

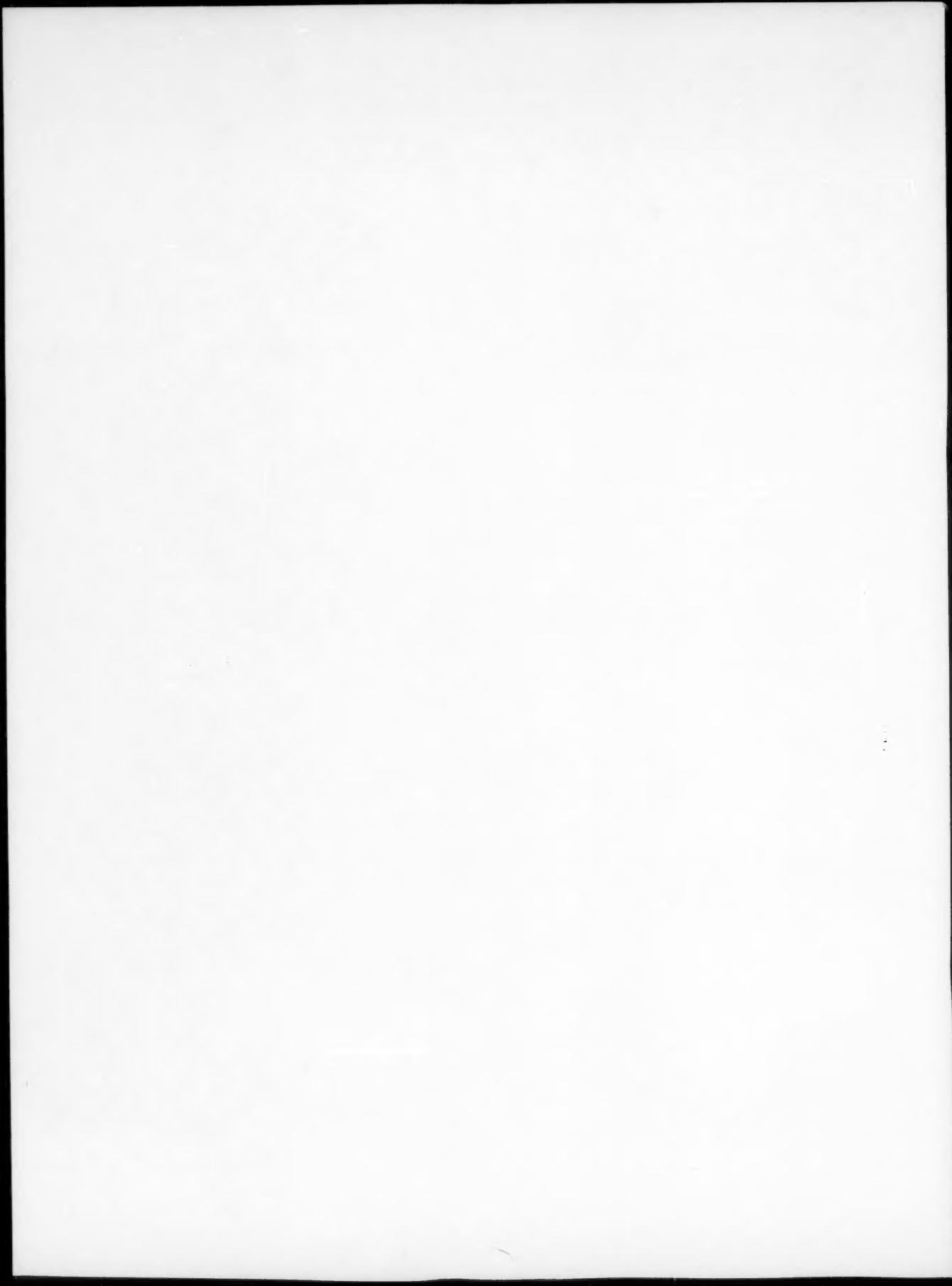
Combined Author Index

Abbaschian, G.J.	93-100A	Chastell, D.J.	913-921A	Foote, R.	603-611B	Hyzak, J.M.	33-43A
Adams, T.N.	153-163B	Chatterjee, D.K.	1837-1841A	Foroush, Z.A.	153-159A		45-52A
Aderibigbe, D.A.	513-515B	Chaubal, P.C.	319-329B	Foulds, J.	173-174A		
Adolph, S.R.	495-497A		331-338B	Fournelle, R.A.	393-399A		
Albrecht, J.	811-820A		339-348B	Frank, R.C.	539-543A		
Alexander, D.J.	1865-1868A	Chawla, K.K.	575-579A		581-584A	Ichinose, Y.	1329-1336A
Allen, R.M.	637-648A	Cheadle, B.A.	1957-1964A	Fritzemeier, L.G.	1951-1955A	Iijima, Y.	1135-1139A
Altstetter, C.	1799-1808A	Chen, G.L.	1951-1955A	Frost, R.T.	1868-1871A	Imagumbai, M.	2131-2141A
Altstetter, C.J.	539-543A	Chicco, B.	1293-1297A	Frydman, S.S.	967-973A	Inoue, A.	337-343A
	581-584A	Cho, K.	901-905A	Fujii, T.	2143-2153A		373-382A
	1355-1365A	Choo, W.Y.	135-140A	Fujitsuka, M.	167-172A	Isaacs, H.S.	2015-2026A
Amin, K.E.	671-673A	Choubey, R.	1957-1964A	Funkensbusch, A.W.	611-618A	Ishii, H.	1521-1529A
An, H.H.	457-472A	Choudhary, M.	35-43B			Iswaran, C.V.	1389-1395A
Anderson, D.L.	91-104B	Christian, J.W.	509-538A			Iwai, M.	311-318B
Andries, B.	545-550A	Chuang, Y.-Y.	379-385B			Iyengar, G.N.K.	387-390B
Anello, J.	2177-2189A	Cielo, P.	479-483B	Gabrielli, F.	1083-1090A		
Angers, R.	5-12A	Closset, B.	945-951A	Gan, D.	2155-2163A	Jacinto, N.	515-517B
Ankem, S.	595-601A	Copley, S.M.	1965-1975A	Gandhi, C.	1233-1238A	Jacob, K.T.	283-285B
	603-609A	Clough, R.B.	259-266B	Garratt-Reed, A.	473-485A		387-390B
Anselli, G.S.	203-211A	Clyne, T.W.	471-478B	Garratt-Reed, A.J.	1347-1353A	Jacobi, H.	2131-2141A
Anton, D.L.	1187-1198A	Cohen, J.B.	1987-1995A	Gayda, J.	1755-1765A	Jahanafooz, A.	1337-1345A
Arieli, A.	717-732A	Cohen, M.	1907-1914A	Gerberich, W.W.	305-311A	Janke, D.	227-235B
Ariga, T.	439-445B	Copley, S.M.	1879-1889A	Gessinger, G.H.	1463-1470A	Jarrett, R.N.	1021-1032A
Arita, M.	1329-1336A	Cornet, M.	141-144A	Ghosh, A.K.	733-743A	Johnson, A.R.	1595-1605A
Arons, R.M.	1453-1462A	Cosandey, F.	603-611B	Giamei, A.F.	1153-1159A	Johnson, D.L.	1101-1102A
Arsenault, R.J.	320-321A		2286-2290A	Glasgow, T.K.	1665-1674A	Johnston, M.H.	85-90B
	1199-1205A		1915-1919A	Glitz, R.	1921-1928A	Jonas, J.J.	1957-1964A
	1429-1434A		1315-1318A	Glowacki, Z.	753-759A	Jones, R.H.	241-249A
Awakura, Y.	311-318B	Courtney, T.H.	873-879A	Gobin, P.F.	1127-1134A	Jones, W.B.	637-648A
			881-887A	Gokhale, A.A.	1101-1102A	Judd, G.	203-211A
Baer, D.R.	241-249A	Covington, J.	2103-2112A	Goldstein, J.I.	1921-1926A	Kadalbal, R.	1153-1159A
Balk, S.	1207-1214A	Craig, B.D.	907-912A	Gordon, P.	457-472A	Kaluba, W.	753-759A
	1215-1221A		1099-1101A	Gorog, J.P.	153-163B	Kane, R.H.	145-152A
Baker, J.E.	581-584A	Cremer, P.	45-52B	Goto, T.	423-427B	Kang, S.S.	1405-1411A
Balluffi, R.W.	527-535B	Crooks, M.J.	1347-1353A	Grimes, H.H.	1933-1938A	Kao, P.	1177-1180A
Bampton, C.C.	2069-2095A	Crosley, P.B.	657-664A	Grugel, R.N.	493-495A	Kao, P.W.	855-864A
	193-198A			Gruzelski, J.E.	945-951A	Kargol, J.A.	1181-1186A
Banerjee, D.	681-684A	Da Cunha Belo, M.	141-144A	Güenü, G.	1127-1134A	Karnowsky, M.M.	345-353A
Banerji, S.K.	827-836A	Dallaire, S.	479-483B	Gummarás, J.R.C.	575-579A	Kashyap, B.P.	53-58A
Baranow, S.	1939-1950A	Das, D.K.	1868-1871A	Guttmann, M.	1821-1826A	Kaspersma, J.H.	267-273B
Bass, M.	1453-1462A	Davenport, W.G.	581-588B	Guthrie, R.I.L.	125-127B	Kasner, M.E.	1977-1986A
Baxter, W.J.	1879-1889A	David, S.A.	1043-1053A	Haglund, J.	193-202B	Kattamis, T.Z.	1153-1159A
	185-192B	Davidson, J.H.	1299-1311A	Hughes, R.	203-211B	Kawecka, E.	71-76B
Baxter, W.J.	1413-1419A	DeBenedetti, B.	1003-1013A	DeHoff, R.T.	1389-1395A	Kayahara, Y.	423-427B
	1421-1427A		1003-1013A	Delobel, P.	251-255A	Kayali, E.S.	1033-1041A
	1927-1932A		1015-1020A	Deruyttere, A.	1015-1020A	Kayashima, M.	1997-2002A
Beck, D.G.	1879-1889A	Doig, P.	913-921A	Gysler, A.	1435-1443A	Kaye, N.A.	975-978A
Begley, J.A.	1003-1013A		1397-1403A			Keller, H.	237-240B
Berkowitz, B.J.	979-984A		1633-1645A			Kenik, E.A.	213-219A
Bernstein, I.M.	33-43A		2177-2189A	Hack, J.E.	1729-1738A	Kennon, N.F.	551-555A
	45-52A		45-52B	Haff, G.R.	1583-1586A		975-978A
	235-239A		293-301B	Hagiwara, M.	373-382A	Kenny, D.	1445-1452A
	811-820A		5-12A	Hajmire, K.	5-12A	Kesternich, W.	213-219A
	1865-1868A		1693-1711A	Hamar-Thibault, S.	545-550A	Khan, K.H.	676-680A
Bertrand, C.	141-144A	Dumoulin, Ph.	551-555A	Hamilton, C.H.	733-743A	Kim, C.	185-191A
Bhatt, R.T.	1933-1938A	Durand-Charre, M.	545-550A	Hamm, C.D.	2281-2285A	Kim, Y.H.	59-72A
Birnbaum, H.K.	174-176A	Dutrizac, J.E.	303-309B	Hanninen, H.	235-239A	Kim, Y.S.	349-356B
	1355-1365A			Hardwick, D.A.	581-588B	King, T.B.	165-173B
	1675-1678A			Harris, R.	589-591B	Kirkaldy, J.S.	2113-2119A
Birocheau, J.	251-255A				1337-1345A	Kleppa, O.J.	251-257B
Biss, V.	185-191A	Eagar, T.W.	1589-1594A	Hasan, F.	1239-1244A	Klundt, R.H.	447-456A
Blander, M.	429-437B	Ebara, R.	1521-1529A	Hauk, V.M.	345-353A	Knoepke, J.R.	15-29B
Blaugher, R.D.	199-202A	Ebert, L.J.	1767-1774A	Hayes, P.C.	117-124B	Koch, D.B.	73-83A
Brebrick, R.F.	1107-1114A	Edington, J.W.	1775-1783A	Heckel, R.W.	1655-1658A	Koczak, M.J.	1501-1510A
Briant, C.L.	745-752A		703-715A	Hecker, S.S.	619-626A	Kojima, Y.	1373-1378A
	1501-1510A	Eisenstein, L.E.	1721-1727A	Heldt, L.A.	627-635A	Korzekwa, D.A.	2061-2064A
	1939-1950A	Eisen, D.	1785-1792A	Helewell, A.	611-618A	Kou, S.	363-371A
Bricknell, R.H.	1223-1232A	El-Raghy, S.M.	473-485A	Hennesen, K.	237-240B	Kou, A.K.	1141-1152A
Brimacombe, J.K.	91-104B	El-Rahaby, S.K.	571-579B	Heshmatpour, B.	53-59B	Kozuka, Z.	673-675A
	105-116B	Emelyanenko, Yu.G.	633-641B	Hibbard, W.R., Jr.	135-139B	Krauss, G.	77-83B
	153-163B	Engh, T.A.	3-4B	Hirano, K.	1135-1139A		1263-1274A
	369-378B	English, G.C.	447-460B	Hirth, J.P.	585-594A		2061-2064A
Brittain, J.O.	2173-2176A	Erm, A.M.	161-166A	Hodsi, F.S.	1245-1255A	Krawitz, A.D.	1069-1076A
Brofman, P.J.	203-211A	Esdale, J.D.	1577-1588A	Hoffeiner, W.	923-927A	Króli, J.	665-669A
Brown, L.C.	25-31A	Esterling, D.M.	2097-2102A	Hoffmann, C.	237-240B	Kuan, T.S.	383-391A
Bruemmer, S.M.	241-249A		1429-1434A	Hölzle, R.	199-202A	Kucera, J.	1658-1659A
Bunk, W.	889-899A	Evans, J.W.	3-13B	Hopkins, R.H.	185-191A	Kumada, K.	337-343A
Butler, E.P.	929-935A		293-301B	Hosford, W.F.	1595-1605A	Kumar, K.	1868-1871A
Byrne, J.G.	855-864A		322-324A		1135-1139A	Kung, C.Y.	328-331A
	1177-1180A	Eylon, D.			1135-1139A	Kuroda, K.	2103-2112A
					1135-1139A	Kurz, W.	259-266B
Carlson, O.N.	995-1001A	Fearing, V.L.	2289A	Hsu, R.	1139-1205A	Kwun, S.I.	393-399A
	1713-1719A		1871-1873A	Hoshino, K.	1135-1139A		
Carmon, B.	645-648B	Fine, M.E.	59-72A	Hotzler, R.K.	1665-1674A		
Carpenter, R.W.	213-219A		1187-1186A	Howson, T.E.	1453-1462A		
Carr, M.J.	1263-1274A	Fiore, N.F.	487-491A		2286-2290A		
Cerisier, P.	429-437B		1181-1186A				
Chakrabarty, A.K.	185-192B	Firrao, D.	1003-1013A	Hu, H.	1257-1262A	Labun, P.A.	2103-2112A
Chakrabortty, S.B.	401-410A	Flemings, M.C.	503-509B	Hua, C.H.	357-367B	Lacombe, P.	1299-1311A
Chandra Narayanan, S.	565-573A		1809-1819A	Huang, T.S.	2173-2176A	Latohi, G.D.	275-288A
Chang, C.W.	1868-1871A	Flewitt, P.E.J.	913-921A	Hudak, S.J., Jr.	1633-1645A	Langdon, T.G.	2289A
Chang, Y.A.	379-385B		1397-1403A	Hunter, G.B.	1589-1594A		689-701A
	1115-1121A		145-152A	Hunter, J.E., Jr.	1063-1067A		2059-2061A
	1123-1126A	Florence, S.	2003-2013A	Hussein, A.A.	837-846A	Lauf, R.J.	539-543A
					847-853A	Laughlin, D.E.	411-425A
					901-905A	Lawley, A.	289-297A

Le, Y.	1141-1152A	Mukherjee, A.K.	717-732A	Ray, R.K.	565-573A	Stein, D.F.	611-618A
Leax, T.R.	1607-1618A	Mukherjee, K.	313-317A	Rayment, J.J.	328-331A	Steinberg, B.G.	2227-2237A
Lederich, R.J.	497-500A	Mulford, R.A.	745-752A	Reid, D.C.	565-570B	Stemple, D.K.	503-509B
Lee, H.G.	403-409B		1223-1232A	Rhines, F.N.	985-993A	Stevenson, D.A.	53-59B
Lee, J.Y.	411-421B	Mulherin, J.H.	657-664A	Ridley, N.	557-563A	Stice, D.	1687-1692A
Leverant, G.R.	1729-1738A	Muller, M.	649-655A		1337-1345A	Stickels, C.A.	613-623B
Levi, C.G.	13-23A	Mura, T.	117-123A	Ripplin, E.J.	1619-1626A	Stone, D.H.	2035-2047A
Lexcellent, C.	221-234A	Murakami, M.	383-391A	Ritchie, R.O.	657-664A	Stout, M.G.	619-626A
Li, D.	251-255A	Murali, T.P.	485-494B		101-110A	Stránský, K.	1658-1659A
Liaw, P.K.	603-611B	Murr, L.E.	627-635A		937-940A	Suery, M.	1809-1819A
	1607-1618A	Murtu, G.S.	53-58A		1627-1631A	Sunwoo, H.	2035-2047A
	1633-1645A				2197-2204A	Surappa, M.K.	485-494B
	2177-2189A				1939-1950A	Suresh, S.	937-940A
Lin, F.S.	401-410A	Nagamori, M.	319-329B	Ritter, A.M.	101-110A		1627-1631A
	2259-2269A		331-338B	Ritter, M.A.	1003-1013A		2271-2280A
Lin, P.L.	61-69B		339-348B	Roberti, R.	1299-1311A	Suutala, N.	2121-2130A
Lipsitt, H.A.	1837-1841A		461-470B	Roques-Carmes, C.	322-324A	Sweett, F.	644-645B
Liu, C.T.	1043-1053A	Naohara, T.	515-517B	Rouze, S.R.	1573-1575A	Szekely, J.	35-43B
Livak, R.J.	1318-1321A	Narita, N.	1355-1365A	Ruano, O.A.	355-361A		513-515B
Livesey, D.W.	1619-1626A	Nathal, M.V.	1767-1774A	Ruth, J.A., Jr.	1785-1792A	Szewczyk, A.F.	1821-1826A
Lloyd, D.J.	1445-1452A		1775-1783A		2289A		
Lorimer, G.W.	1337-1345A	Nayeb-Hashemi, H.	101-110A	Ryeom, Y.J.	1871-1873A	Taha, M.A.	2131-2141A
Loudjani, L.	1299-1311A		2197-2204A		901-905A	Taheri, M.	235-239A
Louthan, M.R., Jr.	2049-2058A	Nesbitt, J.A.	1655-1658A			Takahashi, T.	1373-1378A
Ludika, G.M.	411-425A	Neumann, J.P.	1123-1126A			Takasugi, T.	1471-1481A
Luetjering, G.	1283-1292A	Newman, R.C.	2015-2026A	Saboungi, M.-L.	61-69B	Takeda, Y.	111-116A
Luthra, K.L.	1647-1654A	Niessen, P.	593-602B	Sachdev, A.K.	429-437B	Tamura, I.	176-179A
	1843-1852A	Nix, W.D.	427-437A		1063-1067A	Tanabe, T.	167-172A
	1853-1864A	Notis, M.R.	1921-1926A		1793-1797A	Tanaka, K.	117-123A
Lütjering, G.	1435-1443A				1899-1906A	Tandon, I.C.	495-497A
Lynch, D.C.	285-288B				125-127B	Tangchitvittaya, C.	585-594A
					193-202B	Tangri, K.	1077-1082A
					203-211B	Tauschitz, C.	1483-1489A
Maa, Y.	1115-1121A	Odette, G.R.	299-303A		1521-1529A	Terlinde, G.	1283-1292A
Mack, C.M.	613-623B	Ogura, T.	2205-2207A	Sale, F.R.	625-631B	Thomas, G.	2227-2237A
MacKay, R.A.	1747-1754A	Ohno, R.	175-184B	Saleh, Y.	1275-1281A	Thomas, M.T.	241-249A
Mahajan, Y.	257-268A	Oishi, T.	423-427B	Samarasekera, I.V.	91-104B	Thompson, A.W.	235-239A
Mahoney, M.W.	193-198A	Okafor, I.C.I.	1713-1719A	Sambasiva Rao, G.	2219-2226A	811-820A	
Maier, R.D.	1747-1754A	Olson, G.B.	1907-1914A	Sample, A.	495-501B	1315-1318A	
	1755-1765A	Onyewuenyi, O.A.	423-427B	Sandvik, B.P.J.	777-787A	1531-1532A	
	1767-1774A	Osseso-Asare, K.	2209-2218A	Sastri, S.	789-800A	Thorpe, W.R.	1293-1297A
	1775-1783A	Otsuka, S.	555-564B	Sastray, C.N.	1997-2002A	Tearney, T.C., Jr.	1827-1836A
Maitra, S.	161-166A	Oudehoven, R.W.M.	77-83B	Sastray, S.M.L.	497-500A	Tien, J.K.	603-611B
Majima, H.	311-318B	Owen, W.S.	1239-1244A	Sato, S.	251-257B	Tokizane, M.	1091-1098A
Major, B.	665-669A	Pak, C.S.	1347-1353A	Sato, T.	1373-1378A	Tromans, D.	665-669A
Maki, T.	1379-1388A	Oytana, C.	251-255A	Scanlon, J.C.	979-984A	Tsai, H.-Y.	15-29B
Mangonon, P.L.	319-320A	Ozturk, B.	2289A	Schlosberg, W.H.	1987-1995A	Tscheegg, E.K.	1483-1489A
Mankhand, T.R.	275-282B		1871-1873A	Schmank, M.J.	1069-1076A	Tseng, D.	1077-1082A
Marder, A.R.	85-92A			Schmidt, C.G.	447-456A	Tsuzaki, K.	1379-1388A
Margolin, H.	257-268A			Schuster, W.	1115-1121A		
	289-274A	Page, M.L.	141-152B	Schwerdtfeger, K.	237-240B	Uchida, S.	439-445B
	595-601A	Page, R.A.	305-311A		2131-2141A		
	603-609A	Pak, C.S.	901-905A	Seigle, L.L.	495-497A		
	1275-1281A	Panchanadeeswaran, S.	1177-1180A	Semiatin, S.I.	275-288A		
Martin, D.M.	1713-1719A	Pao, P.S.	497-500A	Shay, R.H.	267-273B	Vaessen, G.J.H.	1239-1244A
Martinez, L.	427-437A	Papazian, J.M.	761-769A	Shea, M.M.	1167-1176A	Vagarali, S.S.	299-303A
Masterson, I.F.	3-13B	Parlee, N.A.D.	357-367B	Shechtman, D.	1891-1898A	Vaidyanathan, T.K.	313-317A
Masumoto, T.	337-343A	Parr, R.A.	85-90B	Sherby, O.D.	355-361A	Vander Sande, J.B.	1347-1353A
	373-382A	Parthasarathi, A.	2027-2033A	Sherman, R.	447-456A	Varschavsky, A.	801-809A
Mateya, M.C.	1263-1274A	Paton, N.E.	1531-1532A	Shewmon, P.G.	1567-1572A	Vasudévan, A.K.	2271-2280A
Matlock, D.K.	2061-2064A	Patterson, B.R.	985-993A	Shikama, T.	167-172A	Voss, D.A.	929-935A
Matsuura, N.	1379-1388A	Paul, S.K.	185-192B	Shimizu, K.	1329-1336A	Wadley, H.N.G.	1965-1975A
Matsuura, Y.	77-83B	Peck, M.G.	1607-1618A	Shioji, Y.	139-145B	Wadsworth, J.	355-361A
Matsuishi, Y.	439-445A	Pelloux, R.M.	73-83A	Siegel, L.L.	1313-1314A	Wadsworth, M.E.	571-579B
Matusiewicz, G.	1997-2002A	Pelton, A.D.	1083-1090A	Sherman, R.	2015-2026A	Wagoner, R.H.	1491-1500A
Maurer, G.E.	1875-1878A	Perkins, J.	61-69B	Shewmon, P.G.	447-460B	Wallace, W.	673-675A
Mauser, J.E.	511-513B	Peterson, D.T.	1367-1372A	Shikama, T.	167-172A	Walser, B.	447-456A
Mazunder, J.	865-871A	Petkovic-Luton, R.	821-825A	Shimizu, K.	1329-1336A	Walter, J.L.	1501-1510A
McAlarney, M.E.	1453-1462A	Petri, H.	237-240B	Shikama, T.	1789-1792A	Warren, G.W.	571-579B
McClintock, F.A.	101-110A	Pickering, H.W.	349-356B	Shimizu, K.	1977-1986A	Warren, I.H.	565-570B
	2197-2204A	Pieprzak, J.A.	613-623B	Shioji, Y.	1781-1873A	Watanabe, R.	167-172A
McEvily, A.J.	439-445A	Pilkington, R.	1739-1745A	Siegel, L.L.	1313-1314A	Watanabe, S.	391-401B
	923-927A	Pilling, J.	557-563A	Sieradzki, K.	2015-2026A	Watkinson, A.P.	369-378B
McMahon, C.J., Jr.	111-116A	Pivin, J.C.	1299-1311A	Sigworth, G.K.	447-460B	Wayman, C.M.	1887-1892A
	176-179A	Plumtree, A.	1033-1041A	Silva, G.	31-34B	Wayman, M.	1693-1711A
McNallan, M.J.	165-173B	Poirier, D.R.	2143-2153A	Simensen, C.J.	2289A	Webster, D.	1511-1519A
Medovar, B.I.	35-43B	Polan, N.W.	2027-2033A	Simkovich, G.	1871-1873A	Weckman, D.C.	593-602B
Mehrabian, R.	13-23A	Pope, D.P.	1471-1481A	Singbeit, D.	1091-1098A	Weertman, J.	2165-2172A
	93-100A	Prasad, P.M.	275-282B	Singer, R.F.	1463-1470A	Weins, W.N.	995-1001A
	221-234A	Prasad, Y.V.R.K.	2219-2226A	Singh, R.	1799-1808A	Welsch, G.	889-899A
Mermet, A.	251-255A	Predel, B.	71-76B	Singh, S.	771-775A	Wert, J.A.	193-198A
Messhi, M.	2035-2047A	Przystupa, M.A.	873-879A	Singh, V.	461-470B	West, A.J., Jr.	2049-2058A
Mezzanotte, D.A.	1181-1186A		881-887A	Sinha, S.N.	289-297A	Williams, R.O.	959-965A
Middleton, L.	551-555A			Skinner, A.	619-626A	Williams, R.S.	1607-1618A
Mikula, A.	1115-1121A			Smith, J.L.	821-825A	Wolf, M.	259-266B
	1123-1126A	Quigley, B.F.	93-100A	Smith, M.F.	1535-1546A	Wood, W.E.	678-680A
Miller, A.K.	1977-1986A			Sommer, F.	515-517B	Woodford, D.A.	1223-1232A
Minakawa, K.	439-445A	Raghavan, M.	953-957A	Sorenson, W.R.	345-353A	Wray, P.J.	125-134A
Minemura, T.	337-343A		979-984A	Souza, M.M.	575-579A	Wright, J.K.	518-520B
Miner, R.V.	1755-1765A	Raj, R.	1207-1214A	Speich, G.R.	2239-2258A	Wunderlin, R.	93-100A
Minni, E.	2281-2285A	Rajan, K.	1215-1221A	Spitzig, W.A.	2239-2258A	Xie, X.	1951-1955A
Mitchell, T.E.	929-935A	Rao, B.V.N.	1161-1166A	Srivastava, K.K.	253-2119A		
	2103-2112A		771-775A	St. John, D.H.	117-124B		
Momokawa, H.	643-644B	Rao, Y.K.	1167-1176A	Stanley, J.T.	1915-1919A		
Montoya-Cruz, J.J.	1153-1159A		1679-1686A	Stanzi, S.E.	1483-1489A		
Moody, N.R.	1055-1061A		1899-1906A	Starke, E.A., Jr.	401-410A		
Moriyama, J.	241-249B			Staudhammer, K.P.	2259-2269A		
	423-427B				619-626A		
Morris, A.E.	15-29B				627-635A		
Morrison, A.L.	518-520B				953-957A		
Moser, Z.	71-76B				965-971A		
Moteff, J.	173-174A	Rapp, R.A.	585-594A				
	1577-1588A	Rashid, M.S.	1679-1686A	Steeds, J.W.			
				Steen, W.M.			

Yang, W.J.S. 324-328A
Yearim, R. 1891-1898A
Yeh, J.T.C. 1547-1562A
Yen, C. 2286-2290A
Yoon, D.N. 1405-1411A
Yorucu, H. 625-631B
Yoshida, H. 167-172A
Young, C.M. 447-456A
Yu, Z.-S. 1587-1572A
Yurek, G.J. 473-485A

Zielinski, A. 487-491A
Zulueta, E.N. 503-509B



Combined Subject Index

Aberration		Alkaline earth metals	
See Distortion		See Magnesium	
Absolute temperature		Strontium	
See Temperature			
Absolute viscosity		Alkalinity	
See Viscosity		See pH	
Absorption (energy)		Alloy steels	
Thermal Effects During Uniaxial Straining of Steels.	1063-1067A	See Austenitic stainless steels	
Absorption (material)		Boron steels	
Prediction of the Effects of Surface-Active Elements on		Chromium manganese steels	
Gas—Liquid Metal Kinetics.	357-367B	Chromium molybdenum steels	
Absorption coefficient		Chromium steels	
See Absorption (energy)		Chromium vanadium steels	
Acid leaching		Dual phase steels	
See also Sulfuric acid leaching		Ferritic stainless steels	
Ferric Ion Leaching of Chalcopyrites From Different Locali-		High alloy steels	
ties.	303-309B	High strength low alloy steels	
Acidity		Low alloy steels	
See pH		Martensitic stainless steels	
Acoustic emission		Nickel chromium molybdenum steels	
Indentation Loading Studies of Acoustic Emission From Tem-		Nickel chromium steels	
per and Hydrogen Embrittled A533B Steel.	1985-1975A	Silicon steels	
Actinide metals		Stainless steels	
See Thorium		TRIP steels	
Activation energy			
Thermal Analysis of Trapped Hydrogen in Pure Iron.	135-140A	Alloying elements, Solubility	
Caustic Stress Corrosion Cracking of Mild Steel.	1091-1098A	Thermodynamics of the Superalloys.	959-965A
Peierls—Nabarro Plastic Deformation in the Presence of So-			
lute Clusters.	1429-1434A		
Short-Range Ordering Kinetics in 316 Austenitic Stainless			
Steel.	1915-1919A		
Strain Aging and Strain Rate Sensitivity of Oxygen-Enriched			
(Alpha + Beta) Zircaloy-2.	1957-1964A		
Activity (chemical)			
Correction to "Self-Diffusion Coefficients of Carbon in Fe ₃ C			
at 723°K Via the Kinetics of Formation of This Compound".	2289A		
Oxygen Pressure Measurements of Silica Saturated			
Fe—O—SiO ₂ Melt by the E.M.F. Method Using Zirconia			
Solid Electrolyte.	423-427B		
Activities of Co ₃ S and FeS in Copper Mattes and the Behavior			
of Cobalt in Copper Smelting.	461-470B		
Thermodynamics of the Superalloys.	959-965A		
Self-Diffusion Coefficients of Carbon in Fe ₃ C at 723°K Via			
the Kinetics of Formation of This Compound.	1871-1873A		
Activity (chemical), Composition effects			
Activities of Oxygen in Liquid Cu—Sb and Cu—Ge Alloys.	77-83B		
Activity of Manganese in Liquid Ni—Mn Alloys.	283-285B		
Activity coefficients			
See Activity (chemical)			
Age hardening			
See Precipitation hardening			
Agents			
See Surfactants			
Aging			
See also Aging (artificial)			
Quench aging			
Secondary hardening			
Strain aging			
The Effects of Copper and Chromium on the Aging Response			
of Dilute Al—Mg—Si Alloys.	1318-1321A		
Aging (artificial)			
See also Secondary hardening			
Modulated Structures and G-P Zones in Al—Mg Alloys.	1373-1378A		
Observations of Aging Effects in a Cu—Sn Shape Memory			
Alloy.	1687-1692A		
The Influence of Cobalt on the Microstructure of the Nickel-			
Base Superalloy MAR-M247.	1775-1783A		
Agitation			
See Electromagnetic stirring			
Aircromatic welding			
See Gas metal arc welding			
Alkali metal compounds			
See Lithium compounds			
Sodium chloride			
Sodium compounds			
Sodium hydroxide			
Alkali metals			
See Lithium			
Sodium			
Alkaline earth metal alloys			
See Strontium			
Alkaline earth metal compounds			
See also Calcium compounds			
Lime			
Alkaline earth metal compounds, Oxidation			
Oxidation of Alkaline Earth Sulfides to Sulfates: Thermody-			
namic Aspects.	387-390B		

Aluminum base alloys

Aluminum base alloys, Crystal growth		Analyzing
The Use of Heat Flow Modeling to Explore Solidification Phenomena.	471-478B	See Auger electron spectroscopy Depth profiling Electrolytic analysis Mathematical analysis Microanalysis Quantitative analysis Stress analysis Surface analysis (chemical) Thermal analysis X ray analysis X ray diffraction X ray stress analysis
Aluminum base alloys, Diffusion		
Evidence for Dislocation Transport of Hydrogen in Aluminum.	811-820A	
Aluminum base alloys, Heat treatment		Andrade method
The Effects of Copper and Chromium on the Aging Response of Dilute Al—Mg—Si Alloys.	1318-1321A	See Crystal growth
Aluminum base alloys, Mechanical properties		Annealing
A Theory of Fatigue Crack Initiation at Inclusions.	117-123A	See Homogenizing
Hydrogen Embrittlement in a 2000 Series Aluminum Alloy.	235-239A	
The Influence of Microstructure and Strength on the Fracture Mode and Toughness of 7XXX Series Aluminum Alloys.	411-425A	Anodic coatings
Microstructural Aspects of Superplasticity.	703-715A	Effect of Oxide Thickness on Electrochemical Detection of Fatigue.
The Rate-Controlling Deformation Mechanisms in Superplasticity—a Critical Assessment.	717-732A	Electrochemical Detection of Fatigue Cracks in Steel.
Structure and Properties of Hypoeutectic Al—Si—Mg Alloys Modified With Pure Strontium.	945-951A	1573-1575A 1927-1932A
Measurement of a Stress Gradient Through the Bulk of an Aluminum Alloy Using Neutrons.	1069-1076A	
Wedge-Type Creep Damage in Low-Cycle Fatigue.	1207-1214A	Anodic dissolution, Field effects
Mechanisms of Creep—Fatigue Interaction.	1215-1221A	Passive and Transpassive Anodic Behavior of Chalcocite in Acid Solutions.
Gel Electrode Imaging of Metal Fatigue. I.—Cracks in 6061-T6 Aluminum.	1413-1419A	571-579B
The Large Strain Deformation of Some Aluminum Alloys.	1445-1452A	
The Influence of Grain Structure on the Ductility of the Al—Cu—Li—Mn—Cd Alloy 2020.	2259-2269A	Anodic polarization
Influence of Corrosion Deposits on Near-Threshold Fatigue Crack Growth Behavior in 2XXX and 7XXX Series Aluminum Alloys.	2271-2280A	Corrosion Behavior of Amorphous Fe—Cr—Al—P—C Ribbon Alloys.
Aluminum base alloys, Metal working		901-905A
Influences of Materials Parameters and Microstructure on Superplastic Forming.	733-743A	
Microstructural Observations of Superplastic Cavitation in Fine-Grained 7475 Al.	1721-1727A	Anodic polarization, Field effects
		Passive and Transpassive Anodic Behavior of Chalcocite in Acid Solutions.
Aluminum base alloys, Microstructure		571-579B
Heating Rate Effects on Recrystallized Grain Size in Two Al—Zn—Mg—Cu Alloys.	193-198A	
Microstructure—Property Relationships of Two Al—3Li—2Cu—0.2Zr—XCd Alloys.	401-410A	Antidomains
The Occurrence of Aligned Microstructures in Directionally Solidified Aluminum—Bismuth Alloys.	493-495A	See Domains
Modulated Structures and G—P Zones in Al—Mg Alloys.	1373-1378A	
Aluminum base alloys, Powder technology		Antimony, Alloying additive
Microstructures of Rapidly Solidified Aluminum Alloy Submicron Powders.	13-23A	Hydrogen Embrittlement of Ultra-Pure Alloys of the Inconel 600 Type: Influence of the Additions of Elements (Carbon, Phosphorus, Tin, Antimony).
The Structure of Rapidly Solidified Al—Fe—Cr Alloys.	1891-1898A	141-144A
Aluminum base alloys, Structural hardening		Antimony, Trace elements
Calorimetric Studies of Precipitation and Dissolution Kinetics in Aluminum Alloys 2219 and 7075.	761-769A	Effect of Sulfur and Antimony on the Intergranular Fracture of Iron at Cathodic Potentials.
Aluminum base alloys, Welding		241-249A
Welding, Glazing and Heat Treating—a Dimensional Analysis of Heat Flow.	363-371A	Antimony base alloys, Solubility
Aluminum brasses, Phase transformations		Activities of Oxygen in Liquid Cu—Sb and Cu—Ge Alloys.
Rapid Solidification Effects in Martensitic Cu—Zn—Al Alloys.	1367-1372A	77-83B
Aluminum bronzes, Phases (state of matter)		Antimony compounds, Thermal properties
The Morphology, Crystallography and Chemistry of Phases in As-Cast Nickel—Aluminum Bronze.	1337-1345A	Heteronuclear Compounds of Arsenic and Antimony.
Aluminum compounds		511-513B
See also Aluminum oxide		
Aluminum compounds, Crystal growth		Arsenides, Physical properties
Recrystallization and Grain Growth in NiAl.	1563-1566A	Standard Free Energy of Formation of NiAsS.
Aluminum compounds, Crystal lattices		285-288B
"C" Component Dislocations in Deformed Ti ₃ Al.	324-328A	
Aluminum compounds, Diffusion		Artificial aging
The Early Stage of Ni ₃ Al Layer Growth in NiAl/Ni Diffusion Couples.	1921-1926A	See Aging (artificial)
Aluminum compounds, Mechanical properties		Aspirating thermocouples
Effect of Defect Structure Upon the Mechanical Behavior of Beta-LiAl Through Dislocation Damping and Hardness Studies.	2173-2176A	See Thermocouples
Aluminum killed steels, Refining		Atmospheres
Effect of Rare Earth Additions on the Inclusions and Properties of a Ca—Al Deoxidized Steel.	185-192B	See Controlled atmospheres Reducing atmospheres
Aluminum oxide, Composite materials		Atmospheric temperature
A Method for Fabrication of Aluminum/Alumina Composites. Work of Fracture in Aluminum Metal-Matrix Composites.	93-100A 289-297A	See Temperature
Amalgams		Atomic diffusion
See Mercury amalgams		See Diffusion
Ambient temperature		Atomization
See Temperature		See Atomizing
Ammonia, Corrosion environments		Atomizing
Stress Corrosion of Cu—Zn and Cu—Zn—Ni Alloys: the Role of Dealloying.	2027-2033A	Heat Flow During Rapid Solidification of Undercooled Metal Droplets.
Amorphous materials		221-234A
See Metallic glasses		
Amorphous structure		Attenuation
Mechanical Properties of Fe—Si—B Amorphous Wires Produced by In-Rotating-Water Spinning Method.	373-382A	See Ultrasonic attenuation
Amplifiers		Auger electron spectroscopy
See Lasers		Surface Segregation in Austenitic Stainless Steel.
Austenite, Crystal growth		745-752A
Recrystallization and Formation of Austenite in Deformed Lath Martensitic Structure of Low-Carbon Steels.		
Austenite, Phase transformations		Austenite
Isothermal Transformation of Austenite to Pearlite and Upper Bainite in Eutectoid Steel.		See also Retained austenite
		The Isothermal Austenite—Ferrite Transformation in Some Deformed Vanadium Steels.
		1347-1353A
		Hydrogen-Related Phase Transformations in Austenitic Stainless Steels.
		1355-1365A
		Austenite, Crystal growth
		Recrystallization and Formation of Austenite in Deformed Lath Martensitic Structure of Low-Carbon Steels.
		1379-1388A
		Austenite, Phase transformations
		Isothermal Transformation of Austenite to Pearlite and Upper Bainite in Eutectoid Steel.
		975-978A

Austenitic stainless steels, Atomic properties		
Short-Range Ordering Kinetics in 316 Austenitic Stainless Steel.	1915-1919A	
Austenitic stainless steels, Corrosion		
The Effect of High-Temperature Low-Cycle Fatigue on the Corrosion Resistance of Austenitic Stainless Steels.	923-927A	
An Examination of Chromium Substitution in Stainless Steels.	2003-2013A	
Stress Corrosion Cracking of Sensitized Type 304 Stainless Steel in Thiosulfate Solutions.	2015-2026A	
On Grain Boundary Segregation in Austenitic Stainless Steels.	2281-2285A	
Austenitic stainless steels, Crystal growth		
Carbide Formation in a Low-Ferrite Austenitic Stainless Steel Weld Metal at 649°C.	173-174A	
Austenitic stainless steels, Diffusion		
A SIMS Study of the Diffusion and Trapping of Deuterium in 302 Stainless Steel.	581-584A	
Austenitic stainless steels, Mechanical properties		
Wedge-Type Creep Damage in Low-Cycle Fatigue.	1207-1214A	
Flow Localization and Shear Band Formation in a Precipitation Strengthened Austenitic Stainless Steel.	1263-1274A	
Correlation of Substructure With Time-Dependent Fatigue Properties of AISI 304 Stainless Steel.	1577-1588A	
Effects of Hydrogen Concentration on Slow Crack Growth in Stainless Steels.	1799-1808A	
Hydrogen Effects on the Tensile Properties of 21-6-9 Stainless Steel.	2049-2058A	
Tensile and Fracture Properties of Type 316 Stainless Steel After Creep.	2155-2163A	
Austenitic stainless steels, Oxidation		
Oxidation Behavior of a Fine-Grained Rapidly Solidified 18-8 Stainless Steel.	473-485A	
Austenitic stainless steels, Phase transformations		
Effects of Strain State and Strain Rate on Deformation-Induced Transformation in 304 Stainless Steel. I.—Magnetic Measurements and Mechanical Behavior.	619-626A	
Effects of Strain State and Strain Rate on Deformation-Induced Transformation in 304 Stainless Steel. II.—Microstructural Study.	627-635A	
Hydrogen-Related Phase Transformations in Austenitic Stainless Steels.	1355-1365A	
Austenitic stainless steels, Structural hardening		
Surface Hardening and Microstructural Changes in 304 Stainless Steel Resulting From Elevated-Temperature Ultrasonic Vibration.	1167-1176A	
The Separate Roles of Subgrains and Forest Dislocations in the Isotropic Hardening of Type 304 Stainless Steel.	1977-1986A	
Austenitic stainless steels, Surface properties		
Surface Segregation in Austenitic Stainless Steel.	745-752A	
Austenitic stainless steels, Welding		
The Effect of Quenching on the Solidification Structure and Transformation Behavior of Stainless Steel Welds.	1141-1152A	
Effect of Manganese and Nitrogen on the Solidification Mode in Austenitic Stainless Steel Welds.	2121-2130A	
Austenitizing		
Intercritical Austenitization of Two Fe—Mn—C Steels.	575-579A	
The Influence of Notch Root Radius and Austenitizing Temperature on Fracture Appearance of As-Quenched Charpy V Type AISI 4340 Steel Specimens.	1003-1013A	
Recrystallization and Formation of Austenite in Deformed Lath Martensitic Structure of Low-Carbon Steels.	1379-1388A	
The Effect of Heat Treatments on the Corrosion Fatigue Properties of 13% Chromium Stainless Steel in 3% NaCl Aqueous Solution.	1521-1529A	
Fracture Toughness of AISI M2 High-Speed Steel and Corresponding Matrix Tool Steel.	1595-1605A	
The Role of Nitrogen in the Embrittlement of Steel.	1939-1950A	
Auto oxidation		
See Oxidation		
Autodiffusion		
See Diffusion		
Autogenous smelting		
See Flash smelting		
Bainite, Crystal growth		
The Bainite Reaction in Fe—Si—C Alloys: the Secondary Stage.	789-800A	
Bainite, Microstructure		
The Bainite Reaction in Fe—Si—C Alloys: the Primary Stage.	777-787A	
Banded structure		
Effects of Strain State and Strain Rate on Deformation-Induced Transformation in 304 Stainless Steel. II.—Microstructural Study.	627-635A	
Flow Localization and Shear Band Formation in a Precipitation Strengthened Austenitic Stainless Steel.	1263-1274A	
The Constitution and Phase Stability of Overlapping Melt Trails in Ag—Cu Alloys Produced by Continuous Laser Melt Quenching.	1879-1889A	
Banded structure, Deformation effects		
The Occurrence of Shear Bands in Isothermal, Hot Forging.	275-288A	
Basicity		
See pH		
Batch type furnaces		
See Bottom blown converters		
BCC metals, Crystal structure		
Pearls—Nabarro Plastic Deformation in the Presence of Solute Clusters.	1429-1434A	
Beehive kilns		
See Kilns		
Bendability		
See Formability		
Binary systems		
Defective Two Sublattice Model for a Binary Liquid.	1107-1114A	
Binary systems, Atomic properties		
Discussion of "A Gaussian-Based Formalism for the Representation of Free Energy as a Function of Composition on Binary Metallic Solutions".	644-645B	
Binary systems, Intermetallics		
Thermodynamic Studies on the Mg—Ga System.	71-76B	
Binary systems, Phase transformations		
The Alpha-Gamma Phase Boundaries and the T_0 for Fe—Mn Alloys.	2113-2119A	
Binary systems, Phases (state of matter)		
Phase Stability Investigations of the Palladium—Cadmium System. I.—Thermodynamic Studies.	1115-1121A	
Phase Stability Investigations of the Palladium—Cadmium System. II.—Structural Studies.	1123-1128A	
A Simple Bisection Technique for the Calculation of a Two-Solid or Two-Liquid Miscibility Gap in Binary Metallic Systems.	2097-2102A	
Binary systems, Solubility		
Activity of Manganese in Liquid Ni—Mn Alloys.	283-285B	
The Coordination Cluster Theory—Description of the Activity Coefficients of Dilute Solutions of Oxygen and Sulfur in Binary Alloys.	429-437B	
Binding energy (nuclear)		
Differential Scanning Calorimetry Evaluations in Alpha Cu—Al Alloys. Energetics.	801-809A	
Bismuth, Alloying elements		
The Occurrence of Aligned Microstructures in Directionally Solidified Aluminum—Bismuth Alloys.	493-495A	
Bismuth, Impurities		
Volatilization of Bismuth in Copper Matte Converting—Computer Simulation.	339-348B	
Bismuth base alloys, Thermal properties		
A Gaussian-Based Formalism for the Representation of Free Energy as a Function of Composition of Binary Metallic Solutions.	213-225B	
Blades		
See Turbine blades		
Blankets (atmospheres)		
See Controlled atmospheres		
Blast furnace practice		
The Reaction of Coke Specimens in an Environment Where Both the Temperature and the Gas Composition Are Time Dependent.	513-515B	
Body centered cubic metals		
See BCC metals		
Boiler scale		
See Scale (corrosion)		
Boiling		
See Nucleate boiling		
Borides, Thermal properties		
Enthalpies of Formation of Borides of Iron, Cobalt and Nickel by Solution Calorimetry in Liquid Copper.	251-257B	
Boron, Composite materials		
Work of Fracture in Aluminum Metal-Matrix Composites.	289-297A	
Boron intensified steels		
See Boron steels		
Boron steels, Mechanical properties		
The Influence of a Duplex Microstructure in Steels on Fatigue Crack Growth in the Near-Threshold Region.	439-445A	
Bottom blown converters		
Hydrodynamics of Gas Stirred Melts. I.—Gas/Liquid Coupling.	193-202B	
Hydrodynamics of Gas Stirred Melts. II.—Axisymmetric Flows.	203-211B	
Boundaries		
See Grain boundaries		
Phase boundary		
Brasses		
See also Aluminum brasses		
Brasses, Mechanical properties		
The Fatigue of Pseudoelastic Polycrystalline Beta-CuZnSn. Plastic Behavior of 70/30 Brass Sheet.	25-31A 1491-1500A	
Brick kilns		
See Kilns		
Bridgman method		
See Crystal growth		
Brine		
See Salt water		
Brittle fracture		
Carbide Formation in a Low-Ferrite Austenitic Stainless Steel Weld Metal at 649°C.	173-174A	

Brittle fracture

Brittle fracture, Composition effects

Effects of Compositional Variations and Aging Treatments on the Fracture Behavior of HY 130 Steel in Air and Hydrogen.

111-116A

Mass Transport of Carbon in One- and Two-Phase Iron—Nickel Alloys in a Temperature Gradient.

Self-Diffusion Coefficients of Carbon in Fe₃C at 723°K Via the Kinetics of Formation of This Compound.

1713-1719A
1871-1873A

Brittleness

See Temper brittleness

Bronzes

See Aluminum bronzes

Bubbling

Fluid Dynamics of Vertical Submerged Gas Jets in Liquid Metal Processing Systems.

Hydrodynamics of Gas Stirred Melts. I.—Gas/Liquid Coupling.

Hydrodynamics of Gas Stirred Melts. II.—Axisymmetric Flows.

165-173B

193-202B

203-211B

Carbon, Ternary systems

Recomputation of Phase Equilibria in the Sodium—Carbon—Oxygen System: Effect of Oxygen.

1101-1102A

Carbon compounds

See Carbides

Titanium carbide

Carbon steels

See also Aluminum killed steels

Dynamic Strain Aging of Various Steels.

1793-1797A

Carbon steels, Casting

The Thermal Distortion of Continuous-Casting Billet Molds. The Influence of Mold Behavior on the Production of Continuously Cast Steel Billets.

91-104B
105-116B

Carbon steels, Coating

On Some Features of Chromium Carbide Diffusion Layer Formation.

753-759A

Carbon steels, Corrosion

An Equation-of-State for Methane for Modeling Hydrogen Attack in Ferritic Steels.

299-303A

Claustic Stress Corrosion Cracking of Mild Steel.

1091-1098A

Carbon steels, Crystal growth

Recrystallization and Formation of Austenite in Deformed Lath Martensitic Structure of Low-Carbon Steels.

1379-1388A

Carbon steels, Directional solidification

Dendrite Morphology of Several Steady State Unidirectionally Solidified Iron-Base Alloys.

2131-2141A

Carbon steels, Heat treatment

Carburizing and Gas Reactions of Hydrocarbon—Nitrogen Mixtures at 850 and 925°C.

267-273B

Gas Carburizing of Steel With Furnace Atmospheres Formed in Situ From Methane and Air and From Butane and Air.

613-623B

Carbon steels, Mechanical properties

Effect of Carbon Content on the Plastic Flow of Plain Carbon Steels at Elevated Temperatures.

125-134A

The Influence of a Duplex Microstructure in Steels on Fatigue Crack Growth in the Near-Threshold Region.

439-445A

Surface Wave Studies of Hydrogen Damage Incubation Time.

487-491A

Fatigue Initiation Study of TMT Eutectoid Steel.

855-864A

The State of Residual Stress in the Near Surface Region of Homogeneous and Heterogeneous Materials After Grinding.

1239-1244A

Hydrogen Cracking in Nominally Pearlitic 1045 Steel.

1315-1318A

Electrochemical Detection of Fatigue Cracks in Steel.

1927-1932A

Plastic Instability in U-Notched Bend Specimens of Spheroidized AISI 1090 Steel.

2209-2218A

Carbon steels, Metallography

The Cleavage Plane of Pearlite.

1865-1868A

Carbon steels, Phase transformations

Isothermal Transformation of Austenite to Pearlite and Upper Bainite in Eutectoid Steel.

975-978A

Carbon steels, Structural hardening

Aging Susceptibility of Retained and Epitaxial Ferrite in Dual-Phase Steels.

2061-2064A

Carbon steels, Thermal properties

Thermal Effects During Uniaxial Straining of Steels.

1063-1067A

Carburization

See Carburizing

Carburizing

See also Gas carburizing

Carburization and Gas Reactions of Hydrocarbon—Nitrogen Mixtures at 850 and 925°C.

267-273B

Case carburizing

See Carburizing

Case hardening

See Carburizing

Gas carburizing

Cast iron

See also White iron

Cast iron, Coating

On Some Features of Chromium Carbide Diffusion Layer Formation.

753-759A

Casting

See also Continuous casting

Direct chill casting

Ingot casting

Melt spinning

Rheocasting

The Effect of Mold Precession on Channel and Macrosegregation in Ammonium Chloride—Water Analog Castings.

495-501B

Casting defects

The Effect of Melt Composition on Solidification Cracking of Steel, With Particular Reference to Continuous Casting.

259-266B

Castings, Mechanical properties

High-Cycle Fatigue Life of the Cast Nickel-Based Superalloys IN 738 LC and IN 939.

1245-1255A

Castings, Welding

High-Cycle Fatigue of Weld Repaired Cast Ti—6Al—4V.

1589-1594A

Cathodes

See Fluidized bed cathodes

Carbides

See also Silicon carbide

Titanium carbide

Fatigue Crack Initiation and Propagation in a Quenched and Tempered Niobium-Bearing HSLA Steel.

393-399A

185-191A

761-769A

2165-2172A

173-174A

213-219A

557-563A

753-759A

979-984A

789-800A

545-550A

141-144A

1293-1297A

485-494B

2289A

1658-1659A

Carbides, Chemical analysis

A New Procedure for Determining Volume Fraction of Primary Carbides in High-Speed and Related Tool Steels.

Carbides, Crystal growth

Carbide Formation in a Low-Ferrite Austenitic Stainless Steel Weld Metal at 649°C.

Irradiation-Induced Mo₂C Precipitation in Ni—Mo.

Tempering of 1.25%Cr—1%Mo Low-Carbon Steels.

On Some Features of Chromium Carbide Diffusion Layer Formation.

Electron Microscopic Analysis of Heterogeneous Precipitates in Hastelloy C-276.

Carbides, Crystal lattices

The Bainite Reaction in Fe—Si—C Alloys: the Secondary Stage.

Carbides, Phase transformations

Carbide Transformations During Aging of Wear-Resistant Cobalt Alloys.

Carbon, Alloying additive

Hydrogen Embrittlement of Ultra-Pure Alloys of the Inconel 600 Type: Influence of the Additions of Elements (Carbon, Phosphorus, Tin, Antimony).

Carbon, Alloying elements

Experimental Determination of the Austenite + Liquid Phase Boundaries of the Fe—C System.

Carbon, Composite materials

Preparation and Properties of Aluminum Alloy Coconut Shell Char Particulate Composites.

Carbon, Diffusion

Correction to "Self-Diffusion Coefficients of Carbon in Fe₃C at 723°K Via the Kinetics of Formation of This Compound". Discussion of "An Approximate Analytical Demonstration of the Famous Darken Experiment".

Caustic soda		
See Sodium hydroxide		
Causticity		
See pH		
Cavitation		
Influences of Materials Parameters and Microstructure on Superplastic Forming.	733-743A	
Compositional Effects on the High-Temperature Ductility of 1Cr—1.25Mo—0.25V Steel.	1471-1481A	
Microstructural Observations of Superplastic Cavitation in Fine-Grained 7475 Al.	1721-1727A	
Cavitation, Deformation effects		
Cavitation and Cavity Growth During Superplastic Flow in Microduplex Cu—Zn—Ni Alloys.	1619-1626A	
Cavities		
See Holes		
Cells		
See Electrolytic cells		
Cellular precipitates		
Combined Recrystallization and Precipitation in a Cu—9Ni—6Sn Alloy.	565-573A	
Phase Transformations in a Wrought Co—Cr—Mo—C Alloy.	1161-1166A	
Cementite, Diffusion		
Correction to "Self-Diffusion Coefficients of Carbon in Fe ₃ C at 723°K Via the Kinetics of Formation of This Compound".	2289A	
Self-Diffusion Coefficients of Carbon in Fe ₃ C at 723°K Via the Kinetics of Formation of This Compound.	1871-1873A	
Ceramics		
See Silicon nitride		
Cerium, Alloying additive		
Understanding the Role of Cerium During VIM Refining of Nickel—Chromium and Nickel—Iron Alloys.	603-611B	
CGF forging process		
See Forging		
Chalcogenides		
See Sulfides		
Chalcopyrite, Beneficiation		
Ferric Ion Leaching of Chalcopyrites From Different Localities.	303-309B	
Chalcopyrite, Electrochemistry		
Passive and Transpassive Anodic Behavior of Chalcopyrite in Acid Solutions.	571-579B	
Charge materials		
Factors Influencing the Production Rate and Quality of Lead Sinter.	15-29B	
Chemical analysis		
See Depth profiling		
Electrolytic analysis		
Microanalysis		
Quantitative analysis		
Surface analysis (chemical)		
Chemical attack		
See Intergranular corrosion		
Preferential attack (corrosion)		
Chemical kinetics		
See Reaction kinetics		
Chemical processes		
See Reactions (chemical)		
Chemical processing industry		
See Reactions (chemical)		
Chemical properties		
See Heat of activation		
Heat of formation		
Chemical reactions		
See Reactions (chemical)		
Chemical reactors		
Thermodynamics of Copper Matte Converting. IV.— <i>A Priori</i> <td>331-338B</td> <td></td>	331-338B	
Chemical tests		
See Depth profiling		
Electrolytic analysis		
Microanalysis		
Quantitative analysis		
Surface analysis (chemical)		
Chemistry		
See Electrochemistry		
Microchemistry		
Surface chemistry		
Thermochemistry		
Chill casting		
See Direct chill casting		
Chlorides		
See also Sodium chloride		
Chlorides, Environment		
Potentiodynamic Polarization Analysis of Silver—Palladium Alloys in Chloride Solutions.	313-317A	
Chlorination		
Kinetics of Chlorination of Cobalt and Co—10 At.-% Pt Alloy by Reaction With HCl Gas.	349-356B	
Chlorine, Reactions (chemical)		
Kinetics and Mechanism of the Reaction of Iron—Chromium and Iron—Chromium—Molybdenum Alloys With Chlorine Gas.		153-159A
Chromalloy process		
See Pack chromizing		
Chromium, Alloying additive		
The Effects of Copper and Chromium on the Aging Response of Dilute Al—Mg—Si Alloys.		1318-1321A
Chromium, Alloying elements		
Microstructures, Mechanical Properties and Electrical Resistivity of Rapidly Quenched Fe—Cr—Al Alloys.		337-343A
Chromium, Diffusion		
Experimental and Theoretical Concentration Profiles at the Surface of Chromized Iron.		495-497A
Chromium, Materials substitution		
An Examination of Chromium Substitution in Stainless Steels.		2003-2013A
Chromium manganese steels, Refining		
Effect of Rare Earth Additions on the Inclusions and Properties of a Ca—Al Deoxidized Steel.		185-192B
Chromium molybdenum nickel steels		
See Nickel chromium molybdenum steels		
Chromium molybdenum steels		
See also Nickel chromium molybdenum steels		
Chromium molybdenum steels, Corrosion		
The Role of Molybdenum in the Enhanced Resistance to Hydrogen Stress Cracking of AISI 4100 Steels.		1099-1101A
An Examination of Chromium Substitution in Stainless Steels.		2003-2013A
Chromium molybdenum steels, Heat treatment		
Tempering of 2.25%Cr—1%Mo Low-Carbon Steels.		557-563A
Chromium molybdenum steels, Mechanical properties		
The Influence of a Duplex Microstructure in Steels on Fatigue Crack Growth in the Near-Threshold Region.		439-445A
The Mechanisms of Crack Initiation and Crack Propagation in Metal-Induced Embrittlement of Metals.		457-472A
Compositional Effects on the High-Temperature Ductility of 1Cr—1.25Mo—0.25V Steel.		1471-1481A
Calorimetric Measurements of the Plastic Work of Fatigue Crack Propagation in 4140 Steel.		2165-2172A
Effects of Friction and High Torque on Fatigue Crack Propagation Mode III.		2197-2204A
Chromium molybdenum steels, Reactions (chemical)		
Kinetics and Mechanism of the Reaction of Iron—Chromium and Iron—Chromium—Molybdenum Alloys With Chlorine Gas.		153-159A
Chromium molybdenum steels, Structural hardening		
Thermomechanical Strengthening of High-Strength, Chromium—Molybdenum Steel.		671-673A
Chromium nickel molybdenum steels		
See Nickel chromium molybdenum steels		
Chromium nickel steels		
See Nickel chromium steels		
Chromium steels		
See also Austenitic stainless steels		
Chromium manganese steels		
Chromium molybdenum steels		
Chromium vanadium steels		
Ferritic stainless steels		
Martensitic stainless steels		
Nickel chromium molybdenum steels		
Nickel chromium steels		
Stainless steels		
Chromium steels, Crystal growth		
Recrystallization and Formation of Austenite in Deformed Lath Martensitic Structure of Low-Carbon Steels.		1379-1388A
Chromium steels, Mechanical properties		
The Effect of Phosphorus Content on the Hydrogen Stress Cracking of High-Strength 4130 Steel.		907-912A
The State of Residual Stress in the Near Surface Region of Homogeneous and Heterogeneous Materials After Grinding.		1239-1244A
Optimization of Fe/Cr/C Base Structural Steels for Improved Strength and Toughness.		2227-2237A
Chromium steels, Reactions (chemical)		
Kinetics and Mechanism of the Reaction of Iron—Chromium and Iron—Chromium—Molybdenum Alloys With Chlorine Gas.		153-159A
Chromium vanadium steels, Mechanical properties		
The Growth of Creep Cavities in a Low-Alloy Steel.		1739-1745A
Chromizing		
See also Pack chromizing		
On Some Features of Chromium Carbide Diffusion Layer Formation.		753-759A
Circuits		
See Integrated circuits		
Cleavage		
Hydrogen Cracking in Nominal Pearlite 1045 Steel. The Cleavage Plane of Pearlite.		1315-1318A 1865-1868A
Coating		
See Chromizing		
Pack chromizing		
Coatings		
See Anodic coatings		
Sprayed coatings		

Cobalt

Cobalt, Alloying elements	
The Influence of Cobalt on the Tensile and Stress Rupture Properties of the Nickel-Base Superalloy MAR-M247.	1767-1774A
The Influence of Cobalt on the Microstructure of the Nickel-Base Superalloy MAR-M247.	1775-1783A
Cobalt, Diffusion	
Internal Friction Studies of Fast Diffusing Solutes in Thorium.	995-1001A
Cobalt, Extraction	
An Investigation of Fluidized Bed Electrowinning of Cobalt Using 50 and 1000 A Cells.	293-301B
Cobalt, Materials substitution	
Effects of Cobalt on Structure, Microchemistry and Properties of Wrought Nickel-Base Superalloy.	1021-1032A
Cobalt, Reactions (chemical)	
Kinetics of Chlorination of Cobalt and Co—10 At.-% Pt Alloy by Reaction With HCl Gas.	349-356B
Cobalt, Recovering	
Activities of CoS and FeS in Copper Mattes and the Behavior of Cobalt in Copper Smelting.	461-470B
Cobalt, Solubility	
Steady-State Rates of Dissolution of Stationary Iron, Cobalt and Nickel Cylinders in Liquid Copper.	175-184B
Cobalt base alloys, Corrosion	
Low-Temperature Hot Corrosion of Cobalt-Base Alloys. I.—Morphology of the Reaction Product.	1843-1852A
Low-Temperature Hot Corrosion of Cobalt-Base Alloys. II.—Reaction Mechanism.	1853-1864A
Cobalt base alloys, Directional solidification	
Enhancement of Coupled Growth of Off-Eutectic Alloys by "Stop-and-Go" Technique.	967-973A
Cobalt base alloys, Mechanical properties	
Fracture in Equiaxed Two Phase Alloys. I.—Fracture in Alloys With Isolated Elastic Particles.	873-879A
Fracture in Equiaxed Two Phase Alloys. II.—Fracture in Alloys With Isolated Plastic Particles.	881-887A
Cobalt base alloys, Microstructure	
Kinetics of Grain Coarsening During Sintering of Co—Cu and Fe—Cu Alloys With Low Liquid Contents.	1405-1411A
Cobalt base alloys, Phase transformations	
Phase Transformations in a Wrought Co—Cr—Mo—C Alloy.	1161-1166A
Cobalt base alloys, Reactions (chemical)	
Kinetics of Chlorination of Cobalt and Co—10 At.-% Pt Alloy by Reaction With HCl Gas.	349-356B
Cobalt base alloys, Structural hardening	
Carbide Transformations During Aging of Wear-Resistant Cobalt Alloys.	545-550A
Cobalt compounds, Crystal growth	
Electromagnetic Containerless Reaction of Samarium With Cobalt for the Formation of Samarium—Cobalt Alloys.	1868-1871A
Cobalt compounds, Reactions (chemical)	
Mechanism of Oxidation—Sulfation Reactions of CoO in the Presence of Na ₂ SO ₄ .	1847-1854A
Cobalt compounds, Thermal properties	
Enthalpies of Formation of Borides of Iron, Cobalt and Nickel by Solution Calorimetry in Liquid Copper.	251-257B
Coefficient of expansion	
See Thermal expansion	
Coefficient of friction	
See Friction	
Coefficient of thermal expansion	
See Thermal expansion	
Coke, Oxidation	
The Reaction of Coke Specimens in an Environment Where Both the Temperature and the Gas Composition Are Time Dependent.	513-515B
Coke breeze	
See Coke	
Cold ductility	
See Ductility	
Cold formability	
See Formability	
Cold forming	
See Cold working	
Cold reduction	
See Cold working	
Cold rolling	
On Penetration of Shear Texture Into Rolled Aluminum and Copper.	665-669A
Cold swaging	
See Swaging	
Cold working	
See also Cold rolling	
High energy rate forming	
Combined Recrystallization and Precipitation in a Cu—9Ni—6Sn Alloy.	565-573A
Structure—Property Relationships in Dual-Phase Cu—Al Alloys. I.—Individual Phases.	837-846A
Effect of the Degree of Prior Cold Work on the Grain Volume Distribution and the Rate of Grain Growth of Recrystallized Aluminum.	985-993A
Columbium	
See Niobium	
Columbium base alloys	
See Niobium base alloys	
Columbium compounds	
See Niobium compounds	
Columnar structure	
The Influence of Gamma Prime on the Recrystallization of an Oxide Dispersion Strengthened Superalloy—MA 6000E.	1665-1674A
Comacts	
See Powder compacts	
Compliance (elasticity)	
See Modulus of elasticity	
Composite materials	
See also Fiber composites	
Composite materials, Mechanical properties	
Effect of Lithium on the Mechanical Properties and Microstructure of SiC Whisker-Reinforced Aluminum Alloys.	1511-1519A
Compression tests	
Splitting of Tungsten Wire in the Knife-Edge Compression Test.	1501-1510A
Compressive modulus	
See Modulus of elasticity	
Computation	
Finite Element Method (FEM) Calculations of Stress—Strain Behavior of Alpha-Beta Ti—Mn Alloys. II.—Stress and Strain Distributions.	603-609A
Computer programs	
Computer Analysis of Phase Diagrams and Thermodynamic Properties of Cryolite-Based Systems. II.—The AlF ₃ —CaF ₂ —LiF, AlF ₃ —CaF ₂ —NaF and CaF ₂ —LiF—NaF Systems.	61-69B
Thermodynamics of Copper Matte Converting. IV.— <i>A Priori</i> <td>331-338B</td>	331-338B
Finite Element Method (FEM) Calculations of Stress—Strain Behavior of Alpha-Beta Ti—Mn Alloys. I.—Stress—Strain Relations.	595-601A
Computer simulation	
The Occurrence of Shear Bands in Isothermal, Hot Forging, Volatilization of Bismuth in Copper Matte Converting—Computer Simulation.	275-288A
Operation of Near-Surface Dislocation Sources.	339-348B
1199-1205A	
Computing	
See Computation	
Concast	
See Continuous casting	
Concentration cell corrosion	
See Pitting (corrosion)	
Conducting sheet analog	
See Heat transmission	
Conductivity	
See Resistivity	
Conductivity (electrical)	
See Resistivity	
Constitutional diagrams	
See Phase diagrams	
Consumption	
See Energy consumption	
Continuous casting	
See also Direct chill casting	
The Thermal Distortion of Continuous-Casting Billet Molds.	91-104B
The Influence of Mold Behavior on the Production of Continuously Cast Steel Billets.	105-116B
The Effect of Melt Composition on Solidification Cracking of Steel, With Particular Reference to Continuous Casting.	259-266B
Controllability	
See Stability	
Controlled atmospheres	
See also Reducing atmospheres	
Carburization and Gas Reactions of Hydrocarbon—Nitrogen Mixtures at 850 and 925°C.	267-273B
Gas Carburizing of Steel With Furnace Atmospheres Formed <i>in Situ</i> From Methane and Air and From Butane and Air.	613-623B
Converters	
See Bottom blown converters	
Cooling	
See Splat cooling	
Cooling rate	
The Influence of Acceleration Forces on Dendritic Growth and Grain Structure.	85-90B
Influence of Cooling Rate on the Microstructure and Retained Austenite in an Intercritically Annealed Vanadium-Containing HSLA Steel.	1899-1906A
Cooling rate, Alloying effects	
The Effects of Copper and Chromium on the Aging Response of Dilute Al—Mg—Si Alloys.	1318-1321A
Copper, Alloying additive	
The Effects of Copper and Chromium on the Aging Response of Dilute Al—Mg—Si Alloys.	1318-1321A

Copper, Alloying elements	
The Constitution and Phase Stability of Overlapping Melt Trajectories in Ag—Cu Alloys Produced by Continuous Laser Melting Quenching.	1879-1889A
Copper, Binary systems	
Thermochemistry of Alloys of Transition Metals: III.—Copper—Silver, —Titanium, —Zirconium and —Hafnium at 1373°K.	391-401B
The Coordination Cluster Theory—Description of the Activity Coefficients of Dilute Solutions of Oxygen and Sulfur in Binary Alloys.	429-437B
A Simple Bisection Technique for the Calculation of a Two-Solid or Two-Liquid Miscibility Gap in Binary Metallic Systems.	2097-2102A
Copper, Crystal lattices	
Operation of Near-Surface Dislocation Sources.	1199-1205A
Copper, Diffusion	
Vacuum Distillation of Liquid Metals. II.—Photographic Study.	589-591B
Copper, Extraction	
Fluidized Bed Electrowinning of Copper: Experiments Using 150 A and 1000 A Cells and Some Mathematical Modeling.	3-13B
Thermodynamics of Copper Matte Converting. III.—Steady-State Volatilization of Gold, Silver, Lead, Zinc, Nickel, Selenium, Tellurium, Bismuth, Antimony and Arsenic From Slag, Matte and Metallic Copper.	319-329B
Thermodynamics of Copper Matte Converting. IV.— <i>A Priori</i> Predictions of the Behavior of Gold, Silver, Lead, Zinc, Nickel, Selenium, Tellurium, Bismuth, Antimony and Arsenic in the Noranda Process Reactor.	331-338B
Activities of CoS and FeS in Copper Mattes and the Behavior of Cobalt in Copper Smelting.	331-338B
The Recovery of Molybdenum From Leach Solutions by Reduction.	461-470B
Passive and Transpassive Anodic Behavior of Chalcopyrite in Acid Solutions.	565-570B
Copper, Heat treatment	
Coarsening of SiO ₂ Particles in Copper and MnS Inclusions in Steel.	2143-2153A
Copper, Mechanical properties	
Near-Threshold Fatigue Crack Growth Behavior in Copper.	1807-1818A
Copper, Rolling	
On Penetration of Shear Texture Into Rolled Aluminum and Copper.	665-669A
Copper, Solubility	
Steady-State Rates of Dissolution of Stationary Iron, Cobalt and Nickel Cylinders in Liquid Copper.	175-184B
Dissolution of Solid Copper Cylinder in Molten Tin—Lead Alloys Under Dynamic Conditions.	439-445B
Copper, Ternary systems	
Extension of the Associated Solution Model to Ternary Metal—Sulfide Melts: Cu—Ni—S.	379-385B
Copper base alloys	
See also Aluminum brasses Aluminum bronzes Brasses	
Copper base alloys, Corrosion	
Stress Corrosion of Cu—Zn and Cu—Zn—Ni Alloys: the Role of Deoxygenation.	2027-2033A
Copper base alloys, Crystal lattices	
Differential Scanning Calorimetry Evaluations in Alpha Cu—Al Alloys, Energetics.	801-809A
Copper base alloys, Diffusion	
Intrinsic Diffusion Coefficients and the Vacancy Flow Factor in Dilute Cu—Zn Alloys.	1135-1139A
Copper base alloys, Heat treatment	
Combined Recrystallization and Precipitation in a Cu—9Ni—6Sn Alloy.	565-573A
Copper base alloys, Mechanical properties	
Structure—Property Relationships in Dual-Phase Cu—Al Alloys. II.—Alloy Behavior.	847-853A
The State of Residual Stress in the Near Surface Region of Homogeneous and Heterogeneous Materials After Grinding.	1239-1244A
Copper base alloys, Microstructure	
Structure—Property Relationships in Dual-Phase Cu—Al Alloys. I.—Individual Phases.	837-846A
Cavitation and Cavity Growth During Superplastic Flow in Microduplex Cu—Zn—Ni Alloys.	1619-1626A
Copper base alloys, Phase transformations	
A Localized Soft Mode Model for the Nucleation of Thermotropic Martensitic Transformation: Application to the Beta → 9R Transformation.	1127-1134A
Observations of Aging Effects in a Cu—Sn Shape Memory Alloy.	1687-1692A
Copper base alloys, Solubility	
Activities of Oxygen in Liquid Cu—Sb and Cu—Ge Alloys.	77-83B
Copper base alloys, Structural hardening	
Aging Effects in Copper-Based Shape Memory Alloys.	551-555A
Copper compounds, Synthesis	
Dry Method Preparation and Melting Point of Cu ₂ SO ₄ .	515-517B
Copper mattes	
Activities of CoS and FeS in Copper Mattes and the Behavior of Cobalt in Copper Smelting.	461-470B
Copper mattes, Reduction (chemical)	
Thermodynamics of Copper Matte Converting. III.—Steady-State Volatilization of Gold, Silver, Lead, Zinc, Nickel, Selenium, Tellurium, Bismuth, Antimony and Arsenic From Slag, Matte and Metallic Copper.	319-329B
Thermodynamics of Copper Matte Converting. IV.— <i>A Priori</i> Predictions of the Behavior of Gold, Silver, Lead, Zinc, Nickel, Selenium, Tellurium, Bismuth, Antimony and Arsenic in the Noranda Process Reactor.	331-338B
Volatilization of Bismuth in Copper Matte Converting—Computer Simulation.	339-348B
Copper ores	
See also Chalcopyrite	
Copper ores, Melting	
A Mineralogical Study of Nickel Mattes From the Kalgoorlie Nickel Smelter, Kalgoorlie, Western Australia.	141-152B
Copper ores, Reduction (chemical)	
Heteronuclear Compounds of Arsenic and Antimony.	511-513B
Core hardness	
See Hardness	
Corrodes	
See Corrosion environments	
Corrosion	
See Corrosion fatigue Corrosion mechanisms Intergranular corrosion Pitting (corrosion) Preferential attack (corrosion) Scale (corrosion) Sulfurization	
Corrosion cracking	
See Stress corrosion cracking	
Corrosion effects	
See Dezincification Pitting (corrosion) Scale (corrosion)	
Corrosion environments	
Influence of Corrosive Environments on Near-Threshold Fatigue Crack Growth in 403 Stainless Steel.	2177-2189A
Corrosion fatigue	
Theoretical Considerations on Corrosion Fatigue Crack Initiation.	649-655A
Corrosion fatigue, Heating effects	
The Effect of Heat Treatments on the Corrosion Fatigue Properties of 13% Chromium Stainless Steel in 3% NaCl Aqueous Solution.	1521-1529A
Corrosion mechanisms	
See also Intergranular corrosion Scale (corrosion)	
Theoretical Considerations on Corrosion Fatigue Crack Initiation.	649-655A
Corrosion products	
See also Scale (corrosion) Observations on the Early Stages of Oxidation of Titanium Carbide.	
Low-Temperature Hot Corrosion of Cobalt-Based Alloys. I.—Morphology of the Reaction Product.	1837-1841A
Low-Temperature Hot Corrosion of Cobalt-Based Alloys. II.—Reaction Mechanism.	1843-1852A
Influence of Corrosion Deposits on Near-Threshold Fatigue Crack Growth Behavior in 2XXX and 7XXX Series Aluminum Alloys.	1853-1864A
Corrosion resistance	
Corrosion Behavior of Amorphous Fe—Cr—Al—P—C Ribbon Alloys.	2271-2280A
Corrosion resistance, Composition effects	
An Examination of Chromium Substitution in Stainless Steels.	901-905A
Corrosion resistance, Deformation effects	
The Effect of High-Temperature Low-Cycle Fatigue on the Corrosion Resistance of Austenitic Stainless Steels.	2003-2013A
CO₂ arc welding	
See Gas metal arc welding	
Crack closure	
Some Considerations on Fatigue Crack Closure at Near-Threshold Stress Intensities Due to Fracture Surface Morphology.	923-927A
Near-Threshold Fatigue Crack Growth Behavior in Copper. A Geometric Model for Fatigue Crack Closure Induced by Fracture Surface Roughness.	1607-1618A
Crack growth	
See Crack propagation	
Crack propagation	
The Effect of Defects on the Fatigue Crack Initiation Process in Two P/M Superalloys. I.—Fatigue Origins.	45-52A
The Effect of Defects on the Fatigue Crack Initiation Process in Two P/M Superalloys. II.—Surface—Subsurface Transition.	59-72A
Fatigue Crack Initiation and Strain-Controlled Fatigue of Some High-Strength Low-Alloy Steels.	101-110A
Mode III Fatigue Crack Propagation in Low-Alloy Steel. Elevated-Temperature Fatigue Crack Growth in Incoloy Alloy 800 in Sulfurizing Environments.	145-152A
Low-Cycle Fatigue Behavior of Ti—6Al—2Sn—4Zr—6Mo. II.—Cyclic Deformation Behavior and Low Cycle Fatigue.	269-274A
The Effect of Hydrogen Source on Crack Initiation in 4340 Steel.	305-311A

Crack propagation

The Mechanisms of Crack Initiation and Crack Propagation in Metal-Induced Embrittlement of Metals.	457-472A	Mechanical Behavior of Alloy 800 at 838°K.	637-648A
Theoretical Considerations on Corrosion Fatigue Crack Initiation.	649-655A	Thermomechanical Strengthening of High-Strength, Chromium-Molybdenum Steel.	671-673A
Fracture in Equiaxed Two Phase Alloys. I.—Fracture in Alloys With Isolated Elastic Particles.	873-879A	Creep rate, Alloying effects	
Fracture in Equiaxed Two Phase Alloys. II.—Fracture in Alloys With Isolated Plastic Particles.	881-887A	The Influence of Cobalt on the Tensile and Stress Rupture Properties of the Nickel-Base Superalloy MAR-M247.	1767-1774A
The Fatigue Crack Growth Behavior of Electron-Beam Welded A286 Superalloy.	1483-1489A	Creep rate, Composition effects	
Near-Threshold Fatigue Crack Growth Behavior in Copper. Indentation Loading Studies of Acoustic Emission From Temper and Hydrogen Embrittled A533B Steel.	1607-1618A	Measurement of Structural Parameters Important in Creep of Ni-Mo and Ni-W Solid Solutions.	1827-1836A
The Plastic Zone and Residual Stress Near a Notch and a Fatigue Crack in HSLA Steel.	1965-1975A	Creep rate, Microstructural effects	
Plastic Instability in U-Notched Bend Specimens of Spheroidized AISI 1090 Steel.	1987-1995A	A Note on the Microstructural Dependence of Creep Strength in Inconel 700.	673-675A
Crack propagation, Corrosion effects	2209-2218A	Creep rate, Stress effects	
Influence of Corrosion Deposits on Near-Threshold Fatigue Crack Growth Behavior in 2XXX and 7XXX Series Aluminum Alloys.	2271-2280A	Study of the Rheological Behavior of the Beta Prime Phase of an Equiatomic Ag-Mg Alloy.	251-255A
Crack propagation, Deformation effects		Creep resistance	
Calorimetric Measurements of the Plastic Work of Fatigue Crack Propagation in 4140 Steel.	2165-2172A	See Creep strength	
Crack propagation, Environmental effects		Creep rupture strength	
Effect of Environment on Fatigue and Creep Crack Growth in Inconel X-750 at Elevated Temperature.	1083-1090A	Creep and Rupture of an ODS Alloy With High Stress Rupture Ductility.	1453-1462A
Influence of Gaseous Environments on Rates of Near-Threshold Fatigue Crack Propagation in NiCrMoV Steel.	1633-1645A	Creep rupture strength, Alloying effects	
Influence of Corrosive Environments on Near-Threshold Fatigue Crack Growth in 403 Stainless Steel.	2177-2189A	The Influence of Cobalt on the Tensile and Stress Rupture Properties of the Nickel-Base Superalloy MAR-M247.	1767-1774A
Crack propagation, Impurity effects		Creep rupture strength, Microstructural effects	
A Theory of Fatigue Crack Initiation at Inclusions.	117-123A	The Influence of Orientation on the Stress Rupture Properties of Nickel-Base Superalloy Single Crystals.	1747-1754A
Effects of Hydrogen Concentration on Slow Crack Growth in Stainless Steels.	1799-1808A	Creep Fracture Processes of Oxide Dispersion Strengthened Mechanically Alloyed Inconel Alloy MA 754.	2286-2290A
Crack propagation, Microstructural effects		Creep strength	
Effects of Texture and Microstructure on the Propagation of Iodine Stress Corrosion Cracks in Zircaloy.	73-83A	Effect of Lithium on the Mechanical Properties and Microstructure of SiC Whisker-Reinforced Aluminum Alloys.	1511-1519A
Low-Cycle Fatigue Behavior of Ti—6Al—2Sn—4Zr—6Mo. I.—The Role of Microstructure in Low-Cycle Crack Nucleation and Early Crack Growth.	257-268A	Creep strength, Microstructural effects	
Fatigue Crack Initiation and Propagation in a Quenched and Tempered Niobium-Bearing HSLA Steel.	393-399A	A Note on the Microstructural Dependence of Creep Strength in Inconel 700.	673-675A
The Influence of a Duplex Microstructure in Steels on Fatigue Crack Growth in the Near-Threshold Region.	439-445A	Creeping	
Fatigue Initiation Study of TMT Eutectoid Steel.	855-864A	See Creep (materials)	
Fracture Toughness: A Rationalization of the Role of Microstructure in an Alpha—Beta Titanium Alloy.	2191-2195A	Crevices	
Crack propagation, Stress effects		See Cracks	
Temperature Dependence of Sustained-Load Subcritical Crack Growth in Ti—6Al—6V—25Ni.	497-500A	Critical temperature	
The Effect of Stress State on Internal Hydrogen-Induced Crack Growth in Ti—6Al—6V—25Ni.	1055-1061A	An Examination of the Validity of Existing Empirical Formulas for the Calculation of M_s Temperature.	328-331A
Effects of Friction and High Torque on Fatigue Crack Propagation in Mode III.	2197-2204A	Cross tension test	
Crack resistance		See Tension tests	
See Crack propagation		Cryolite	
Cracking (fracturing)		Computer Analysis of Phase Diagrams and Thermodynamic Properties of Cryolite Based Systems. II.—The $\text{AlF}_3\text{—CaF}_2\text{—LiF}$, $\text{AlF}_3\text{—CaF}_2\text{—NaF}$ and $\text{CaF}_2\text{—LiF—NaF}$ Systems.	61-69B
See also Stress corrosion cracking		Crystal defects	
Self-Fracture of Hydrogen-Charged Niobium.	320-321A	See also Burgers vector Dislocation loops Dislocations Glide dislocations Lattice vacancies Stacking faults	
Cracks		Thermal Analysis of Trapped Hydrogen in Pure Iron.	135-140A
The Effect of Melt Composition on Solidification Cracking of Steel. With Particular Reference to Continuous Casting.	259-266B	Crystal growth	
Electrochemical Detection of Fatigue Cracks in Steel.	1927-1932A	See also Epitaxial growth	
Creep (materials)		Crystal growth, Diffusion effects	
See also Creep rate		On Some Features of Chromium Carbide Diffusion Layer Formation.	753-759A
Creep rupture strength		Crystal lattices	
Creep strength		See Superlattices	
Correction "The Significance of the Dimensionless Constant in the Rate Equation for Superplastic Flow".	2289A	Crystal orientation	
A Numerical Study of Cavity Growth Controlled by Coupled Surface and Grain Boundary Diffusion.	427-437A	See Crystal structure	
Effect of Environment on Fatigue and Creep Crack Growth in Inconel X-750 at Elevated Temperature.	1083-1090A	Crystal structure	
Wedge-Type Creep Damage in Low-Cycle Fatigue.	1207-1214A	See also Substructures (crystalline) Identification of the Interface Phase in Titanium Alloys.	681-684A
Mechanisms of Creep—Fatigue Interaction.	1215-1221A	The Growth of Hematite Blades During the High-Temperature Oxidation of Iron.	929-935A
Correlation of Substructure With Time-Dependent Fatigue Properties of AISI 304 Stainless Steel.	1577-1588A	Crystallinity	
The Growth of Creep Cavities in a Low-Alloy Steel.	1739-1745A	See Crystal structure	
Fatigue and Creep—Fatigue Deformation of Several Nickel-Based Superalloys at 850°C.	1755-1765A	Crystallization	
Induced Creep and Creep/Fatigue of a Nickel-Base Superalloy at Ambient Temperatures.	1951-1955A	See Recrystallization	
The Significance of the Dimensionless Constant in the Rate Equation for Superplastic Flow.	2059-2061A	Crystallography	
Tensile and Fracture Properties of Type 316 Stainless Steel After Creep.	2155-2163A	The Morphology, Crystallography and Chemistry of Phases in As-Cast Nickel—Aluminum Bronze.	1337-1345A
Creep (materials), Composition effects	1021-1032A	Pearls—Nabarro Plastic Deformation in the Presence of Solute Clusters.	1429-1434A
Effects of Cobalt on Structure, Microchemistry and Properties of a Wrought Nickel-Base Superalloy.		Crystals	
See Creep (materials)		See Single crystals	
Creep (materials), Impurity effects		Curves	
Creep of Hydrogen-Charged Ti—5Al—2.5Sn at Room Temperature.	1531-1532A	See Stress strain curves	
Creep limit		Cutting	
See Creep (materials)		See Grinding	
Creep properties		Cycles	
See Creep (materials)		See Thermal cycling	
Creep rate		Cyclic loads	
Temperature Dependence of Sustained-Load Subcritical Crack Growth in Ti—6Al—6V—25Ni.	497-500A	Low-Cycle Fatigue Behavior of Ti—6Al—2Sn—4Zr—6Mo. II.—Cyclic Deformation Behavior and Low Cycle Fatigue.	269-274A

Stress-Substructure Relationships in Cyclically and Monotonically Deformed Wavy Slip Mode Metals.	1033-1041A	Description	Prediction of the Effects of Surface-Active Elements on Gas—Liquid Metal Kinetics.	357-367B
Cyclic Deformation of Pearlite Eutectoid Rail Steel.	2035-2047A			
Cyclical heating		Desulfurizing	Hydrodynamics of Gas Stirred Melts. II.—Axisymmetric Flows.	203-211B
<i>See Thermal cycling</i>				
Czochralski process		Detection	<i>See also</i> Flaw detection Effect of Oxide Thickness on Electrochemical Detection of Fatigue. Electrochemical Detection of Fatigue Cracks in Steel.	1573-1575A 1927-1932A
<i>See Crystal growth</i>				
D H process		Deuterium, Diffusion	A SIMS Study of the Diffusion and Trapping of Deuterium in 302 Stainless Steel.	581-584A
<i>See Vacuum degassing</i>				
Decarburizing	199-202A	Dezinification	Stress Corrosion of Cu—Zn and Cu—Zn—Ni Alloys: the Role of Dealloying.	2027-2033A
Primary Recrystallization Textures in Dilute Fe—C Alloys.				
Rate of Decarburization of Iron—Carbon Melts. I.—Experimental Determination of the Effect of Sulfur.	403-409B	Diagrams	<i>See also</i> Phase diagrams Solution Chemistry of Tungsten Leaching Systems.	555-564B
Rate of Decarburization of Iron—Carbon Melts. II.—A Mixed-Control Model.	411-421B			
Decomposing		Diffraction	<i>See</i> Electron diffraction Neutron diffraction X ray diffraction	
<i>See Decomposition</i>				
Decomposition		Diffusion	Correction to "Self-Diffusion Coefficients of Carbon in Fe ₃ C at 723°K Via the Kinetics of Formation of This Compound". Correction to "The Significance of the Dimensionless Constant in the Rate Equation for Superplastic Flow". Tracer Diffusivity of O ¹⁸ in CaO—SiO ₂ Melts at 1600°C. A Numerical Study of Cavity Growth Controlled by Coupled Surface and Grain Boundary Diffusion. Chemical and Kinetic Factors Related to Hydrogen Removal From Aluminum. Application of the McNabb—Foster Trapping Equations to the Diffusion of Oxygen in Dilute Niobium Alloys. Grain Boundary Diffusion Mechanisms in Metals. A SIMS Study of the Diffusion and Trapping of Deuterium in 302 Stainless Steel.	2289A 2289A 237-240B 427-437A 447-460B 539-543A 527-553B 581-584A 717-732A 811-820A 995-1001A 1135-1139A 1313-1314A 1405-1411A 1655-1658A 1658-1659A 1871-1873A 2059-2061A 2069-2095A
<i>See also</i> Phase decomposition Spinodal decomposition				
Microstructural Features Produced by the Reduction of Wüstite in H ₂ /H ₂ O Gas Mixtures.	117-124B			
Deep carburizing		Diffusion, Alloying effects	Interdiffusion Coefficients in the Ni ₂ Al ₃ (Gamma) Phase of the Ni—Al System. Kinetics of Grain Coarsening During Sintering of Co—Cu and Fe—Cu Alloys With Low Liquid Contents. Discussion of "Diffusion-Controlled Phase Transformation in a Finite Region". Discussion of "An Approximate Analytical Demonstration of the Famous Darken Experiment". Self-Diffusion Coefficients of Carbon in Fe ₃ C at 723°K Via the Kinetics of Formation of This Compound. The Significance of the Dimensionless Constant in the Rate Equation for Superplastic Flow. Grain Boundary Diffusion Mechanisms in Metals.	
<i>See Carburizing</i>				
Deep hardening				
<i>See Hardening</i>				
Defects		Diffusion, Temperature effects	Coarsening of SiO ₂ Particles in Copper and MnS Inclusions in Steel.	2143-2153A
<i>See</i> Burgers vector				
Casting defects				
Crystal defects				
Dislocation loops				
Dislocations				
Glide dislocations				
Lattice vacancies				
Stacking faults				
Surface defects				
Deformability		Diffusion, Al alloying effects	Thermotransport of Hydrogen and Deuterium in Vanadium, Niobium and Tantalum. Mass Transport of Carbon in One- and Two-Phase Iron—Nickel Alloys in a Temperature Gradient.	821-825A 1713-1719A
<i>See Formability</i>				
Deformation		Diffusion coating (process)	See Chromizing Pack chromizing	
<i>See Plastic deformation</i>				
Degasification		Diffusion coefficient	<i>See</i> Diffusion	
<i>See Degassing</i>				
Degassing		Diffusion couples	<i>See</i> Diffusion	
<i>See also</i> Vacuum degassing				
Chemical and Kinetic Factors Related to Hydrogen Removal From Aluminum.	447-460B	Diffusion layers, Crystal lattices	On Some Features of Chromium Carbide Diffusion Layer Formation.	753-759A
Demetalization		Diffusion layers, Intermetallics	Interdiffusion Coefficients in the Ni ₂ Al ₃ (Gamma) Phase of the Ni—Al System.	1313-1314A
<i>See</i> Dezincification				
Dendrite		Diffusion layers, Phases (state of matter)	The Early Stage of Ni ₃ Al Layer Growth in NiAl/Ni Diffusion Couples.	1921-1926A
<i>See Dendritic structure</i>				
Dendritic structure		Diffusivity	Mathematical Treatment of Permeation for Cylindrical Geometry. Changes in Diffusivity Due to Sintering in Metallized Iron Oxide Pellets.	174-176A 518-520B
The Influence of Acceleration Forces on Dendritic Growth and Grain Structure.	85-90B		Hydrogen Transport in Nickel-Based Stainless Alloys. Measurement of Structural Parameters Important in Creep of Ni—Mo and Ni—W Solid Solutions.	1811-1886A 1827-1836A
Enhancement of Coupled Growth of Off-Eutectic Alloys by "Stop-and-Go" Technique.	967-973A			
The Effect of Quenching on the Solidification Structure and Transformation Behavior of Stainless Steel Welds.	1141-1152A	Diffusivity, Alloying effects	The Influence of Solutes on Kinetics and Thermodynamics of Liquid Indium—Oxygen Systems.	53-59B
Coarsening and Microsegregation During Solidification of Ni—Al—Cr Dendritic Monocrystals.	1153-1159A			
Dendrite Morphology of Several Steady State Unidirectionally Solidified Iron-Base Alloys.	2131-2141A	Diffusivity, Composition effects	Hydrogen Diffusion in Nb—Ta Alloys.	1675-1678A
Dendritic structure, Pressure effects				
Effect of Strain Rate on Deformation Behavior of Semisolid Dendritic Alloys.	1809-1819A			
Densification, Stress effects				
Enhanced Densification of White Cast Iron Powders by Cyclic Phase Transformations Under Stress.	355-361A			
Dental alloys				
Potentiodynamic Polarization Analysis of Silver—Palladium Alloys in Chloride Solutions.	313-317A			
Dental amalgams				
<i>See</i> Mercury amalgams				
Deoxidation				
<i>See</i> Deoxidizing				
Deoxidizing				
Effects of the Electromagnetic Stirring on the Removal of Inclusions of Oxide From Liquid Steel.	45-52B			
Effect of Rare Earth Additions on the Inclusions and Properties of a Ca—Al Deoxidized Steel.	185-192B			
Oxygen Probes Based on Calcia-Doped Hafnia or Calcium Zirconate for Use in Metallic Melts.	227-235B			
Deoxidation of High-Melting-Point Metals and Alloys in Vacuum.	241-249B			
Dephosphorizing				
The Effect of Oxygen Potential on Phosphorus in the CaO—Al ₂ O ₃ System.	643-644B			
Deposition				
<i>See</i> Chromizing Pack chromizing Vapor deposition				
Depth profiling				
Experimental and Theoretical Concentration Profiles at the Surface of Chromized Iron.	495-497A			

Dimensions

Dimensions		
See Particle size		
Wall thickness		
Direct chill casting		
A Numerical Simulation of the D.C. Continuous Casting Process including Nucleate Boiling Heat Transfer.	593-602B	
Direct reduction		
See also Hydrogen reduction		
Changes in Diffusivity Due to Sintering in Metallized Iron Oxide Pellets.	518-520B	
Directional solidification		
The Occurrence of Aligned Microstructures in Directionally Solidified Aluminum—Bismuth Alloys.	493-495A	
Enhancement of Coupled Growth of Off-Eutectic Alloys by "Stop-and-Go" Technique.	967-973A	
Dendrite Morphology of Several Steady State Unidirectionally Solidified Iron-Base Alloys.	2131-2141A	
Discontinuous precipitates		
See Cellular precipitates		
Dislocation climb		
See Dislocation mobility		
Dislocation density		
Low-Temperature Strain Behavior of Lead Thin Films on a Substrate.	383-391A	
Positron Trapping at Phase Interfaces and Dislocations in Pearlite Eutectoid Steel.	1177-1180A	
Operation of Near-Surface Dislocation Sources.	1199-1205A	
Influence of Grain Size and Age-Hardening on Dislocation Pile-Ups and Tensile Fracture for a Ti—Al Alloy.	1283-1292A	
The Separate Roles of Subgrains and Forest Dislocations in the Isotropic Hardening of Type 304 Stainless Steel.	1977-1986A	
Dislocation loops, Composition effects		
Effect of Defect Structure Upon the Mechanical Behavior of Beta-LiAl Through Dislocation Damping and Hardness Studies.	2173-2176A	
Dislocation mobility		
Microstructural Aspects of Superplasticity.	703-715A	
Evidence for Dislocation Transport of Hydrogen in Aluminum.	811-820A	
Dislocation mobility, Composition effects		
Effect of Defect Structure Upon the Mechanical Behavior of Beta-LiAl Through Dislocation Damping and Hardness Studies.	2173-2176A	
Dislocation pinning		
See Pinning (dislocation)		
Dislocations		
See also Burgers vector		
Dislocation loops		
Glide dislocations		
"C" Component Dislocations in Deformed Ti ₃ Al.	324-328A	
Peierls—Nabarro Plastic Deformation in the Presence of Solute Clusters.	1429-1434A	
Dispersion hardening		
Convergent Beam Diffraction Analysis of Dispersoids in Oxide Dispersion-Strengthened Alloys.	953-957A	
Dispersion hardening alloys, Casting		
Preparation and Properties of Aluminum Alloy Coconut Shell Char Particulate Composites.	485-494B	
Dispersion hardening alloys, Crystal growth		
The Influence of Hot Working on the Subsequent Recrystallization of a Dispersion Strengthened Superalloy—MA 6000.	1463-1470A	
The Influence of Gamma Prime on the Recrystallization of an Oxide Dispersion Strengthened Superalloy—MA 6000E.	1665-1674A	
Dispersion hardening alloys, Mechanical properties		
Creep and Rupture of an ODS Alloy With High Stress Rupture Ductility.	1453-1462A	
Creep Fracture Processes of Oxide Dispersion Strengthened Mechanically Alloyed Inconel Alloy MA 754.	2286-2290A	
Dispersion hardening alloys, Phase transformations		
The Effect of an Inert Oxide Particle Dispersion on the Morphology of Martensite in Fe—27Ni—0.025C Alloys.	203-211A	
Dispersions, Chemical analysis		
Convergent Beam Diffraction Analysis of Dispersoids in Oxide Dispersion-Strengthened Alloys.	953-957A	
Dispersoids		
See Dispersions		
Disposal		
See Waste disposal		
Dissociation energy		
See Free energy of formation		
Dissolution		
See also Anodic dissolution		
Steady-State Rates of Dissolution of Stationary Iron, Cobalt and Nickel Cylinders in Liquid Copper.	175-184B	
Ferric Ion Leaching of Chalcocyanides From Different Localities.	303-309B	
Solution Chemistry of Tungsten Leaching Systems.	555-564B	
Dissolution, Alloying effects		
Coarsening of SiO ₂ Particles in Copper and MnS Inclusions in Steel.	2143-2153A	
Dissolution, Composition effects		
Dissolution of Solid Copper Cylinder in Molten Tin—Lead Alloys Under Dynamic Conditions.	439-445B	
Dissolution, Heating effects		
Calorimetric Studies of Precipitation and Dissolution Kinetics in Aluminum Alloys 2219 and 7075.	761-769A	
Distilling		
See Distillation		
Distortion		
The Thermal Distortion of Continuous-Casting Billet Molds.	91-104B	
Domains		
Differential Scanning Calorimetry Evaluations in Alpha Cu—Al Alloys, Energetics.	801-809A	
Drawing (heat treatment)		
See Tempering		
Drive shafts		
See Shafts (power)		
Dual phase steels, Alloy development		
Studies on the Development of High-Strength Dual-Phase Steel Sheets With High r_m Values.	1257-1262A	
Dual phase steels, Heat treatment		
Intercritical Austenitizing of Two Fe—Mn—C Steels.	575-579A	
Dual phase steels, Mechanical properties		
Deformation Characteristics of Dual-Phase Steels.	85-92A	
Tempering Characteristics of a Vanadium-Containing Dual-Phase Steel.	1679-1686A	
A Study of the Deformation and Fracture of a Dual-Phase Steel.	1821-1826A	
Optimization of Fe/Cr/C Base Structural Steels for Improved Strength and Toughness.	2227-2237A	
Dual phase steels, Structural hardening		
Dynamic Strain Aging of Various Steels.	1793-1797A	
Aging Susceptibility of Retained and Epitaxial Ferrite in Dual-Phase Steels.	2061-2064A	
Ductile fracture		
A Study of the Deformation and Fracture of a Dual-Phase Steel.	1821-1826A	
Plastic Instability in U-Notched Bend Specimens of Spherodized AISI 1090 Steel.	2209-2218A	
Ductility		
Hydrogen Embrittlement in a 2000 Series Aluminum Alloy. Influences of Materials Parameters and Microstructure on Superplastic Forming.	235-239A	
Creep and Rupture of an ODS Alloy With High Stress Rupture Ductility.	733-743A	
Ductility, Composition effects		
Compositional Effects on the High-Temperature Ductility of 1Cr—1.25Mo—0.25V Steel.	1471-1481A	
Ductility, Impurity effects		
Effect of Volume Fraction and Shape of Sulfide Inclusions on Through-Thickness Ductility and Impact Energy of High-Strength 4340 Plate Steels.	2239-2258A	
Ductility, Microstructural effects		
Deformation Characteristics of Dual-Phase Steels.	85-92A	
The Influence of Grain Structure on the Ductility of the Al—Cu—Li—Mn—Cd Alloy 2020.	2259-2269A	
Ductility, Welding effects		
Weld Metal Grain Structure and Mechanical Properties of a Thallium-Doped Ir—0.3% W Alloy (DOP-26).	1043-1053A	
Dynamics		
See Kinetics		
Elastic constants		
See also Modulus of elasticity		
A Localized Soft Mode Model for the Nucleation of Thermelastic Martensitic Transformation: Application to the Beta → 9R Transformation.	1127-1134A	
Elastic modulus		
See Modulus of elasticity		
Elastic properties		
See Elastic constants		
Electric circuits		
See Integrated circuits		
Electric conductors (materials)		
See Electrolytes		
Electric generators		
See Turbogenerators		
Electric potential, Corrosion effects		
Deterioration of Electromotive Force of Chromel—Alumel Thermocouples in Reducing Atmospheres at High Temperatures.	167-172A	
Electric welding		
See Electron beam welding		
Gas metal arc welding		
Gas tungsten arc welding		
Electrical conductance		
See Electrical resistance		
Electrical conductivity		
See Resistivity		
Electrical impedance		
See Electrical resistance		
Electrical phenomena		
See Electric potential		

Electrical properties		
<i>See Resistivity</i>		
<i>Thermoelectricity</i>		
Electrical resistance, Temperature effects		
<i>Short-Range Ordering Kinetics in 316 Austenitic Stainless Steel.</i>	1915-1919A	
Electrical resistivity		
<i>See Resistivity</i>		
Electroanalysis		
<i>See Electrolytic analysis</i>		
Electrochemistry		
<i>Gel Electrode Imaging of Metal Fatigue. I.—Cracks in 6061-T6 Aluminum.</i>	1413-1419A	
<i>Gel Electrode Imaging of Metal Fatigue. II.—Deformation in 1100 Aluminum.</i>	1421-1427A	
<i>Effect of Oxide Thickness on Electrochemical Detection of Fatigue.</i>	1573-1575A	
Electrocoatings		
<i>See Anodic coatings</i>		
Electrodes		
<i>See Fluidized bed cathodes</i>		
Electrogas welding		
<i>See Gas metal arc welding</i>		
Electrolysis		
<i>See Electrowinning</i>		
<i>Fluidized bed electrolysis</i>		
Electrolytes		
<i>Gel Electrode Imaging of Metal Fatigue. I.—Cracks in 6061-T6 Aluminum.</i>	1413-1419A	
<i>Gel Electrode Imaging of Metal Fatigue. II.—Deformation in 1100 Aluminum.</i>	1421-1427A	
Electrolytic analysis		
<i>Oxygen Probes Based on Calcium-Doped Hafnia or Calcium Zirconate for Use in Metallic Melts.</i>	227-235B	
Electrolytic cells		
<i>Fluidized Bed Electrowinning of Copper; Experiments Using 150 A and 1000 A Cells and Some Mathematical Modeling.</i>	3-13B	
Electrolytic dissolution		
<i>See Anodic dissolution</i>		
Electromagnetic fields		
<i>Electromagnetic Containerless Reaction of Samarium With Cobalt for the Formation of Samarium—Cobalt Alloys.</i>	1888-1871A	
Electromagnetic stirring		
<i>Effects of the Electromagnetic Stirring on the Removal of Inclusions of Oxide From Liquid Steel.</i>	45-52B	
Electromotive force		
<i>See Electric potential</i>		
Electron beam melting		
<i>Doxidation of High-Melting-Point Metals and Alloys in Vacuum.</i>	241-249B	
<i>Lime-Enhanced Hydrogen Reduction of Molybdenite.</i>	275-282B	
Electron beam vacuum melting		
<i>See Electron beam melting</i>		
Electron beam welding		
<i>The Fatigue Crack Growth Behavior of Electron-Beam Welded A286 Superalloy.</i>	1483-1489A	
Electron diffraction		
<i>Convergent Beam Diffraction Analysis of Dispersoids in Oxide Dispersion-Strengthened Alloys.</i>	953-957A	
Electron microscopy		
<i>See also Scanning electron microscopy</i>		
<i>Transmission electron microscopy</i>		
<i>Electron Microscopic Analysis of Heterogeneous Precipitates in Hastelloy C-276.</i>	979-934A	
Electron paramagnetic resonance		
<i>CaS Formation and Oxidation in the System CaO—SiO₂—Al₂O₃ Measured by Electron Paramagnetic Resonance.</i>	1997-2002A	
Electron spectroscopy		
<i>See Auger electron spectroscopy</i>		
Electron spin resonance		
<i>See Electron paramagnetic resonance</i>		
Electropotential		
<i>See Electric potential</i>		
Electroreduction		
<i>See Electrowinning</i>		
Electrorefining		
<i>See Electroslag refining</i>		
Electroslag process		
<i>See Electroslag refining</i>		
Electroslag refining		
<i>The Velocity Field in the Molten Slag Region of ESR Systems: A Comparison of Measurements in a Model System With Theoretical Predictions.</i>	35-43B	
Electrowinning		
<i>An Investigation of Fluidized Bed Electrowinning of Cobalt Using 50 and 1000 A Cells.</i>	293-301B	
Elevated temperature		
<i>See High temperature</i>		
Embrittlement		
<i>See also Hydrogen embrittlement</i>		
<i>Liquid metal embrittlement</i>		
<i>The Fracture Behavior of Quenched and Tempered Manganese Steels.</i>	827-836A	
<i>The Detection of Monolayer Grain Boundary Segregations in Steels Using STEM-EDS X-Ray Microanalysis.</i>	1397-1403A	
Embrittlement, Impurity effects		
<i>The Role of Sulfur in the Air Embrittlement of Nickel and Its Alloys.</i>	1223-1232A	
<i>The Role of Nitrogen in the Embrittlement of Steel.</i>	1939-1950A	
Embrittlement, Microstructural effects		
<i>Influence of Grain Size and Age-Hardening on Dislocation Pile-Ups and Tensile Fracture for a Ti—Al Alloy.</i>	1283-1292A	
Emission		
<i>See Acoustic emission</i>		
Energy		
<i>See Activation energy</i>		
<i>Binding energy (nuclear)</i>		
<i>Free energy</i>		
<i>Free energy of formation</i>		
<i>Free energy of transformation</i>		
<i>Heat of activation</i>		
<i>Heat of formation</i>		
<i>Heat of fusion</i>		
<i>Heat of mixing</i>		
<i>Stacking fault energy</i>		
<i>Surface energy</i>		
Energy consumption		
<i>Fluidized Bed Electrowinning of Copper; Experiments Using 150 A and 1000 A Cells and Some Mathematical Modeling.</i>	3-13B	
<i>An Investigation of Fluidized Bed Electrowinning of Cobalt Using 50 and 1000 A Cells.</i>	293-301B	
Energy of activation		
<i>See Activation energy</i>		
Energy of dissociation		
<i>See Free energy of formation</i>		
Energy of formation		
<i>See Free energy of formation</i>		
Enthalpy		
<i>Enthalpies of Formation of Borides of Iron, Cobalt and Nickel by Solution Calorimetry in Liquid Copper.</i>	251-257B	
Environment		
<i>See Corrosion environments</i>		
Epitaxial growth		
<i>Observations on the Early Stages of Oxidation of Titanium Carbide.</i>	1837-1841A	
Equations		
<i>See Equations of state</i>		
Equations of state		
<i>An Equation-of-State for Methane for Modeling Hydrogen Attack in Ferritic Steels.</i>	299-303A	
Equilibrium diagrams		
<i>See Phase diagrams</i>		
Eutectics, Crystal growth		
<i>Enhancement of Coupled Growth of Off-Eutectic Alloys by "Stop-and-Go" Technique.</i>	967-973A	
Eutectics, Metal working		
<i>Superplastic Behavior of the Sn—Pb Eutectic in the As-Worked State.</i>	53-58A	
Evaporation		
<i>See Nucleate boiling</i>		
<i>Vacuum distillation</i>		
Expansion		
<i>See Thermal expansion</i>		
Extractive metallurgy		
<i>See Hydrometallurgy</i>		
Extrusion		
<i>Superplastic Behavior of the Sn—Pb Eutectic in the As-Worked State.</i>	53-58A	
Extrusion pressing		
<i>See Extrusion</i>		
Face centered cubic metals		
<i>See FCC metals</i>		
Failure analysis		
<i>See Fractography</i>		
Fatigue (materials)		
<i>See also Corrosion fatigue</i>		
<i>Fatigue life</i>		
<i>Fatigue strength</i>		
<i>Low cycle fatigue</i>		
<i>Some Considerations on Fatigue Crack Closure at Near-Threshold Stress Intensities Due to Fracture Surface Morphology.</i>	937-940A	
<i>Effect of Environment on Fatigue and Creep Crack Growth in Inconel X-750 at Elevated Temperature.</i>	1083-1090A	
<i>Effect of Oxide Thickness on Electrochemical Detection of Fatigue.</i>	1573-1575A	
<i>Near-Threshold Fatigue Crack Growth Behavior in Copper. A Geometric Model for Fatigue Crack Closure Induced by Fracture Surface Roughness.</i>	1607-1618A	
<i>Fatigue and Creep—Fatigue Deformation of Several Nickel-Based Superalloys at 650°C.</i>	1627-1631A	
<i>Elevated temperature</i>		
<i>See High temperature</i>		

Fatigue (materials)

Electrochemical Detection of Fatigue Cracks in Steel.	1927-1932A	Ferrite, Alloying effects	
The Plastic Zone and Residual Stress Near a Notch and a Fatigue Crack in HSLA Steel.	1987-1995A	Effect of Manganese and Nitrogen on the Solidification Mode in Austenitic Stainless Steel Welds.	2121-2130A
Influence of Corrosive Environments on Near-Threshold Fatigue Crack Growth in 403 Stainless Steel.	2177-2189A	Ferritic stainless steels, Mechanical properties	
Fatigue (materials), Environmental effects		The Influence of Substructure on the Elevated- and Room-Temperature Strength of a 26Cr-1Mo Ferritic Stainless Steel.	447-458A
Influence of Gaseous Environments on Rates of Near-Threshold Fatigue Crack Propagation in NiCrMoV Steel.	1633-1645A	Ferritic stainless steels, Welding	
Fatigue (materials), Microstructural effects		The Effect of Quenching on the Solidification Structure and Transformation Behavior of Stainless Steel Welds.	1141-1152A
The Influence of a Duplex Microstructure in Steels on Fatigue Crack Growth in the Near-Threshold Region.	439-445A	Ferrous alloys	
Fatigue cracking		See also Cast iron Steels	
See Fatigue failure		Ferrous alloys, Corrosion	
Fatigue failure		Elevated-Temperature Fatigue Crack Growth in Incoloy Alloy 800 in Sulfidizing Environments.	145-152A
The Effect of Defects on the Fatigue Crack Initiation Process in Two P/M Superalloys. II.—Surface—Subsurface Transition.	45-52A	Corrosion Behavior of Amorphous Fe—Cr—Al—P—C Ribbon Alloys.	901-905A
Mechanical Behavior of Alloy 800 at 838°K.	637-648A	The Effect of High-Temperature Low-Cycle Fatigue on the Corrosion Resistance of Austenitic Stainless Steels.	923-927A
The Effect of Phosphorus Content on the Hydrogen Stress Cracking of High-Strength 4130 Steel.	907-912A	Corrosion of Fe—Ni—Cr, Fe—Cr—Al and Fe—Ni—Cr—Al Alloys in $H_2/O/H_2O$ Mixtures at 1200°C.	1299-1311A
Wedge-Type Creep Damage in Low-Cycle Fatigue.	1207-1214A	Ferrous alloys, Crystal growth	
Gel Electrode Imaging of Metal Fatigue. I.—Cracks in 6061-T6 Aluminum.	1413-1419A	Primary Recrystallization Textures in Dilute Fe—C Alloys.	199-202A
Gel Electrode Imaging of Metal Fatigue. II.—Deformation in 1100 Aluminum.	1421-1427A	Ferrous alloys, Diffusion	
The Fatigue Crack Growth Behavior of Electron-Beam Welded A286 Superalloy.	1483-1489A	Mass Transport of Carbon in One- and Two-Phase Iron—Nickel Alloys in a Temperature Gradient.	1713-1719A
Fatigue failure, Corrosion effects		Ferrous alloys, Mechanical properties	
Influence of Corrosion Deposits on Near-Threshold Fatigue Crack Growth Behavior in 2XXX and 7XXX Series Aluminum Alloys.	2271-2280A	Microstructures, Mechanical Properties and Electrical Resistivity of Rapidly Quenched Fe—Cr—Al Alloys.	337-343A
Fatigue failure, Environmental effects		Mechanical Properties of Fe—Si—B Amorphous Wires Produced by In-Rotating Water Spinning Method.	373-382A
Elevated-Temperature Fatigue Crack Growth in Incoloy Alloy 800 in Sulfidizing Environments.	145-152A	Mechanical Behavior of Alloy 800 at 838°K.	637-648A
Fatigue failure, Impurity effects		Ferrous alloys, Microstructure	
The Effect of Defects on the Fatigue Crack Initiation Process in Two P/M Superalloys. I.—Fatigue Origins.	33-43A	The Usefulness of Integral Mean Curvature Measurements in the Study of the Kinetics of Coarsening.	1389-1395A
A Theory of Fatigue Crack Initiation at Inclusions.	117-123A	Kinetics of Grain Coarsening During Sintering of Co—Cu and Fe—Cu Alloys With Low Liquid Contents.	1405-1411A
Fatigue failure, Microstructural effects		Ferrous alloys, Oxidation	
Fatigue Crack Initiation and Strain-Controlled Fatigue of Some High-Strength Low-Alloy Steels.	59-72A	Microstructural Investigation of the Oxidation of an Fe—3% Cr Alloy.	2103-2112A
Fatigue failure, Stress effects		Ferrous alloys, Phases (state of matter)	
Induced Creep and Creep/Fatigue of a Nickel-Based Superalloy at Ambient Temperatures.	1951-1955A	Experimental Determination of the Austenite + Liquid Phase Boundaries of the Fe—C System.	1293-1297A
Fatigue fracture		Ferrous alloys, Powder technology	
See Fatigue failure		The Effect of an Inert Oxide Particle Dispersion on the Morphology of Martensite in Fe—27Ni—0.025C Alloys.	203-211A
Fatigue life		Characterization of a Rapidly Solidified Iron-Based Superalloy.	1535-1546A
Mode III Fatigue Crack Propagation in Low-Alloy Steel.	101-110A	Ferrous alloys, Refining	
Low-Cycle Fatigue Behavior of Ti—6Al—2Sn—4Zr—6Mo. I.—The Role of Microstructure in Low-Cycle Crack Nucleation and Early Crack Growth.	257-268A	Rate of Decarburization of Iron—Carbon Melts. I.—Experimental Determination of the Effect of Sulfur.	403-409B
Fatigue Crack Initiation and Propagation in a Quenched and Tempered Nickel-Bearing HSLA Steel.	393-399A	Rate of Decarburization of Iron—Carbon Melts. II.—A Mixed-Control Model.	411-421B
Theoretical Considerations on Corrosion Fatigue Crack Initiation.	649-655A	Ferrous alloys, Structural hardening	
Mechanisms of Creep—Fatigue Interaction.	1215-1221A	Effect of Composition and High-Energy Rate Forging on the Onset of Precipitation in an Iron-Based Superalloy.	345-353A
High-Cycle Fatigue Life of the Cast Nickel-Based-Superalloys IN 738 LC and IN 939.	1245-1255A	Ferrous alloys, Welding	
Gel Electrode Imaging of Metal Fatigue. II.—Deformation in 1100 Aluminum.	1421-1427A	The Fatigue Crack Growth Behavior of Electron-Beam Welded A286 Superalloy.	1483-1489A
The Influence of Microstructure on the Susceptibility of Titanium Alloys to Internal Hydrogen Embrittlement.	1729-1738A	Ferrous compounds	
Fatigue life, Microstructural effects		See Iron compounds	
The Fatigue of Pseudoelastic Polycrystalline Beta-CuZnSn.	25-31A	Ferrous metals	
Low-Cycle Fatigue Behavior of Ti—6Al—2Sn—4Zr—6Mo. II.—Cyclic Deformation Behavior and Low Cycle Fatigue.	269-274A	See Ferrous alloys	
Low-Cycle Fatigue Behavior of Ti—M Alloys: Fatigue Life.	1275-1281A	Fiber composites, Mechanical properties	
Fatigue life, Stress effects		A Method for Fabrication of Aluminum/Alumina Composites.	93-100A
Effects of Friction and High Torque on Fatigue Crack Propagation in Mode III.	2197-2204A	Work of Fracture in Aluminum Metal-Matrix Composites.	289-297A
Fatigue life, Vibration effects		Fatigue Behavior of SiC Reinforced Ti(6Al—4V) at 650°C.	1933-1938A
Effects of Dwell on High-Temperature Low-Cycle Fatigue of a Titanium Alloy.	322-324A	Fiber metallurgy	
Fatigue life, Welding effects		See also Fiber composites	
High-Cycle Fatigue of Weld Repaired Cast Ti—6Al—4V.	1589-1594A	A Method for Fabrication of Aluminum/Alumina Composites.	93-100A
Fatigue properties		Fibrous structure	
See Fatigue (materials)		The Occurrence of Aligned Microstructures in Directionally Solidified Aluminum—Bismuth Alloys.	493-495A
Fatigue strength		Fields (physics)	
Effect of Rare Earth Additions on the Inclusions and Properties of a Ca—Al Dodecagonal Steel.	185-192B	See Electromagnetic fields Magnetic fields	
Fatigue Behavior of SiC Reinforced Ti(6Al—4V) at 650°C.	1933-1938A	Finite element method	
Cyclic Deformation of Pearlite Eutectoid Rail Steel.	2035-2047A	A Numerical Simulation of the D.C. Continuous Casting Process Including Nucleate Boiling Heat Transfer.	593-602B
Fatigue strength, Microstructural effects		Discussion of "Diffusion-Controlled Phase Transformation in a Finite Region".	1655-1658A
Fatigue Initiation Study of TMT Eutectoid Steel.	855-864A	Finsider process	
FCC metals, Diffusion		See Direct reduction	
Grain Boundary Diffusion Mechanisms in Metals.	527-553B	Fissures	
Grain Boundary Diffusion Mechanisms in Metals.	2069-2095A	See Cracks	
Ferric compounds		Flame reduction process	
See Iron compounds		See Direct reduction	
Ferrite		Flash smelting	
The Isothermal Austenite—Ferrite Transformation in Some Deformed Vanadium Steels.	1347-1353A	A Mineralogical Study of Nickel Mattes From the Kalgoorlie Nickel Smelter, Kalgoorlie, Western Australia.	141-152B
Tempering Characteristics of a Vanadium-Containing Dual-Phase Steel.	1679-1686A		
Aging Susceptibility of Retained and Epitaxial Ferrite in Dual-Phase Steels.	2061-2064A		

Fused salts

Flaw detection	
Gel Electrode Imaging of Metal Fatigue. I.—Cracks in 6061-T6 Aluminum.	1413-1419A
Gel Electrode Imaging of Metal Fatigue. II.—Deformation in 1100 Aluminum.	1421-1427A
Flexural vibration	
See Fatigue (materials)	
Flow	
See Fluid flow	
Gas flow	
Plastic flow	
Flow stress	
See Shear strength	
Fluid flow	
See also Gas flow	
The Effect of Mold Precession on Channel and Macrosegregation in Ammonium Chloride—Water Analog Castings.	495-501B
Fluid flow, Field effects	
Effect of Wave Motion on Chill Cast Surfaces.	503-509B
Fluidity	
See Viscosity	
Fluidized bed cathodes	
An Investigation of Fluidized Bed Electrowinning of Cobalt Using 50 and 1000 A Cells.	293-301B
Fluidized bed electrodes	
See Fluidized bed cathodes	
Fluidized bed electrolysis	
Fluidized Bed Electrowinning of Copper; Experiments Using 150 A and 1000 A Cells and Some Mathematical Modeling.	3-13B
Fluidized beds	
The Production of Niobium/Tin Powders by Vapor Deposition Processes.	625-631B
Fluxmeters (magnetic)	
See Magnetic measurements	
Force	
See Cyclic loads	
Torque	
Forecasting	
The Velocity Field in the Molten Slag Region of ESR Systems: a Comparison of Measurements in a Model System With Theoretical Predictions.	35-43B
Forging	
See also Hot forging	
Liquid metal forging	
Superplastic Behavior of the Sn—Pb Eutectic in the As-Worked State.	53-58A
Flow Localization and Shear Band Formation in a Precipitation Strengthened Austenitic Stainless Steel.	1263-1274A
Formability	
The Large Strain Deformation of Some Aluminum Alloys.	1445-1452A
Forming	
See Cold rolling	
Extrusion	
Forging	
High energy rate forming	
Hot rolling	
Liquid metal forging	
Superplastic forming	
Swaging	
Thermomechanical treatment	
Fractography	
Effects of Texture and Microstructure on the Propagation of Iodine Stress Corrosion Cracks in Zircaloy.	73-83A
Further Observations on the Fracture of a Quenched and Tempered Steel in Hydrogen.	176-179A
Hydrogen Embrittlement in a 2000 Series Aluminum Alloy.	235-239A
Self-Fracture of Hydrogen-Charged Niobium.	320-321A
Microstructure—Property Relationships of Two Al—3Li—2Cu—0.2Zr—Xcd Alloys.	401-410A
Temperature Dependence of Sustained-Load Subcritical Crack Growth in Ti—6Al—6V—2Sn.	497-500A
Crack Arrest Toughness of Two High-Strength Steels (AISI 4140 and AISI 4340).	657-664A
The Fracture Behavior of Quenched and Tempered Martensite Steels.	827-836A
The Effect of Phosphorus Content on the Hydrogen Stress Cracking of High-Strength 4130 Steel.	907-912A
Some Considerations on Fatigue Crack Closure at Near-Threshold Stress Intensities Due to Fracture Surface Morphology.	937-940A
The Influence of Notch Root Radius and Austenitizing Temperature on Fracture Appearance of As-Quenched Charpy-V Type AISI 4340 Steel Specimens.	1003-1013A
The Effect of Stress State on Internal Hydrogen-Induced Crack Growth in Ti—6Al—6V—2Sn.	1055-1061A
Effect of Environment on Fatigue and Creep Crack Growth in Inconel X-750 at Elevated Temperature.	1083-1090A
Caustic Stress Corrosion Cracking of Mild Steel.	1091-1098A
A Study of the Deformation and Fracture of a Dual-Phase Steel.	1821-1826A
Fractography, Microstructural effects	
The Influence of Microstructure and Strength on the Fracture Mode and Toughness of 7XXX Series Aluminum Alloys.	411-425A
Fracture mechanics	
See also J integral	
Mechanisms of Creep—Fatigue Interaction.	1215-1221A
On Fracture Initiation Mechanisms and Dynamic Recrystallization During Hot Deformation of Pure Nickel.	1233-1238A
High-Cycle Fatigue Life of the Cast Nickel-Based-Superalloys IN 738 LC and IN 939.	1245-1255A
Influence of Gaseous Environments on Rates of Near-Threshold Fatigue Crack Propagation in NiCrMoV Steel.	1633-1645A
Indentation Loading Studies of Acoustic Emission From Temper and Hydrogen Embrittled A533B Steel.	1965-1975A
Hydrogen Effects on the Tensile Properties of 21-6-9 Stainless Steel.	2049-2058A
Fracture mechanics, Composition effects	
Stress Corrosion of Cu—Zn and Cu—Zn—Ni Alloys: the Role of Dealloying.	2027-2033A
Fracture toughness	
Further Observations on the Fracture of a Quenched and Tempered Steel in Hydrogen.	176-179A
Effect of Rare Earth Additions on the Inclusions and Properties of a Ca—Al Deoxidized Steel.	185-192B
Fracture in Equiaxed Two Phase Alloys. I.—Fracture in Alloys With Isolated Elastic Particles.	873-879A
Fracture in Equiaxed Two Phase Alloys. II.—Fracture in Alloys With Isolated Plastic Particles.	881-887A
Fracture toughness, Heating effects	
Work of Fracture in Aluminum Metal-Matrix Composites.	289-297A
The Influence of Notch Root Radius and Austenitizing Temperature on Fracture Appearance of As-Quenched Charpy-V Type AISI 4340 Steel Specimens.	1003-1013A
Fracture Toughness of AISI M2 High-Speed Steel and Corresponding Matrix Tool Steel.	1595-1605A
Fracture toughness, Microstructural effects	
The Influence of Microstructure and Strength on the Fracture Mode and Toughness of 7XXX Series Aluminum Alloys.	411-425A
Fracture Toughness: a Rationalization of the Role of Microstructure in an Alpha—Beta Titanium Alloy.	2191-2195A
Optimization of Fe/Cr/C Base Structural Steels for Improved Strength and Toughness.	2227-2237A
Fracture toughness, Temperature effects	
Crack Arrest Toughness of Two High-Strength Steels (AISI 4140 and AISI 4340).	657-664A
Fracturing	
See also Brittle fracture	
Ductile fracture	
Intergranular fracture	
Fracturing, Stress effects	
Tensile and Fracture Properties of Type 316 Stainless Steel After Creep.	2155-2163A
Free energy	
See also Activation energy	
Free energy of formation	
Free energy of transformation	
Stacking fault energy	
A Gaussian-Based Formalism for the Representation of Free Energy as a Function of Composition of Binary Metallic Solutions.	213-225B
Discussion of "A Gaussian-Based Formalism for the Representation of Free Energy as a Function of Composition on Binary Metallic Solutions".	644-645B
Free energy of activation	
See Activation energy	
Free energy of dissociation	
See Free energy of formation	
Free energy of formation	
Thermodynamics of the Superalloys.	959-965A
Thermodynamics of the Ti—H System.	1329-1336A
Free energy of formation, Temperature effects	
Standard Free Energy of Formation of NiAsS.	285-288B
Free energy of transformation	
Thermodynamics of the Ti—H System.	1329-1336A
Freezing points	
See Melting points	
Frequencies	
Effect of Environment on Fatigue and Creep Crack Growth in Inconel X-750 at Elevated Temperature.	1083-1090A
Friction	
Effects of Friction and High Torque on Fatigue Crack Propagation in Mode III.	2197-2204A
Fuel elements	
See Nuclear fuel elements	
Fuels	
See Coke	
Fugacity, Pressure effects	
An Equation-of-State for Methane for Modeling Hydrogen Attack in Ferritic Steels.	299-303A
Furnaces	
See Bottom blown converters	
Kilns	
Rotary furnaces	
Fused salts, Phases (state of matter)	
Computer Analysis of Phase Diagrams and Thermodynamic Properties of Cryolite Based Systems. II.—The $\text{AlF}_3\text{—CaF}_2\text{—LiF}$, $\text{AlF}_3\text{—CaF}_2\text{—NaF}$ and $\text{CaF}_2\text{—LiF—NaF}$ Systems.	61-69B

Fusion welding

Fusion welding		
<i>See</i> Electron beam welding		
Gas metal arc welding		
Gas tungsten arc welding		
Laser beam welding		
Gallium, Binary systems		
<i>Thermodynamic Studies on the Mg—Ga System.</i>	71-76B	
Galvanic cells		
<i>See</i> Electrolytic cells		
Gas carburizing		
<i>Gas Carburizing of Steel With Furnace Atmospheres Formed in Situ From Methane and Air and From Butane and Air.</i>	613-623B	
Gas flow		
<i>Fluid Dynamics of Vertical Submerged Gas Jets in Liquid Metal Processing Systems.</i>	165-173B	
<i>Hydrodynamics of Gas Stirred Melts. I.—Gas/Liquid Coupling.</i>	193-202B	
<i>Hydrodynamics of Gas Stirred Melts. II.—Axisymmetric Flows.</i>	203-211B	
<i>Vacuum Distillation of Liquid Metals. II—Photographic Study.</i>	589-591B	
Gas metal arc welding		
<i>Weld Metal Grain Structure and Mechanical Properties of a Thallium-Doped Ir—0.3% W Alloy (DOP-26).</i>	1043-1053A	
Gas permeability		
<i>See</i> Permeability		
Gas phases, Diffusion		
<i>Mathematical Treatment of Permeation for Cylindrical Geometry.</i>	174-176A	
Gas tungsten arc welding		
<i>Carbide Formation in a Low-Ferrite Austenitic Stainless Steel Weld Metal at 649°C.</i>	173-174A	
<i>Welding, Glazing and Heat Treating—a Dimensional Analysis of Heat Flow.</i>	363-371A	
<i>High-Cycle Fatigue of Weld Repaired Cast Ti—6Al—4V. Effect of Manganese and Nitrogen on the Solidification Mode in Austenitic Stainless Steel Welds.</i>	1589-1594A	
<i>Morphology of the Reaction Product.</i>	2121-2130A	
Gas turbines		
<i>Mechanism of Oxidation—Sulfation Reactions of CoO in the Presence of Na₂SO₄.</i>	1647-1654A	
<i>Fatigue and Creep—Fatigue Deformation of Several Nickel-Based Superalloys at 650°C.</i>	1755-1765A	
<i>Low-Temperature Hot Corrosion of Cobalt-Based Alloys. I.—Morphology of the Reaction Product.</i>	1843-1852A	
Gaussian distribution		
<i>See</i> Normal distribution		
Generators		
<i>See</i> Turbogenerators		
Germanium base alloys, Solubility		
<i>Activities of Oxygen in Liquid Cu—Sb and Cu—Ge Alloys.</i>	77-83B	
Gibbs free energy		
<i>See</i> Free energy		
Glass		
<i>See also</i> Metallic glasses		
Glass, Phases (state of matter)		
<i>CaS Formation and Oxidation in the System CaO—SiO₂—Al₂O₃ Measured by Electron Paramagnetic Resonance.</i>	1997-2002A	
Glazing		
<i>Welding, Glazing and Heat Treating—a Dimensional Analysis of Heat Flow.</i>	363-371A	
Glissile dislocations		
<i>Low-Temperature Strain Behavior of Lead Thin Films on a Substrate.</i>	383-391A	
<i>Deformation Modes of the Alpha-Phase of Ti—6Al—4V as a Function of Oxygen Concentration and Aging Temperature.</i>	889-899A	
GP zone		
<i>See</i> Guinier Preston zone		
Gradometers		
<i>See</i> Magnetic measurements		
Grain boundaries		
<i>Effect of Sulfur and Antimony on the Intergranular Fracture of Iron at Cathodic Potentials.</i>	241-249A	
<i>A Numerical Study of Cavity Growth Controlled by Coupled Surface and Grain Boundary Diffusion.</i>	427-437A	
<i>The Influence of Grain Boundary Phosphorus Concentration on Liquid Metal and Hydrogen Embrittlement of Monel 400. The Role of Sulfur in the Air Embrittlement of Nickel and Its Alloys.</i>	611-618A	
<i>The Detection of Monolayer Grain Boundary Segregations in Steels Using STEM-EDS X-Ray Microanalysis.</i>	1223-1232A	
<i>Compositional Effects on the High-Temperature Ductility of 1Cr—1.25Mo—0.25 Steel.</i>	1397-1403A	
<i>Splitting of Tungsten Wire in the Knife-Edge Compression Test.</i>	1471-1481A	
<i>The Thermodynamics of Interactive Cosegregation of Phosphorus and Alloying Elements in Iron and Temper-Brittite Steels.</i>	1501-1510A	
<i>The Growth of Creep Cavities in a Low-Alloy Steel. A Study of the Deformation and Fracture of a Dual-Phase Steel.</i>	1693-1711A	
<i>Diffusion Driven Grain Boundary Migration in Iron During Zincification.</i>	1739-1745A	
<i>Grain Boundary Diffusion Mechanisms in Metals.</i>	1821-1826A	
<i>Grain Boundary Diffusion Mechanisms in Metals. II—Copper—Silver, —Titanium, —Zirconium and —Hafnium at 1373°K.</i>	1567-1572A	
Grain boundaries, Diffusion		
<i>Grain Boundary Diffusion Mechanisms in Metals.</i>	527-553B	
<i>Diffusion Driven Grain Boundary Migration in Iron During Zincification.</i>		
Grain boundary sliding		
<i>The Mechanical Properties of Superplastic Materials.</i>	689-701A	
<i>Microstructural Aspects of Superplasticity.</i>	703-715A	
<i>The Rate-Controlling Deformation Mechanisms in Superplasticity—a Critical Assessment.</i>	717-732A	
Grain growth		
<i>Kinetics of Grain Coarsening During Sintering of Co—Cu and Fe—Cu Alloys With Low Liquid Contents.</i>	1405-1411A	
<i>Recrystallization and Grain Growth in NiAI.</i>	1563-1566A	
<i>The Influence of Gamma Prime on the Recrystallization of an Oxide Dispersion Strengthened Superalloy—MA 6000E.</i>	1665-1674A	
Grain growth, Deformation effects		
<i>Effect of the Degree of Prior Cold Work on the Grain Volume Distribution and the Rate of Grain Growth of Recrystallized Aluminum.</i>	985-993A	
<i>The Influence of Hot Working on the Subsequent Recrystallization of a Dispersion Strengthened Superalloy—MA 6000.</i>	1463-1470A	
Grain orientation		
<i>The Influence of Orientation on the Stress Rupture Properties of Nickel-Based Superalloy Single Crystals.</i>	1747-1754A	
Grain refinement		
<i>Coarsening and Microsegregation During Solidification of Ni—Al—Cr Dendritic Monocrystals.</i>	1153-1159A	
Grain size		
<i>The Fatigue of Pseudoelastic Polycrystalline Beta-CuZnSn. Oxidation Behavior of a Fine-Grained Rapidly Solidified 18-8 Stainless Steel.</i>	25-31A	
<i>Influence of Grain Size and Age-Hardening on Dislocation Pile-Ups and Tensile Fracture for a Ti—Al Alloy.</i>	473-485A	
<i>Rapid Solidification Effects in Martensitic Cu—Zn—Al Alloys.</i>	1283-1292A	
<i>Recrystallization and Formation of Austenite in Deformed Lath Martensitic Structure of Low-Carbon Steels.</i>	1377-1388A	
<i>Influence of Test Temperature and Microstructure on the Tensile Properties of Titanium Alloys.</i>	1435-1443A	
Grain size, Deformation effects		
<i>Superplastic Behavior of the Sn—Pb Eutectic in the As-Worked State.</i>	53-58A	
<i>Grain Boundary Strengthening in Strongly Textured Magnesium Produced by Hot Rolling.</i>	2219-2226A	
Grain size, Heating effects		
<i>Heating Rate Effects on Recrystallized Grain Size in Two Al—Zn—Mg—Cu Alloys.</i>	193-198A	
Grain structure		
<i>The Isothermal Austenite—Ferrite Transformation in Some Deformed Vanadium Steels.</i>	1347-1353A	
<i>Rapid Solidification Effects in Martensitic Cu—Zn—Al Alloys.</i>	1367-1372A	
<i>Kinetics of Grain Coarsening During Sintering of Co—Cu and Fe—Cu Alloys With Low Liquid Contents.</i>	1405-1411A	
Grain structure, Deformation effects		
<i>The Influence of Grain Structure on the Ductility of the Al—Cu—Li—Mn—Cd Alloy 2020.</i>	2259-2269A	
Grain structure, Welding effects		
<i>Weld Metal Grain Structure and Mechanical Properties of a Thallium-Doped Ir—0.3% W Alloy (DOP-26).</i>	1043-1053A	
Gravitation		
<i>The Influence of Acceleration Forces on Dendritic Growth and Grain Structure.</i>	85-90B	
<i>The Effect of Mold Precession on Channel and Macrosegregation in Ammonium Chloride—Water Analog Castings.</i>	495-501B	
Gravity		
<i>See</i> Gravitation		
Grinding		
<i>The State of Residual Stress in the Near Surface Region of Homogeneous and Heterogeneous Materials After Grinding.</i>	1239-1244A	
Growth		
<i>See</i> Crystal growth		
<i>Epitaxial growth</i>		
<i>Grain growth</i>		
<i>Growth rate</i>		
Growth rate		
<i>Mechanism of the Solid-State Displacement Reaction Between Iron and Nickel Oxide at 1000°C. Coarsening and Microsegregation During Solidification of Ni—Al—Cr Dendritic Monocrystals.</i>	585-594A	
<i>Recrystallization and Grain Growth in NiAI.</i>	1153-1159A	
<i>Stress-Assisted Isothermal Martensitic Transformation: Application to TRIP Steels.</i>	1563-1566A	
<i>1907-1914A</i>		
Guinier Preston zone		
<i>Modulated Structures and G—P Zones in Al—Mg Alloys.</i>	1373-1378A	
Guinier Preston zone, Solubility		
<i>Calorimetric Studies of Precipitation and Dissolution Kinetics in Aluminum Alloys 2219 and 7075.</i>	761-769A	
Hafnium, Binary systems		
<i>Thermochemistry of Alloys of Transition Metals: III—Copper—Silver, —Titanium, —Zirconium and —Hafnium at 1373°K.</i>	391-401B	
Halides		
<i>See</i> Chlorides		
<i>Sodium chloride</i>		
Halogenation		
<i>See</i> Chlorination		

Halogens	Heavy metals
<i>See Chlorine</i>	<i>See Antimony</i>
Iodine	Bismuth
Hardenability	Cadmium
<i>See Quench hardenability</i>	Lead (metal)
Strain hardenability	Mercury (metal)
Hardenability (quench)	Tin
<i>See Quench hardenability</i>	
Hardening	Heliarc welding
<i>See also Aging (artificial)</i>	<i>See Gas tungsten arc welding</i>
Carburizing	
Dispersion hardening	Heimholz free energy
Gas carburizing	<i>See Free energy</i>
Precipitation hardening	Hematite, Crystal growth
Secondary hardening	<i>The Growth of Hematite Blades During the High-Temperature Oxidation of Iron.</i>
Solution strengthening	
Strain aging	HERF
Strain hardening	<i>See High energy rate forming</i>
Surface hardening	High alloy steels
Structure—Property Relationships in Dual-Phase Cu—Al Alloys. II.—Alloy Behavior.	<i>See also Austenitic stainless steels</i>
	Ferritic stainless steels
	Martensitic stainless steels
	Stainless steels
Hardness	High alloy steels, Directional solidification
<i>See also Microhardness</i>	<i>Dendrite Morphology of Several Steady State Unidirectionally Solidified Iron-Base Alloys.</i>
Mechanical Properties of Fe—Si—B Amorphous Wires Produced by In-Rotating-Water Spinning Method.	
Athermal Solid Solution Hardening in Tantalum.	<i>2131-2141A</i>
	High alloy steels, Phase transformations
	<i>An Examination of the Validity of Existing Empirical Formulas for the Calculation of M_3 Temperature.</i>
Hazelett process	
<i>See Continuous casting</i>	High energy rate forming
Heat affected zone	<i>Effect of Composition and High-Energy Rate Forging on the Onset of Precipitation in an Iron-Base Superalloy.</i>
The Fatigue Crack Growth Behavior of Electron-Beam Welded A286 Superalloy.	
	<i>345-353A</i>
Heat flow	High speed tool steels, Mechanical properties
<i>See Heat transmission</i>	<i>Fracture Toughness of AISI M2 High-Speed Steel and Corresponding Matrix Tool Steel.</i>
Heat flux	
<i>See Heat transmission</i>	<i>1595-1805A</i>
Heat of activation	High speed tool steels, Microstructure
Thermotransport of Hydrogen and Deuterium in Vanadium, Niobium and Tantalum.	<i>A New Procedure for Determining Volume Fraction of Primary Carbides in High-Speed and Related Tool Steels.</i>
	<i>185-191A</i>
Heat of decomposition	High strength low alloy steels
<i>See Heat of formation</i>	<i>See also Dual phase steels</i>
Heat of dissociation	<i>Dynamic Strain Aging of Various Steels.</i>
<i>See Heat of formation</i>	
Heat of formation	<i>1793-1797A</i>
Thermodynamic Studies on the Mg—Ga System.	High strength low alloy steels, Mechanical properties
Enthalpies of Formation of Borides of Iron, Cobalt and Nickel by Solution Calorimetry in Liquid Copper.	<i>Fatigue Crack Initiation and Strain-Controlled Fatigue of Some High-Strength Low-Alloy Steels.</i>
Phase Stability Investigations of the Palladium—Cadmium System. II.—Structural Studies.	
	<i>59-72A</i>
	<i>Fatigue Crack Initiation and Propagation in a Quenched and Tempered Niobium-Bearing HSLA Steel.</i>
	<i>393-399A</i>
	<i>The Plastic Zone and Residual Stress Near a Notch and a Fatigue Crack in HSLA Steel.</i>
	<i>1987-1995A</i>
Heat of fusion	High strength low alloy steels, Microstructure
Enthalpies of Formation of Borides of Iron, Cobalt and Nickel by Solution Calorimetry in Liquid Copper.	<i>Influence of Cooling Rate on the Microstructure and Retained Austenite in an Intercritically Annealed Vanadium-Containing HSLA Steel.</i>
	<i>1899-1908A</i>
Heat of mixing	High strength low alloy steels, Phase transformations
Computer Analysis of Phase Diagrams and Thermodynamic Properties of Cryolite Based Systems. II.—The $\text{AlF}_3-\text{CaF}_2-\text{LiF}$, $\text{AlF}_3-\text{CaF}_2-\text{NaF}$ and $\text{CaF}_2-\text{LiF}-\text{NaF}$ Systems.	<i>The Isothermal Austenite—Ferrite Transformation in Some Deformed Vanadium Steels.</i>
Thermochemistry of Alloys of Transition Metals: III.—Copper—Silver, —Titanium, —Zirconium and —Hafnium at 1373°K.	
	<i>1347-1353A</i>
	<i>The Alpha-Gamma Phase Boundaries and the T_0 for Fe—Mn Alloys.</i>
	<i>2113-2119A</i>
Heat of solidification	High strength low alloy steels, Thermal properties
<i>See Heat of fusion</i>	<i>Thermal Effects During Uniaxial Straining of Steels.</i>
Heat resistant alloys	
<i>See Superalloys</i>	High temperature
Heat transfer	<i>The Effect of High-Temperature Low-Cycle Fatigue on the Corrosion Resistance of Austenitic Stainless Steels.</i>
Regenerative Heat Transfer in Rotary Kilns (for Limestone).	
Heat Flow During Rapid Solidification of Undercooled Metal Droplets.	<i>923-927A</i>
A Numerical Simulation of the D.C. Continuous Casting Process Including Nucleate Boiling Heat Transfer.	High temperature tests
	<i>Effect of Carbon Content on the Plastic Flow of Plain Carbon Steels at Elevated Temperatures.</i>
	<i>125-134A</i>
	<i>Creep and Rupture of an ODS Alloy With High Stress Rupture Ductility.</i>
	<i>1453-1462A</i>
Heat transmission	Holes
The Influence of Mold Behavior on the Production of Continuously Cast Steel Billets.	<i>A Numerical Study of Cavity Growth Controlled by Coupled Surface and Grain Boundary Diffusion.</i>
Welding, Glazing and Heat Treating—a Dimensional Analysis of Heat Flow.	
The Use of Heat Flow Modeling to Explore Solidification Phenomena.	<i>427-437A</i>
	Homogenizing
	<i>Coarsening of SiO_2 Particles in Copper and MnS Inclusions in Steel.</i>
	<i>2143-2153A</i>
Heat treatment	Hot cracking
<i>See also Aging (artificial)</i>	<i>See Cracking (fracturing)</i>
Austenitizing	Hot ductility
Carburizing	<i>See Ductility</i>
Gas carburizing	Hot forging
Grain refinement	<i>The Occurrence of Shear Bands in Isothermal, Hot Forging.</i>
Homogenizing	
Precipitation hardening	<i>275-288A</i>
Quench aging	Hot hardness
Quenching and tempering	<i>See Hardness</i>
Secondary hardening	Hot reduction
Tempering	<i>See Hot working</i>
Optimization of Fe/Cr/C Base Structural Steels for Improved Strength and Toughness.	Hot rolling
	<i>Grain Boundary Strengthening in Strongly Textured Magnesium Produced by Hot Rolling.</i>
	<i>2219-2226A</i>
Heating	Hot roughing
<i>See Laser beam heating</i>	<i>See Hot rolling</i>
Heats (energies)	Hot strength
<i>See Heat of activation</i>	<i>See Tensile strength</i>
Heat of formation	
Heat of fusion	Hot swaging
Heat of mixing	<i>See Swaging</i>

Hot tensile strength

Hot tensile strength See Tensile strength		
Hot torsion tests See Torsion tests		
Hot working See also Hot forging Hot rolling	1233-1238A	
On Fracture Initiation Mechanisms and Dynamic Recrystallization During Hot Deformation of Pure Nickel.	1463-1470A	
The Influence of Hot Working on the Subsequent Recrystallization of a Dispersion Strengthened Superalloy—MA 6000.		
Hydrogen See also Deuterium		
Hydrogen, Binary systems Thermodynamics of the Ti—H System.	1329-1336A	
Hydrogen, Diffusion The Effect of Hydrogen Source on Crack Initiation in 4340 Steel. Self-Fracture of Hydrogen-Charged Niobium. Evidence for Dislocation Transport of Hydrogen in Aluminum. Thermotransport of Hydrogen and Deuterium in Vanadium, Niobium and Tantalum. Hydrogen Transport in Nickel-Based Stainless Alloys. Hydrogen Diffusion in Nb-Ta Alloys. Effect of Hydrogen Concentration on Slow Crack Growth in Stainless Steels.	305-311A 320-321A 811-820A 821-825A 1181-1186A 1675-1678A 1799-1808A	
Hydrogen, Environment Influence of Gaseous Environments on Rates of Near-Threshold Fatigue Crack Propagation in NiCrMoV Steel.	1633-1645A	
Hydrogen, Impurities Thermal Analysis of Trapped Hydrogen in Pure Iron. Creep of Hydrogen-Charged Ti—5Al—2.5Sn at Room Temperature.	135-140A 1531-1532A	
Hydrogen, Solubility Chemical and Kinetic Factors Related to Hydrogen Removal From Aluminum.	447-460B	
Hydrogen, Sorption Hydrogen Effects on the Tensile Properties of 21-6-9 Stainless Steel.	2049-2058A	
Hydrogen compounds See Hydrogen sulfide Sulfuric acid		
Hydrogen embrittlement Further Observations on the Fracture of a Quenched and Tempered Steel in Hydrogen. Hydrogen Embrittlement in a 2000 Series Aluminum Alloy. An Equation-of-State for Methane for Modeling Hydrogen Attack in Ferritic Steels. The Effect of Hydrogen Source on Crack Initiation in 4340 Steel. Surface Wave Studies of Hydrogen Damage Incubation Time. The Influence of Grain Boundary Phosphorus Concentration on Liquid Metal and Hydrogen Embrittlement of Monel 400. Hydrogen Cracking in Nominally Pearlitic 1045 Steel. Hydrogen-Relief Phase Transformations in Austenitic Stainless Steels. Effects of Hydrogen Concentration on Slow Crack Growth in Stainless Steels. Indentation Loading Studies of Acoustic Emission From Temper and Hydrogen Embrittled A533B Steel. Hydrogen Effects on the Tensile Properties of 21-6-9 Stainless Steel.	176-179A 235-239A 299-303A 305-311A 487-491A 611-618A 1315-1318A 1355-1365A 1799-1808A 1965-1975A 2049-2058A	
Hydrogen embrittlement, Alloying effects Hydrogen Embrittlement of Ultra-Pure Alloys of the Inconel 600 Type: Influence of the Additions of Elements (Carbon, Phosphorus, Tin, Antimony). The Role of Molybdenum in the Enhanced Resistance to Hydrogen Stress Cracking of AISI 4100 Steels.	141-144A 1099-1101A	
Hydrogen embrittlement, Composition effects Effects of Compositional Variations and Aging Treatments on the Fracture Behavior of HY 130 Steel in Air and Hydrogen.	111-116A	
Hydrogen embrittlement, Impurity effects The Effect of Phosphorus Content on the Hydrogen Stress Cracking of High-Strength 4130 Steel.	907-912A	
Hydrogen embrittlement, Microstructural effects The Influence of Microstructure on the Susceptibility of Titanium Alloys to Internal Hydrogen Embrittlement.	1729-1738A	
Hydrogen embrittlement, Stress effects The Effect of Stress State on Internal Hydrogen-Induced Crack Growth in Ti—6Al—6V—2Sn.	1055-1061A	
Hydrogen ion concentration See pH.		
Hydrogen reduction Microstructural Features Produced by the Reduction of Wüstite in H ₂ /H ₂ O Gas Mixtures. Lime-Enhanced Hydrogen Reduction of Molybdenite. Dry Method Preparation and Melting Point of Cu ₂ SO ₄ . The Recovery of Molybdenum From Leach Solutions by Reduction.	117-124B 275-282B 515-517B 565-570B	
Hydrogen sulfide, Environment Elevated-Temperature Fatigue Crack Growth in Incoloy Alloy 800 in Sulidizing Environments. The Role of Molybdenum in the Enhanced Resistance to Hydrogen Stress Cracking of AISI 4100 Steels. Corrosion of Fe—Ni—Cr, Fe—Cr—Al and Fe—Ni—Cr—Al Alloys in H ₂ /H ₂ O/H ₂ S Mixtures at 1200°C.	145-152A 1099-1101A 1299-1311A	
Hydrogenation Creep of Hydrogen-Charged Ti—5Al—2.5Sn at Room Temperature.		1531-1532A
Hydrometallurgy Solution Chemistry of Tungsten Leaching Systems.		555-564B
Hydroxides See Sodium hydroxide		
IR drop See Electric potential		
Impact strength Effects of Compositional Variations and Aging Treatments on the Fracture Behavior of HY 130 Steel in Air and Hydrogen.		111-116A
Impact strength, Impurity effects Effect of Volume Fraction and Shape of Sulfide Inclusions on Through-Thickness Ductility and Impact Energy of High-Strength 4340 Plate Steels.		2239-2258A
Impact toughness See Impact strength		
Impedance See Electrical resistance		
Impermeability See Permeability		
Impurities Thermodynamics of Copper Matte Converting. III.—Steady-State Volatilization of Gold, Silver, Lead, Zinc, Nickel, Selenium, Tellurium, Bismuth, Antimony and Arsenic From Slag, Matte and Metallic Copper.		319-329B
Thermodynamics of Copper Matte Converting. IV.— <i>A Priori</i> Predictions of the Behavior of Gold, Silver, Lead, Zinc, Nickel, Selenium, Tellurium, Bismuth, Antimony and Arsenic in the Noranda Process Reactor.		331-338B
Inchromizing See Chromizing		
Inclusions See also Nonmetallic inclusions The Effect of Melt Refining Upon Inclusions in Aluminum. A Theory of Fatigue Crack Initiation at Inclusions.		31-34B 117-123A
Indium, Diffusion The Mechanisms of Crack Initiation and Crack Propagation in Metal-Induced Embrittlement of Metals.		457-472A
Indium, Solubility The Influence of Solutes on Kinetics and Thermodynamics of Liquid Indium—Oxygen Systems.		53-59B
Indium base alloys, Mechanical properties Characterization of In-Based Eutectic Alloys Used in Josephson Packaging.		1547-1562A
Indium base alloys, Thermal properties The Influence of Solutes on Kinetics and Thermodynamics of Liquid Indium—Oxygen Systems.		53-59B
Induction melting See Vacuum induction melting		
Inert gas welding See Gas tungsten arc welding		
Ingot casting Effect of Wave Motion on Chill Cast Surfaces.		503-509B
Ingot molds The Thermal Distortion of Continuous-Casting Billet Molds.		91-104B
Ingot molds, Thermal properties The Influence of Mold Behavior on the Production of Continuously Cast Steel Billets.		105-116B
Inorganic acids See Sulfuric acid		
Instability See Stability		
Integrated circuits Characterization of In-Based Eutectic Alloys Used in Josephson Packaging.		1547-1562A
Intensity See Stress intensity		
Intercrystalline structure See Intergranular structure		
Interfaces Intercritical Austenitization of Two Fe—Mn—C Steels. Identification of the Interface Phase in Titanium Alloys.		575-579A 681-684A
Characterization of In-Based Eutectic Alloys Used in Josephson Packaging.		1547-1562A
Discussion of "Diffusion-Controlled Phase Transformation in a Finite Region".		1655-1658A
Interfaces, Diffusion Deformation by Moving Interfaces.		509-538A
Interfacial energy See Surface energy		
Intergranular corrosion, Environmental effects Environmental Factors Affecting Localized Corrosion of 7075-T7351 Aluminum Alloy Plate.		161-166A
Intergranular corrosion, Heating effects On Grain Boundary Segregation in Austenitic Stainless Steels.		2281-2285A
Intergranular fracture The Fatigue of Pseudoelastic Polycrystalline Beta-CuZnSn.		25-31A

Microstructural Observations of Superplastic Cavitation in Fine-Grained 7475 Al.	1721-1727A	
The Growth of Creep Cavities in a Low-Alloy Steel.	1739-1745A	
Intergranular fracture, Alloying effects		
Hydrogen Embrittlement of Ultra-Pure Alloys of the Inconel 600 Type: Influence of the Additions of Elements (Carbon, Phosphorus, Tin, Antimony).	141-144A	
Intergranular fracture, Diffusion effects		
Evidence for Dislocation Transport of Hydrogen in Aluminum.	811-820A	
Intergranular fracture, Environmental effects		
Influence of Corrosive Environments on Near-Threshold Fatigue Crack Growth in 403 Stainless Steel.	2177-2189A	
Intergranular fracture, Impurity effects		
Effect of Sulfur and Antimony on the Intergranular Fracture of Iron at Cathodic Potentials.	241-249A	
Intergranular precipitation		
Microstructures, Mechanical Properties and Electrical Resistivity of Rapidly Quenched Fe—Cr—Al Alloys.	337-343A	
The Bainite Reaction in Fe—Si—C Alloys: the Primary Stage.	777-787A	
The Stress Corrosion Susceptibility of a Quenched and Tempered 12% CrMoV Martensitic Stainless Steel.	913-921A	
The Role of Nitrogen in the Embrittlement of Steel.	1939-1950A	
On Grain Boundary Segregation in Austenitic Stainless Steels.	2281-2285A	
Intergranular structure		
Mechanisms of Creep—Fatigue Interaction.	1215-1221A	
Intermetallic compounds		
See Intermetallics		
Intermetallic phases		
Phase Analysis of Sintered and Heat Treated Alloy 718.	5-12A	
Intermetallics		
Thermochemistry of Alloys of Transition Metals: III.—Copper—Silver, —Titanium, —Zirconium and —Hafnium at 1373°K.	391-401B	
Intermetallics, Crystal growth		
Thermodynamic Studies on the Mg—Ga System.	71-76B	
The Early Stage of Ni ₂ Al Layer Growth in NiAl/Ni Diffusion Couples.	1921-1926A	
Intermetallics, Diffusion		
Interdiffusion Coefficients in the Ni ₂ Al ₃ (Gamma) Phase of the Ni—Al System.	1313-1314A	
Internal friction		
Internal Friction Studies of Fast Diffusing Solutes in Thorium.	995-1001A	
Internal friction, Microstructural effects		
Effect of Defect Structure Upon the Mechanical Behavior of Beta-LiAl Through Dislocation Damping and Hardness Studies.	2173-2176A	
Internal stress		
See Residual stress		
Iodine, Environment		
Effects of Texture and Microstructure on the Propagation of Iodine Stress Corrosion Cracks in Zircaloy.	73-83A	
Iridium base alloys, Welding		
Weld Metal Grain Structure and Mechanical Properties of a Thallium-Doped Ir—0.3% W Alloy (DOP-26).	1043-1053A	
Iron		
See also Cast iron White iron		
Iron, Alloying additive		
The Occurrence of Aligned Microstructures in Directionally Solidified Aluminum—Bismuth Alloys.	493-495A	
Iron, Binary systems		
The Alpha-Gamma Phase Boundaries and the T_0 for Fe—Mn Alloys.	2113-2119A	
Iron, Coating		
Experimental and Theoretical Concentration Profiles at the Surface of Chromized Iron.	495-497A	
Iron, Crystal lattices		
Thermal Analysis of Trapped Hydrogen in Pure Iron.	135-140A	
Iron, Diffusion		
Correction to "Self-Diffusion Coefficients of Carbon in Fe ₃ C at 723°K Via the Kinetics of Formation of This Compound". Activities of CoS and FeS in Copper Mattes and the Behavior of Cobalt in Copper Smelting.	2289A	
Internal Friction Studies of Fast Diffusing Solutes in Thorium. Diffusion Driven Grain Boundary Migration in Iron During Zincification.	461-470B	
Self-Diffusion Coefficients of Carbon in Fe ₃ C at 723°K Via the Kinetics of Formation of This Compound.	995-1001A	
Iron, Extraction		
Microstructural Features Produced by the Reduction of Wustite in H ₂ /H ₂ O Gas Mixtures.	117-124B	
Iron, Mechanical properties		
Effect of Sulfur and Antimony on the Intergranular Fracture of Iron at Cathodic Potentials.	241-249A	
Iron, Oxidation		
Oxidation of Fe(II) in Sulfuric Acid Solutions With Dissolved Molecular Oxygen.	311-318B	
The Growth of Hematite Blades During the High-Temperature Oxidation of Iron.	929-935A	
Iron, Physical properties		
Fluid Dynamics of Vertical Submerged Gas Jets in Liquid Metal Processing Systems.		165-173B
Iron, Reactions (chemical)		
Mechanism of the Solid-State Displacement Reaction Between Iron and Nickel Oxide at 1000°C.		585-594A
Iron, Solubility		
Steady-State Rates of Dissolution of Stationary Iron, Cobalt and Nickel Cylinders in Liquid Copper.		175-184B
Iron, Sorption		
Prediction of the Effects of Surface-Active Elements on Gas—Liquid Metal Kinetics.		357-367B
Iron and steel making		
See Steel making		
Iron base alloys		
See Ferrous alloys		
Iron compounds		
See also Hematite Iron oxides Wustite		
Iron compounds, Thermal properties		
Enthalpies of Formation of Borides of Iron, Cobalt and Nickel by Solution Calorimetry in Liquid Copper.		251-257B
Iron ores		
See Hematite		
Iron oxides		
See also Hematite Wustite		
Iron oxides, Reduction (chemical)		
Changes in Diffusivity Due to Sintering in Metallized Iron Oxide Pellets.		518-520B
Iron powder		
See Iron		
J integral		
The Influence of Notch Root Radius and Austenitizing Temperature on Fracture Appearance of As-Quenched Charpy-V Type AISI 4340 Steel Specimens.		1003-1013A
Joints		
See Butt joints Welded joints		
Junghans Rossi casting		
See Continuous casting		
Killed steels		
See Aluminum killed steels		
Kilns		
Regenerative Heat Transfer in Rotary Kilns (for Limestone). Limestone Calcination in a Rotary Kiln.		153-163B 369-378B
Kinetics		
See also Reaction kinetics The Usefulness of Integral Mean Curvature Measurements in the Study of the Kinetics of Coarsening.		1389-1395A
Ladle additions		
Effective Viscosity Models for Gas Stirred Ladles.		125-127B
Lamellar structure		
Cyclic Deformation of Pearlite Eutectoid Rail Steel.		2035-2047A
Lanthanide metal compounds		
See Samarium compounds		
Lanthanide metals		
See Cerium		
Laser beam heating		
Welding, Glazing and Heat Treating—a Dimensional Analysis of Heat Flow.		363-371A
Laser beam welding		
Microstructure and Mechanical Properties of Laser Welded Titanium 6Al—4V.		865-871A
Laser welding		
See Laser beam welding		
Lasers		
The Constitution and Phase Stability of Overlapping Melt Trails in Ag—Cu Alloys Produced by Continuous Laser Melt Quenching.		1879-1889A
Latent heat		
See Heat of fusion		
Latent heat of fusion		
See Heat of fusion		
Lattice constant		
See Lattice parameters		
Lattice defects		
See Crystal defects		
Lattice parameters		
Silicide Precipitation in Alloy Ti—6Al—5Zr—0.5Mo—0.2Si. Phase Stability Investigations of the Palladium—Cadmium System. II.—Structural Studies.		771-775A 1123-1126A
Lattice vacancies		
Defective Two Sublattice Model for a Binary Liquid.		1107-1114A
Lattice vacancies, Diffusion		
Intrinsic Diffusion Coefficients and the Vacancy Flow Factor in Dilute Cu—Zn Alloys.		1135-1139A

Lattices

Lattices

See Superlattices

Leaching

See also Acid leaching

Sulfuric acid leaching

Solution Chemistry of Tungsten Leaching Systems.

The Recovery of Molybdenum From Leach Solutions by Reduction.

Lead (metal), Alloying elements

The Influence of Acceleration Forces on Dendritic Growth and Grain Structure.

555-564B

565-570B

85-90B

429-437B

2097-2102A

383-391A

53-58A

165-173B

439-445B

213-225B

633-641B

1868-1871A

275-282B

153-163B

369-378B

457-472A

611-618A

1809-1819A

644-645B

165-173B

581-588B

589-591B

357-367B

1293-1297A

2097-2102A

1107-1114A

Lithium, Composite materials

Effect of Lithium on the Mechanical Properties and Microstructure of SiC Whisker-Reinforced Aluminum Alloys.

1511-1519A

Lithium compounds, Mechanical properties

Effect of Defect Structure Upon the Mechanical Behavior of Beta-LiAl Through Dislocation Damping and Hardness Studies.

2173-2176A

Live loads

See Cyclic loads

Lixiviation

See Leaching

Loads (forces)

See Cyclic loads

Long range order

Study of the Rheological Behavior of the Beta Prime Phase of an Equiatomic Ag-Mg Alloy.

251-255A

Loops (dislocation)

See Dislocation loops

Loss of coolant accident

Deformation Behavior of Duplex Zircaloy-4—Oxygen Alloys.

1077-1082A

Low alloy steels

See also Boron steels

Silicon steels

Low alloy steels, Crystal lattices

Positron Trapping at Phase Interfaces and Dislocations in Pearlite Eutectoid Steel.

1177-1180A

Low alloy steels, Mechanical properties

Crack Arrest Toughness of Two High-Strength Steels (AISI 4140 and AISI 4340).

657-664A

The Thermodynamics of Interactive Cosegregation of Phosphorus and Alloying Elements in Iron and Temper-Brittle Steels.

1693-1711A

Indentation Loading Studies of Acoustic Emission From Tempered and Hydrogen Embrittled A533B Steel.

1965-1975A

Low alloy steels, Phase transformations

An Examination of the Validity of Existing Empirical Formulas for the Calculation of M_3 Temperature.

328-331A

Low cycle fatigue

Low-Cycle Fatigue Behavior of Ti-6Al-2Sn-4Zr-6Mo. I.—The Role of Microstructure in Low-Cycle Crack Nucleation and Early Crack Growth.

257-268A

Low-Cycle Fatigue Behavior of Ti-6Al-2Sn-4Zr-6Mo. II.—Cyclic Deformation Behavior and Low Cycle Fatigue.

269-274A

Effects of Dwell on High-Temperature Low-Cycle Fatigue of a Titanium Alloy.

322-324A

The Effect of High-Temperature Low-Cycle Fatigue on the Corrosion Resistance of Austenitic Stainless Steels.

923-927A

Wedge-Type Creep Damage in Low-Cycle Fatigue.

1207-1214A

Low-Cycle Fatigue Behavior of Ti-Mn Alloys: Fatigue Life.

1275-1281A

Correlation of Substructure With Time-Dependent Fatigue Properties of AISI 304 Stainless Steel.

1577-1588A

Machining

See Grinding

Macrofractography

See Fractography

Magnesium, Alloying additive

Preparation and Properties of Aluminum Alloy Coconut Shell Char Particulate Composites.

485-494B

Magnesium, Alloying elements

Study of the Rheological Behavior of the Beta Prime Phase of an Equiatomic Ag-Mg Alloy.

251-255A

Magnesium, Binary systems

Thermodynamic Studies on the Mg-Ga System.

71-76B

Magnesium, Mechanical properties

Grain Boundary Strengthening in Strongly Textured Magnesium Produced by Hot Rolling.

2219-2226A

Magnetic fields

Effect of Wave Motion on Chill Cast Surfaces.

503-509B

Magnetic flux welding

See Gas metal arc welding

Magnetic force

See Magnetic fields

Magnetic measurements

Effects of Strain State and Strain Rate on Deformation-Induced Transformation in 304 Stainless Steel. I.—Magnetic Measurements and Mechanical Behavior.

619-626A

Magnetic resonance

See Electron paramagnetic resonance

Manganese, Alloying additive

The Fracture Behavior of Quenched and Tempered Manganese Steels.

827-836A

Effect of Manganese and Nitrogen on the Solidification Mode in Austenitic Stainless Steel Welds.

2121-2130A

Manganese, Alloying elements

Finite Element Method (FEM) Calculations of Stress-Strain Behavior of Alpha-Beta Ti-Mn Alloys. I.—Stress-Strain Relations.

595-601A

Finite Element Method (FEM) Calculations of Stress-Strain Behavior of Alpha-Beta Ti-Mn Alloys. II.—Stress and Strain Distributions.

603-609A

Low-Cycle Fatigue Behavior of Ti-Mn Alloys: Fatigue Life.

1275-1281A

Manganese, Binary systems

Activity of Manganese in Liquid Ni-Mn Alloys.

283-285B

Mechanical tests

The Alpha-Gamma Phase Boundaries and the T_0 for Fe—Mn Alloys.	2113-2119A	The Thermal Distortion of Continuous-Casting Billet Molds. Effective Viscosity Models for Gas Stirred Ladles. Hydrodynamics of Gas Stirred Melts. II.—Axisymmetric Flows.	91-104B 125-127B
Manganese, Dopants		Heat Flow During Rapid Solidification of Undercooled Metal Droplets.	203-211B
Compositional Effects on the High-Temperature Ductility of 1Cr—1.25Mo—0.25 Steel.	1471-1481A	An Equation-of-State for Methane for Modeling Hydrogen Attack in Ferritic Steels.	221-234A
Manganese compounds, Thermal properties		Thermodynamics of Copper Matte Converting. III.—Steady-State Volatilization of Gold, Silver, Lead, Zinc, Nickel, Selenium, Tellurium, Bismuth, Antimony and Arsenic From Slag, Matte and Metallic Copper.	299-303A
Enthalpies of Formation of Borides of Iron, Cobalt and Nickel by Solution Calorimetry in Liquid Copper.	251-257B	Welding, Glazing and Heat Treating—a Dimensional Analysis of Heat Flow.	319-329B
Manganese steels		Extension of the Associated Solution Model to Ternary Metal—Sulfur Melts: Cu—Ni—S.	363-371A
See Chromium-manganese steels		Rate of Decarburization of Iron—Carbon Melts. II.—A Mixed-Control Model.	379-385B
Martensite		A Numerical Study of Cavity Growth Controlled by Coupled Surface and Grain Boundary Diffusion.	411-421B
Deformation Characteristics of Dual-Phase Steels.	85-92A	The Coordination Cluster Theory—Description of the Activity Coefficients of Dilute Solutions of Oxygen and Sulfur in Binary Alloys.	427-437A
Structure—Property Relationships in Dual-Phase Cu—Al Alloys. I.—Individual Phases.	837-846A	The Use of Heat Flow Modeling to Explore Solidification Phenomena.	429-437B
Recrystallization and Formation of Austenite in Deformed Lath Martensitic Structure of Low-Carbon Steels.	1379-1388A	Application of the McNabb—Foster Trapping Equations to the Diffusion of Oxygen in Dilute Niobium Alloys.	471-478B
Martensite, Phase transformations		Vacuum Distillation of Liquid Metals. I.—Theory and Experimental Study.	539-543A
Structure—Property Relationships in Dual-Phase Cu—Al Alloys. II.—Alloy Behavior.	847-853A	Kinetics of Vaporization of Lead Sulfide.	581-588B
Martensitic stainless steels, Corrosion		Discussion of "A Gaussian-Based Formalism for the Representation of Free Energy as a Function of Composition on Binary Metallic Solutions".	633-641B
The Stress Corrosion Susceptibility of a Quenched and Tempered 12% CrMo Martensitic Stainless Steel.	913-921A	The Rate-Controlling Deformation Mechanisms in Superplasticity—a Critical Assessment.	644-645B
The Effect of Heat Treatments on the Corrosion Fatigue Properties of 13% Chromium Stainless Steel in 3% NaCl Aqueous Solution.	1521-1529A	Fracture in Eutectoid Two Phase Alloys. I.—Fracture in Alloys With Isolated Elastic Particles.	717-732A
Martensitic stainless steels, Mechanical properties		Fracture in Eutectoid Two Phase Alloys. II.—Fracture in Alloys With Isolated Plastic Particles.	873-879A
Influence of Corrosive Environments on Near-Threshold Fatigue Crack Growth in 403 Stainless Steel.	2177-2189A	Defective Two Sublattice Model for a Binary Liquid.	881-887A
Martensitic transformations		A Localized Soft Mode Model for the Nucleation of Thermelastic Martensitic Transformation: Application to the Beta— β A Transformation.	1107-1114A
An Examination of the Validity of Existing Empirical Formulas for the Calculation of M_s Temperature.	328-331A	Wedge-Type Creep Damage in Low-Cycle Fatigue.	1127-1134A
Deformation by Moving Interfaces.	509-538A	A Geometric Model for Fatigue Crack Closure Induced by Fracture Surface Roughness.	1207-1214A
Aging Effects in Copper-Based Shape Memory Alloys.	551-555A	Discussion of "An Approximate Analytical Demonstration of the Famous Darken Experiment".	1627-1631A
A Localized Soft Mode Model for the Nucleation of Thermelastic Martensitic Transformation: Application to the Beta— β A Transformation.	1127-1134A	Mass Transport of Carbon in One- and Two-Phase Iron—Nickel Alloys in a Temperature Gradient.	1658-1659A
Rapid Solidification Effects in Martensitic Cu—Zn—Al Alloys.	1367-1372A	The Early Stage of Ni_3Al Layer Growth in NiAl/Ni Diffusion Couples.	1713-1719A
The Alpha-Gamma Phase Boundaries and the T_0 for Fe—Mn Alloys.	2113-2119A	The Significance of the Dimensionless Constant in the Rate Equation for Superplastic Flow.	1921-1926A
Martensitic transformations, Alloying effects		Coarsening of SiO_2 Particles in Copper and MnS Inclusions in Steel.	2059-2061A
The Effect of an Inert Oxide Particle Dispersion on the Morphology of Martensite in Fe—27Ni—0.025C Alloys.	203-211A	Effects of Friction and High Torque on Fatigue Crack Propagation in Mode III.	2143-2153A
Martensitic transformations, Deformation effects		Mathematics	2197-2204A
Effects of Strain State and Strain Rate on Deformation-Induced Transformation in 304 Stainless Steel. I.—Magnetic Measurements and Mechanical Behavior.	619-626A	See Finite element method Mathematical analysis Mathematical models	
Effects of Strain State and Strain Rate on Deformation-Induced Transformation in 304 Stainless Steel. II.—Microstructural Study.	627-635A		
Mechanical Stability of Retained Austenite in Quenched and Tempered AISI 4340 Steel.	676-680A		
Martensitic transformations, Heating effects		Mattes	
Observations of Aging Effects in a Cu—Sn Shape Memory Alloy.	1687-1692A	See also Copper mattes	
Martensitic transformations, Stress effects			
Stress-Assisted Isothermal Martensitic Transformation: Application to TRIP Steels.	1907-1914A	Mattes, Chemical analysis	
Mass transfer		A Mineralogical Study of Nickel Mattes From the Kalgoorlie Nickel Smelter, Kalgoorlie, Western Australia.	141-152B
Vacuum Distillation of Liquid Metals. I.—Theory and Experimental Study.	581-588B		
Kinetics of Vaporization of Lead Sulfide.	633-641B		
Mass Transport of Carbon in One- and Two-Phase Iron—Nickel Alloys in a Temperature Gradient.	1713-1719A		
Low-Temperature Hot Corrosion of Cobalt-Based Alloys. II.—Reaction Mechanism.	1853-1864A		
Measuring instruments			
See Calorimeters Oxygen probes Thermocouples			
Mechanical properties			
See Creep (materials)			
Creep rate			
Creep rupture strength			
Creep strength			
Ductility			
Elastic constants			
Fatigue (materials)			
Fatigue life			
Fatigue strength			
Fracture toughness			
Hardness			
Hydrogen embrittlement			
Impact strength			
Microhardness			
Modulus of elasticity			
Notch sensitivity			
Plastic flow			
Plasticity			
Residual stress			
Shear strength			
Shear stress			
Superplasticity			
Temper brittleness			
Tensile properties			
Tensile strength			
Yield strength			
Mathematical models			
Correction to "The Significance of the Dimensionless Constant in the Rate Equation for Superplastic Flow".	2289A		
Fluidized Bed Electrowinning of Copper; Experiments Using 150 A and 1000 A Cells and Some Mathematical Modeling.	3-13B		
The Velocity Field in the Molten Slag Region of ESR Systems: A Comparison of Measurements in a Model System With Theoretical Predictions.	35-43B		
Mechanical tests			
See Compression tests Tension tests Torsion tests			

Mechanics

Mechanics	
See J Integral	
Kinetics	
Melt spinning	
Mechanical Properties of Fe—Si—B Amorphous Wires Produced by In-Rotating-Water Spinning Method.	373-382A
Melting	
See Electron beam melting	
Levitation melting	
Vacuum induction melting	
Melting furnaces	
See Bottom blown converters	
Melting points	
Dry Method Preparation and Melting Point of Cu ₂ SO ₄ .	515-517B
Memory (shape)	
See Shape memory	
Mercury (metal)	
The Velocity Field in the Molten Slag Region of ESR Systems: A Comparison of Measurements in a Model System With Theoretical Predictions.	35-43B
Mercury amalgams, Thermal properties	
A Gaussian-Based Formalism for the Representation of Free Energy as a Function of Composition of Binary Metallic Solutions.	213-225B
Mercury base alloys	
See Mercury amalgams	
Metal carbides	
See Titanium carbide	
Metal powders, Microstructure	
Microstructures of Rapidly Solidified Aluminum Alloy Sub-micron Powders.	13-23A
Metal powders, Synthesis	
The Production of Niobium/Tin Powders by Vapor-Deposition Processes.	625-631B
Metal scrap, Recovering	
The Extractive Metallurgy of Old Scrap Recycle.	135-139B
Metal scrap, Refining	
Vacuum Distillation of Liquid Metals. I.—Theory and Experimental Study.	581-588B
Vacuum Distillation of Liquid Metals. II.—Photographic Study.	589-591B
Metal working	
See Cold rolling	
Cold working	
Forging	
High energy rate forming	
Hot rolling	
Hot working	
Liquid metal forging	
Superplastic forming	
Swaging	
Thermomechanical treatment	
Metallic glasses, Corrosion	
Corrosion Behavior of Amorphous Fe—Cr—Al—P—C Ribbon Alloys.	901-905A
Metaliferous minerals	
See Ores	
Metallographic structures	
See Microstructure	
Metallography	
See Specimen preparation	
Metalloid compounds	
See Arsenic compounds	
Arsenides	
Silicon carbide	
Metalloids	
See Boron	
Tellurium	
Microalloyed steels	
See High strength low alloy steels	
Microanalysis	
Phase Analysis of Sintered and Heat Treated Alloy 718.	5-12A
The Morphology, Crystallography and Chemistry of Phases in As-Cast Nickel—Aluminum Bronze.	1337-1345A
The Detection of Monolayer Grain Boundary Segregations in Steels Using STEM-EDS X-Ray Microanalysis.	1397-1403A
Microchemistry	
Microstructural Investigation of the Oxidation of an Fe—3% Cr Alloy.	2103-2112A
Microfractography	
See Fractography	
Microhardness, Heating effects	
Structure—Property Relationships in Dual-Phase Cu—Al Alloys. I.—Individual Phases.	837-846A
Microhardness, Microstructural effects	
Effect of Defect Structure Upon the Mechanical Behavior of Beta-LiAl Through Dislocation Damping and Hardness Studies.	2173-2176A
Microparticles	
See Particles	
Microscopy	
See Electron microscopy	
Optical microscopy	
Scanning electron microscopy	
Transmission electron microscopy	
Microstructure	
See also Fibrous structure	
Lamellar structure	
Fatigue Crack Initiation and Strain-Controlled Fatigue of Some High-Strength Low-Alloy Steels.	59-72A
Microstructural Features Produced by the Reduction of Wustite in H ₂ /H ₂ O Gas Mixtures.	117-124B
Carbide Formation in a Low-Ferrite Austenitic Stainless Steel Weld Metal at 649°C.	173-174A
Intercritical Austenitization of Two Fe—Mn—C Steels.	575-579A
Fatigue Initiation Study of TMT Eutectoid Steel.	855-864A
Fracture in Equiaxed Two Phase Alloys. I.—Fracture in Alloys With Isolated Elastic Particles.	873-879A
Fracture in Equiaxed Two Phase Alloys. II.—Fracture in Alloys With Isolated Plastic Particles.	881-887A
Isothermal Transformation of Austenite to Pearlite and Upper Bainite in Eutectoid Steel.	975-978A
Position Trapping at Phase Interfaces and Dislocations in Pearlite Eutectoid Steel.	1177-1180A
Hydrogen Cracking in Nominally Pearlitic 1045 Steel.	1315-1318A
The Morphology, Crystallography and Chemistry of Phases in As-Cast Nickel—Aluminum Bronze.	1337-1345A
Splitting of Tungsten Wire in the Knife-Edge Compression Test.	1501-1510A
Characterization of a Rapidly Solidified Iron-Based Superalloy.	1535-1546A
Electromagnetic Containerless Reaction of Samarium With Cobalt for the Formation of Samarium—Cobalt Alloys.	1868-1871A
Microstructure, Alloying effects	
Structure and Properties of Hypoeutectic Al—Si—Mg Alloys Modified With Pure Strontium.	945-951A
The Influence of Cobalt on the Microstructure of the Nickel-Base Superalloy MAR-M247.	1775-1783A
Microstructure, Composition effects	
Effects of Cobalt on Structure, Microchemistry and Properties of a Wrought Nickel-Base Superalloy.	1021-1032A
Microstructure, Cooling effects	
Microstructures of Rapidly Solidified Aluminum Alloy Sub-micron Powders.	13-23A
The Effect of Quenching on the Solidification Structure and Transformation Behavior of Stainless Steel Welds.	1141-1152A
Influence of Cooling Rate on the Microstructure and Retained Austenite in an Intercritically Annealed Vanadium-Containing HSLA Steel.	1899-1906A
Microstructure, Deformation effects	
Fatigue and Creep—Fatigue Deformation of Several Nickel-Based Superalloys at 650°C.	1755-1765A
Microstructure, Heating effects	
Modulated Structures and G—P Zones in Al—Mg Alloys.	1373-1378A
Microstructure, Welding effects	
Microstructure and Mechanical Properties of Laser Welded Titanium 6Al—4V.	865-871A
Mig arc welding	
See Gas metal arc welding	
Mill scale	
See Scale (corrosion)	
Mineralogy	
A Mineralogical Study of Nickel Mattes From the Kalgoorlie Nickel Smelter, Kalgoorlie, Western Australia.	141-152B
Miscibility	
A Simple Bisection Technique for the Calculation of a Two-Solid or Two-Liquid Miscibility Gap in Binary Metallic Systems.	2097-2102A
Mobility	
See Dislocation mobility	
Modification	
Structure and Properties of Hypoeutectic Al—Si—Mg Alloys Modified With Pure Strontium.	945-951A
Modulus of elasticity	
Effect of Lithium on the Mechanical Properties and Microstructure of SiC Whisker-Reinforced Aluminum Alloys.	1511-1519A
Molds	
See Ingot molds	
Molten metals	
See Liquid metals	
Molten salts	
See Fused salts	
Molybdenum, Alloying additive	
The Role of Molybdenum in the Enhanced Resistance to Hydrogen Stress Cracking of AISI 4100 Steels.	1099-1101A
Molybdenum, Alloying elements	
Irradiation-Induced Mo ₂ C Precipitation in Ni—Mo.	213-219A
Relative Hardenabilities and Interaction Effects of Molybdenum and Vanadium in 4330 Alloy Steel.	319-320A
Measurement of Structural Parameters Important in Creep of Ni—Mo and Ni—W Solid Solutions.	1827-1836A
Molybdenum, Crystal lattices	
Operation of Near-Surface Dislocation Sources.	1199-1205A
Molybdenum, Powder technology	
Lime-Enhanced Hydrogen Reduction of Molybdenite.	275-282B

Nickel molybdenum chromium steels

Molybdenum, Recovering		Creep and Rupture of an ODS Alloy With High Stress Rupture Ductility.	1453-1462A
The Recovery of Molybdenum From Leach Solutions by Reduction.	565-570B	The Influence of Orientation on the Stress Rupture Properties of Nickel-Base Superalloy Single Crystals.	1747-1754A
Molybdenum, Refining		Fatigue and Creep—Fatigue Deformation of Several Nickel-Base Superalloys at 650°C.	1755-1765A
Deoxidation of High-Melting-Point Metals and Alloys in Vacuum.	241-249B	The Influence of Cobalt on the Tensile and Stress Rupture Properties of the Nickel-Base Superalloy MAR-M247.	1767-1774A
Molybdenum chromium nickel steels		Measurement of Structural Parameters Important in Creep of Ni—Mo and Ni—W Solid Solutions.	1827-1836A
See Nickel chromium molybdenum steels		Induced Creep and Creep Fatigue of a Nickel-Base Superalloy at Ambient Temperatures.	1951-1955A
Molybdenum chromium steels		Creep Fracture Processes of Oxide Dispersion Strengthened Mechanically Alloyed Inconel Alloy MA 754.	2286-2290A
See Chromium molybdenum steels			
Molybdenum compounds		Nickel base alloys, Metallography	
See also Molybdenum disulfide		Phase Analysis of Sintered and Heat Treated Alloy 718.	5-12A
Molybdenum compounds, Reduction (chemical)		Nickel base alloys, Microstructure	
The Recovery of Molybdenum From Leach Solutions by Reduction.	565-570B	The Influence of Cobalt on the Microstructure of the Nickel-Base Superalloy MAR-M247.	1775-1783A
Molybdenum disulfide, Reduction (chemical)		Nickel base alloys, Powder technology	
Lime-Enhanced Hydrogen Reduction of Molybdenite.	275-282B	The Effect of Defects on the Fatigue Crack Initiation Process in Two P/M Superalloys. I.—Fatigue Origins.	33-43A
Molybdenum nickel chromium steels		The Effect of Defects on the Fatigue Crack Initiation Process in Two P/M Superalloys. II.—Surface—Subsurface Transition.	45-52A
See Nickel chromium molybdenum steels		Nickel base alloys, Refining	
Molybdenum steels		Understanding the Role of Cerium During VIM Refining of Nickel—Chromium and Nickel—Iron Alloys.	603-611B
See Chromium molybdenum steels		Nickel base alloys, Structural hardening	
Nickel chromium molybdenum steels		Convergent Beam Diffraction Analysis of Dispersoids in Oxide Dispersion-Strengthened Alloys.	953-957A
Monocrystals		Electron Microscopic Analysis of Heterogeneous Precipitates in Hastelloy C-276.	979-984A
See Single crystals		Nickel base alloys, Thermal properties	
Neutron diffraction		Thermodynamics of the Superalloys.	959-965A
Measurement of a Stress Gradient Through the Bulk of an Aluminum Alloy Using Neutrons.	1069-1076A	Nickel chromium alloys, Corrosion	
Nickel, Alloying elements		Corrosion of Fe—Ni—Cr, Fe—Cr—Al and Fe—Ni—Cr—Al Alloys in H ₂ /H ₂ O/H ₂ S Mixtures at 1200°C.	1299-1311A
The Effect of an Inert Oxide Particle Dispersion on the Morphology of Martensite in Fe—27Ni—0.025C Alloys.	203-211A	Nickel chromium molybdenum steels, Corrosion	
Nickel, Binary systems		Theoretical Considerations on Corrosion Fatigue Crack Initiation.	649-655A
Activity of Manganese in Liquid Ni—Mn Alloys.	283-285B	Nickel chromium molybdenum steels, Heat treatment	
Nickel, Coatings		Coarsening of SiO ₂ Particles in Copper and MnS Inclusions in Steel.	2143-2153A
Pulsed Laser Treatment of Plasma-Sprayed Coatings.	479-483B	Nickel chromium molybdenum steels, Mechanical properties	
Nickel, Diffusion		Mode III Fatigue Crack Propagation in Low-Alloy Steel.	101-110A
Internal Friction Studies of Fast Diffusing Solutes in Thorium. The Early Stage of Ni ₃ Al Layer Growth in NiAl/Ni Diffusion Couples.	995-1001A	Effects of Compositional Variations and Aging Treatments on the Fracture Behavior of HY 130 Steel in Air and Hydrogen.	111-116A
1921-1926A		A Theory of Fatigue Crack Initiation at Inclusions.	117-123A
Nickel, Materials substitution		Further Observations on the Fracture of a Quenched and Tempered Steel in Hydrogen.	176-179A
Effects of Cobalt on Structure, Microchemistry and Properties of a Wrought Nickel-Base Superalloy.	1021-1032A	The Effect of Hydrogen Source on Crack Initiation in 4340 Steel.	305-311A
Nickel, Mechanical properties		The Influence of Notch Root Radius and Austenitizing Temperature on Fracture Appearance of As-Quenched Charpy-V Type AISI 4340 Steel Specimens.	1003-1013A
The Role of Sulfur in the Air Embrittlement of Nickel and Its Alloys.	1223-1232A	Influence of Gaseous Environments on Rates of Near-Threshold Fatigue Crack Propagation in NiCrMoV Steel.	1633-1645A
On Fracture Initiation Mechanisms and Dynamic Recrystallization During Hot Deformation of Pure Nickel.	1233-1238A	The Thermodynamics of Interactive Cosegregation of Phosphorus and Alloying Elements in Iron and Temper-Brittle Steels.	1693-1711A
Nickel, Solubility		Effect of Volume Fraction and Shape of Sulfide Inclusions on Through-Thickness Ductility and Impact Energy of High-Strength 4340 Plate Steels.	2239-2258A
Steady-State Rates of Dissolution of Stationary Iron, Cobalt and Nickel Cylinders in Liquid Copper.	175-184B	Nickel chromium molybdenum steels, Phase transformations	
Nickel, Ternary systems		Mechanical Stability of Retained Austenite in Quenched and Tempered AISI 4340 Steel.	678-680A
Extension of the Associated Solution Model to Ternary Metal—Sulfur Melts: Cu—Ni—S.	379-385B	Nickel chromium molybdenum steels, Structural hardening	
Nickel base alloys		Relative Hardenabilities and Interaction Effects of Molybdenum and Vanadium in 4330 Alloy Steel.	319-320A
See also Nickel chromium alloys		Nickel chromium steels	
Nickel base alloys, Coating		See also Nickel chromium molybdenum steels	
Interdiffusion Coefficients in the Ni ₂ Al ₃ (Gamma) Phase of the Ni—Al System.	1313-1314A	Nickel chromium steels, Mechanical properties	
Nickel base alloys, Crystal growth		The Fracture Behavior of Quenched and Tempered Manganese Steels.	827-836A
The Influence of Hot Working on the Subsequent Recrystallization of a Dispersion Strengthened Superalloy—MA 6000.	1463-1470A	The Role of Nitrogen in the Embrittlement of Steel.	1939-1950A
The Influence of Gamma Prime on the Recrystallization of an Oxide Dispersion Strengthened Superalloy—MA 6000E.	1665-1674A	Temper Embrittlement Diagram of NiCr Steel Doped With Phosphorus.	2205-2207A
Nickel base alloys, Diffusion		Nickel compounds, Crystal growth	
Hydrogen Transport in Nickel-Base Stainless Alloys.	1181-1186A	Recrystallization and Grain Growth in NiAl.	1563-1566A
Nickel base alloys, Directional solidification		Nickel compounds, Diffusion	
Coarsening and Microsegregation During Solidification of Ni—Al—Cr Dendritic Monocrystals.	1153-1159A	The Early Stage of Ni ₃ Al Layer Growth in NiAl/Ni Diffusion Couples.	1921-1926A
Nickel base alloys, Electrical properties		Nickel compounds, Physical properties	
Deterioration of Electromotive Force of Chromel—Alumel Thermocouples in Reducing Atmospheres at High Temperatures.	167-172A	Standard Free Energy of Formation of Ni ₃ As.	285-288B
Nickel base alloys, Irradiation		Nickel compounds, Reactions (chemical)	
Irradiation-Induced Mo ₂ C Precipitation in Ni—Mo.	213-219A	Mechanism of the Solid-State Displacement Reaction Between Iron and Nickel Oxide at 1000°C.	585-594A
Nickel base alloys, Mechanical properties		Nickel compounds, Thermal properties	
Hydrogen Embrittlement of Ultra-Pure Alloys of the Inconel 600 Type: Influence of the Additions of Elements (Carbon, Phosphorus, Tin, Antimony).	141-144A	Enthalpies of Formation of Borides of Iron, Cobalt and Nickel by Solution Calorimetry in Liquid Copper.	251-257B
Surface Wave Studies of Hydrogen Damage Incubation Time.	487-491A		
The Influence of Grain Boundary Phosphorus Concentration on Liquid Metal and Hydrogen Embrittlement of Monel 400.	611-618A	Nickel molybdenum chromium steels	
A Note on the Microstructural Dependence of Creep Strength in Inconel 700.	673-675A	See Nickel chromium molybdenum steels	
Effects of Cobalt on Structure, Microchemistry and Properties of a Wrought Nickel-Base Superalloy.	1021-1032A		
Effect of Environment on Fatigue and Creep Crack Growth in Inconel X-750 at Elevated Temperature.	1083-1090A		
Cyclic Hardening of Ni—14.4 Al-% Al Alloy Containing Coherent Precipitates.	1187-1198A		
The Role of Sulfur in the Air Embrittlement of Nickel and Its Alloys.	1223-1232A		
High-Cycle Fatigue Life of the Cast Nickel-Base-Superalloys IN 738 LC and IN 939.	1245-1255A		

Nickel molybdenum steels

Nickel molybdenum steels
See Nickel chromium molybdenum steels

Nickel ores, Melting

A Mineralogical Study of Nickel Mattes From the Kalgoorlie Nickel Smelter, Kalgoorlie, Western Australia.

141-152B

Nickel steels

See Nickel chromium molybdenum steels
Nickel chromium steels

Niobium, Alloying additive

The Role of Molybdenum in the Enhanced Resistance to Hydrogen Stress Cracking of AISI 4100 Steels.

1099-1101A

Niobium, Diffusion

Thermotransport of Hydrogen and Deuterium in Vanadium, Niobium and Tantalum.

821-825A

Niobium, Mechanical properties

Self-Fracture of Hydrogen-Charged Niobium.

320-321A

Niobium base alloys, Diffusion

Application of the McNabb—Foster Trapping Equations to the Diffusion of Oxygen in Dilute Niobium Alloys.
Hydrogen Diffusion in Nb-Ta Alloys.

539-543A
1675-1678A

Niobium base alloys, Refining

Deoxidation of High-Melting-Point Metals and Alloys in Vacuum.

241-249B

Niobium compounds, Powder technology

The Production of Niobium/Tin Powders by Vapor-Deposition Processes.

625-631B

Nitrides, Environment

Environmental Factors Affecting Localized Corrosion of 7075-T7351 Aluminum Alloy Plate.

161-166A

Nitrides

See Silicon nitride

Nitrogen, Alloying additive

Effect of Manganese and Nitrogen on the Solidification Mode in Austenitic Stainless Steel Welds.

2121-2130A

Nitrogen, Environment

Carburization and Gas Reactions of Hydrocarbon—Nitrogen Mixtures at 850 and 925°C.

267-273B

Nitrogen, Impurities

The Role of Nitrogen in the Embrittlement of Steel.

1939-1950A

Nitrogen, Sorption

Prediction of the Effects of Surface-Active Elements on Gas—Liquid Metal Kinetics.

357-367B

Nitrogen compounds

See Ammonia

Nitrates

Nonferrous alloys, Microstructure

The Usefulness of Integral Mean Curvature Measurements in the Study of the Kinetics of Coarsening.

1389-1395A

Nonferrous smelting

See Smelting

Nonmetallic inclusions

The Effect of Defects on the Fatigue Crack Initiation Process in Two P/M Superalloys. I.—Fatigue Origins.

33-43A

The Effect of Defects on the Fatigue Crack Initiation Process in Two P/M Superalloys. II.—Surface—Subsurface Transition.

45-52A

Effects of the Electromagnetic Stirring on the Removal of Inclusions of Oxide From Liquid Steel.

45-52B

Effect of Rare Earth Additions on the Inclusions and Properties of a Ca—Al Deoxidized Steel.

185-192B

Creep Fracture Processes of Oxide Dispersion Strengthened Mechanically Alloyed Inconel Alloy MA 754.

2286-2290A

Nonmetallic inclusions, Crystal growth

Coarsening of SiO₂ Particles in Copper and MnS Inclusions in Steel.

2143-2153A

Nonmetallic inclusions, Impurities

Effect of Volume Fraction and Shape of Sulfide Inclusions on Through-Thickness Ductility and Impact Energy of High-Strength 4340 Plate Steels.

2239-2258A

Normal distribution

Discussion of "A Gaussian-Based Formalism for the Representation of Free Energy as a Function of Composition on Binary Metallic Solutions".

644-645B

Notch ductility

See Ductility

Notch effect

See Notch sensitivity

Notch impact strength

See Impact strength

Notch sensitivity

The Influence of Notch Root Radius and Austenitizing Temperature on Fracture Appearance of As-Quenched Charpy-V Type AISI 4340 Steel Specimens.

1003-1013A

The Plastic Zone and Residual Stress Near a Notch and a Fatigue Crack in HSLA Steel.

1987-1995A

Notched bar tensile test

See Tension tests

Nuclear binding energy

See Binding energy (nuclear)

Nuclear forces

See Binding energy (nuclear)

Nuclear fuel claddings
See Nuclear fuel elements

Nuclear fuel elements

Deformation Behavior of Duplex Zircaloy-4—Oxygen Alloys. 1077-1082A

Nucleate boiling

A Numerical Simulation of the D.C. Continuous Casting Process Including Nucleate Boiling Heat Transfer.

593-602B

Nucleation

Effects of Strain State and Strain Rate on Deformation-Induced Transformation in 304 Stainless Steel. II.—Microstructural Study.

627-635A

Nuclei (transformation)

See Nucleation

Optical masers

See Lasers

Optical microscopy

Phase Analysis of Sintered and Heat Treated Alloy 718.

5-12A

Order disorder

See also Long range order

Short range order

Differential Scanning Calorimetry Evaluations in Alpha Cu—Al Alloys. Energetics.

801-809A

Structure—Property Relationships in Dual-Phase Cu—Al Alloys. I.—Individual Phases.

837-846A

Phase Stability Investigations of the Palladium—Cadmium System. I.—Thermodynamic Studies.

1115-1121A

Ordering

See Order disorder

Ores

See also Chalcocrite

Copper ores

Hematite

Nickel ores

Standard Free Energy of Formation of NiAsS.

285-288B

Orientation

See also Grain orientation

The Bainite Reaction in Fe—Si—C Alloys: the Secondary Stage.

789-800A

Oxidation

Deterioration of Electromotive Force of Chromel—Alumel Thermocouples in Reducing Atmospheres at High Temperatures.

167-172A

The Growth of Hematite Blades During the High-Temperature Oxidation of Iron.

929-935A

Corrosion of Fe—Ni—Cr, Fe—Cr—Al and Fe—Ni—Cr—Al Alloys in H₂O/H₂S Mixtures at 1200°C.

1299-1311A

Mechanism of Oxidation—Sulfation Reactions of CoO in the Presence of Na₂SO₄.

1647-1654A

CaS Formation and Oxidation in the System CaO—SiO₂—Al₂O₃ Measured by Electron Paramagnetic Resonance.

1997-2002A

Oxidation resistance

Oxidation Behavior of a Fine-Grained Rapidly Solidified 18-8 Stainless Steel.

473-485A

Microstructural Investigation of the Oxidation of an Fe—3% Cr Alloy.

2103-2112A

Oxide coatings

See Anodic coatings

Oxides

See also Aluminum oxide

Iron oxides

Lime

Wustite

Oxides, Reactions (chemical)

Mechanism of the Solid-State Displacement Reaction Between Iron and Nickel Oxide at 1000°C.

585-594A

Mechanism of Oxidation—Sulfation Reactions of CoO in the Presence of Na₂SO₄.

1647-1654A

Oxidizing

See Oxidation

Oxygen

Oxidation of Fe(II) in Sulfuric Acid Solutions With Dissolved Molecular Oxygen.

311-318B

Oxygen, Chemical analysis

Oxygen Probes Based on Calcia-Doped Hafnia or Calcium Zirconate for Use in Metallic Melts.

227-235B

Oxygen, Diffusion

Tracer Diffusivity of O¹⁸ in CaO—SiO₂ Melts at 1600°C.

237-240B

Application of the McNabb—Foster Trapping Equations to the Diffusion of Oxygen in Dilute Niobium Alloys.

539-543A

Oxygen, Solubility

The Influence of Solutes on Kinetics and Thermodynamics of Liquid Indium—Oxygen Systems.

53-59B

Activities of Oxygen in Liquid Cu—Sb and Cu—Ge Alloys.

77-83B

Oxygen Pressure Measurements of Silica Saturated Fe—O—SiO₂ Melts by the E.M.F. Method Using Zirconia Solid Electrolyte.

423-427B

The Coordination Cluster Theory—Description of the Activity Coefficients of Dilute Solutions of Oxygen and Sulfur in Binary Alloys.

429-437B

Oxygen, Ternary systems

Recomputation of Phase Equilibria in the Sodium—Carbon—Oxygen System: Effect of Oxygen.

1101-1102A

Oxygen, Trace elements

Deformation Modes of the Alpha-Phase of Ti—6Al—4V as a Function of Oxygen Concentration and Aging Temperature.

889-899A

Deformation Behavior of Duplex Zircaloy-4—Oxygen Alloys.	1077-1082A	pH factor	
Strain Aging and Strain Rate Sensitivity of Oxygen-Enriched (Alpha + Beta) Zircaloy-2.	1957-1964A	See pH	
Oxygen probes, Materials selection		pH value	
Oxygen Probes Based on Calcium-Doped Hafnia or Calcium Zirconate for Use in Metallic Melts.	227-235B	See pH	
Pack chromizing		Phase boundary	
Experimental and Theoretical Concentration Profiles at the Surface of Chromized Iron.	495-497A	Experimental Determination of the Austenite + Liquid Phase Boundaries of the Fe—C System.	1293-1297A
Packing (crystal density)		Phase decomposition	
See Crystal structure		See also Spindal decomposition The Bainite Reaction in Fe—Si—C Alloys: the Secondary Stage.	789-800A
Packing fraction		Phase diagram reactions	
See Binding energy (nuclear)		See Austenitizing Martensitic transformations Phase decomposition Spindal decomposition	
Palladium, Binary systems		Phase diagrams	
Phase Stability Investigations of the Palladium—Cadmium System. I.—Thermodynamic Studies.	1115-1121A	Computer Analysis of Phase Diagrams and Thermodynamic Properties of Cryolite-Based Systems. II.—The $\text{AlF}_3-\text{CaF}_2-\text{LiF}$, $\text{AlF}_3-\text{CaF}_2-\text{NaF}$ and $\text{CaF}_2-\text{LiF}-\text{NaF}$ Systems.	61-69B
Phase Stability Investigations of the Palladium—Cadmium System. II.—Structural Studies.	1123-1126A	Extension of the Associated Solution Model to Ternary Metal—Sulfur Melts: Cu—Ni—S.	379-385B
Palladium base alloys, Electrochemistry		Recomputation of Phase Equilibria in the Sodium— Carbon—Oxygen System: Effect of Oxygen.	1101-1102A
Potentiodynamic Polarization Analysis of Silver—Palladium Alloys in Chloride Solutions.	313-317A	Phase Stability Investigations of the Palladium—Cadmium System. II.—Structural Studies.	1123-1126A
Paramagnetic resonance		Experimental Determination of the Austenite + Liquid Phase Boundaries of the Fe—C System.	1293-1297A
See Electron paramagnetic resonance		Hydrogen-Related Phase Transformations in Austenitic Stainless Steels.	1355-1365A
Parameters		The Constitution and Phase Stability of Overlapping Melt Trails in Ag—Cu Alloys Produced by Continuous Laser Melt Quenching.	1879-1889A
See Lattice parameters		The Alpha-Gamma Phase Boundaries and the T_0 for Fe—Mn Alloys.	2113-2119A
Particle shape		Phase stability	
The Effect of Defects on the Fatigue Crack Initiation Process in Two P/M Superalloys. II.—Surface—Subsurface Transi- tion.	45-52A	Mechanical Stability of Retained Austenite in Quenched and Tempered AISI 4340 Steel.	676-680A
The Usefulness of Integral Mean Curvature Measurements in the Study of the Kinetics of Coarsening.	1389-1395A	Phase Stability Investigations of the Palladium—Cadmium System. II.—Structural Studies.	1123-1126A
Particle size		Hydrogen-Related Phase Transformations in Austenitic Stainless Steels.	1355-1365A
Heat Flow During Rapid Solidification of Undercooled Metal Droplets.	221-234A	Effects of Hydrogen Concentration on Slow Crack Growth in Stainless Steels.	1799-1808A
Low-Cycle Fatigue Behavior of Ti—6Al—2Sn—4Zr—6Mo. I.—The Role of Microstructure in Low-Cycle Crack Nucle- ation and Early Crack Growth.	257-268A		
Limestone Calcination in a Rotary Kiln.	369-378B		
Calorimetric Studies of Precipitation and Dissolution Kinetics in Aluminum Alloys 2219 and 7075.	761-769A		
Cyclic Hardening of Ni—14.4 At.-% Al Alloy Containing Co- herent Precipitates.	1187-1198A		
Low-Cycle Fatigue Behavior of Ti—Mn Alloys: Fatigue Life.	1275-1281A		
Particle size, Cooling effects		Phase transformations	
Microstructures of Rapidly Solidified Aluminum Alloy Sub- micron Powders.	13-23A	See also Austenitizing Martensitic transformations	
The Effect of Melt Refining Upon Inclusions in Aluminum.	31-34B	Enhanced Densification of White Cast Iron Powders by Cy- clic Phase Transformations Under Stress.	355-361A
Preparation and Properties of Aluminum Alloy Coconut Shell Char Particulate Composites.	485-494B	Carbide Transformations During Aging of Wear-Resistant Cob- alt Alloys.	545-550A
Tempering of 2.25%Cr—1%Mo Low-Carbon Steels.	557-563A	Intercritical Austenitization of Two Fe—Mn—C Steels.	575-579A
Finite Element Method (FEM) Calculations of Stress—Strain Behavior of Alpha-Beta Ti—Mn Alloys. I.—Stress—Strain Relations.	595-601A	The Bainite Reaction in Fe—Si—C Alloys: the Primary Stage.	777-787A
Finite Element Method (FEM) Calculations of Stress—Strain Behavior of Alpha-Beta Ti—Mn Alloys. II.—Stress and Strain Distributions.	603-609A	The Effect of Quenching on the Solidification Structure and Transformation Behavior of Stainless Steel Welds.	1141-1152A
A Note on the Microstructural Dependence of Creep Strength in Inconel 700.	673-675A	The Isothermal Austenite—Ferrite Transformation in Some Deformed Vanadium Steels.	1347-1353A
The Usefulness of Integral Mean Curvature Measurements in the Study of the Kinetics of Coarsening.	1389-1395A	Hydrogen-Related Phase Transformations in Austenitic Stainless Steels.	1355-1365A
Characterization of a Rapidly Solidified Iron-Based Super- alloy.	1535-1546A	Discussion of "Diffusion-Controlled Phase Transformation in a Finite Region".	1655-1658A
The Structure of Rapidly Solidified Al—Fe—Cr Alloys.	1891-1898A		
Coarsening of SiO_2 Particles in Copper and MnS Inclusions in Steel.	2143-2153A	Phase transformations, Heating effects	
		Phase Transformations in a Wrought Co—Cr—Mo—C Alloy.	1161-1168A
Particle size distribution, Radiation effects		Phase transformations, Temperature effects	
Irradiation-Induced Mo_2C Precipitation in Ni—Mo.	213-219A	Isothermal Transformation of Austenite to Pearlite and Upper Bainite in Eutectoid Steel.	975-978A
Particles		Phases (state of matter)	
Fracture in Equiaxed Two Phase Alloys. I.—Fracture in Al- loys With Isolated Elastic Particles.	873-879A	See also Gas phases Intermetallic phases Liquid phases	
Fracture in Equiaxed Two Phase Alloys. II.—Fracture in Al- loys With Isolated Plastic Particles.	881-887A	Finite Element Method (FEM) Calculations of Stress—Strain Behavior of Alpha-Beta Ti—Mn Alloys. I.—Stress—Strain Relations.	595-601A
Passivation		Finite Element Method (FEM) Calculations of Stress—Strain Behavior of Alpha-Beta Ti—Mn Alloys. II.—Stress and Strain Distributions.	603-609A
Potentiodynamic Polarization Analysis of Silver—Palladium Alloys in Chloride Solutions.	313-317A	The Morphology, Crystallography and Chemistry of Phases in As-Cast Nickel—Aluminum Bronze.	1337-1345A
Stress Corrosion Cracking of Sensitized Type 304 Stainless Steel in Thiosulfate Solutions.	2015-2026A	Phases (state of matter), Crystal lattices	
Pearlite, Metallography		The Constitution and Phase Stability of Overlapping Melt Trails in Ag—Cu Alloys Produced by Continuous Laser Melt Quenching.	1879-1889A
The Cleavage Plane of Pearlite.	1865-1868A		
Pellets		Phosphorus, Alloying additive	
Factors Influencing the Production Rate and Quality of Lead Sinter.	15-29B	Hydrogen Embrittlement of Ultra-Pure Alloys of the Inconel 600 Type: Influence of the Additions of Elements (Carbon, Phosphorus, Tin, Antimony).	141-144A
Pellets, Reduction (chemical)		Phosphorus, Alloying elements	
Changes in Diffusivity Due to Sintering in Metallized Iron Oxide Pellets.	518-520B	Studies on the Development of High-Strength Dual-Phase Steel Sheets With High r_m Values.	1257-1262A
Perforations		Phosphorus, Diffusion	
See Holes		On Grain Boundary Segregation in Austenitic Stainless Steels.	2281-2285A
Permeability		Phosphorus, Dopants	
Mathematical Treatment of Permeation for Cylindrical Geom- etry.	174-176A	The Fracture Behavior of Quenched and Tempered Manga- nese Steels.	827-836A
Hydrogen Transport in Nickel-Base Stainless Alloys.	1181-1186A	Compositional Effects on the High-Temperature Ductility of 1Cr—1.25Mo—0.25V Steel.	1471-1481A
pH			
The Relative Uptake of Several Vaporized Radiotracers at 1300°C as a Function of Basicity in Selected Oxide Melts.	645-648B		

Phosphorus

Temper Embrittlement Diagram of NiCr Steel Doped With Phosphorus.	2205-2207A	
Phosphorus, Impurities		
The Thermodynamics of Interactive Cosegregation of Phosphorus and Alloying Elements in Iron and Temper-Brittle Steels.	1693-1711A	
Phosphorus, Trace elements		
The Influence of Grain Boundary Phosphorus Concentration on Liquid Metal and Hydrogen Embrittlement of Monel 400.	611-618A	
The Effect of Phosphorus Content on the Hydrogen Stress Cracking of High-Strength 4130 Steel.	907-912A	
Photo oxidation		
See Oxidation		
Physical properties		
See Diffusivity		
Heat of activation		
Heat of formation		
Heat of fusion		
Heat of mixing		
Melting points		
Miscibility		
Permeability		
Porosity		
Resistivity		
Solubility		
Texture		
Thermal expansion		
Thermoelectricity		
Thixotropy		
Vapor pressure		
Viscosity		
Piezoresistance		
See Electrical resistance		
Pinning (dislocation)		
Differential Scanning Calorimetry Evaluations in Alpha Cu—Al Alloys, Energetics.	801-809A	
Pitting (corrosion), Environmental effects		
Environmental Factors Affecting Localized Corrosion of 7075-T7351 Aluminum Alloy Plate.	161-166A	
Plasma arc casting		
See Casting		
Plasma arc plating		
See Plasma spraying		
Plasma arc spraying		
See Plasma spraying		
Plasma jet spraying		
See Plasma spraying		
Plasma spraying		
Pulsed Laser Treatment of Plasma-Sprayed Coatings.	479-483B	
Plaster of Paris		
See Calcium compounds		
Plastic deformation		
Deformation by Moving Interfaces.	509-538A	
Plastic flow		
The Occurrence of Shear Bands in Isothermal, Hot Forging.	275-288A	
Plastic flow, Composition effects		
Effect of Carbon Content on the Plastic Flow of Plain Carbon Steels at Elevated Temperatures.	125-134A	
Plastic flow, Deformation effects		
Flow Localization and Shear Band Formation in a Precipitation Strengthened Austenitic Stainless Steel.	1263-1274A	
Plastic flow, Temperature effects		
Stress-Assisted Isothermal Martensitic Transformation: Application to TRIP Steels.	1907-1914A	
Plastic strain		
See Plastic deformation		
Plasticity		
See also Superplasticity		
Plastic Behavior of 70/30 Brass Sheet.	1491-1500A	
The Plastic Zone and Residual Stress Near a Notch and a Fatigue Crack in HSLA Steel.	1987-1995A	
Plastic Instability in U-Notted Bend Specimens of Spheroidized AISI 1090 Steel.	2209-2218A	
Platinum metal alloys		
See Iridium base alloys		
Palladium base alloys		
Platinum metals		
See Palladium		
Point defects		
See Lattice vacancies		
Polarization (electrodes)		
See also Anodic polarization		
Polarization (electrodes), Composition effects		
Potentiodynamic Polarization Analysis of Silver—Palladium Alloys in Chloride Solutions.	313-317A	
Pole figures		
On Penetration of Shear Texture into Rolled Aluminum and Copper.	665-669A	
Poling		
See Deoxidizing		
Pores		
See Porosity		
Porosity		
The Effect of Defects on the Fatigue Crack Initiation Process in Two P/M Superalloys. I.—Fatigue Origins.	33-43A	
The Effect of Defects on the Fatigue Crack Initiation Process in Two P/M Superalloys. II.—Surface—Subsurface Transition.	45-52A	
High-Cycle Fatigue Life of the Cast Nickel-Base-Superalloys IN 738 LC and IN 939.	1245-1255A	
Positron annihilation		
Positron Trapping at Phase Interfaces and Dislocations in Pearlite Eutectoid Steel.	1177-1180A	
Potential (electric)		
See Electric potential		
Pots (electrolytic)		
See Electrolytic cells		
Powder compacts, Mechanical properties		
Characterization of a Rapidly Solidified Iron-Based Superalloy.	1535-1546A	
Superplasticity in Rapidly Solidified White Cast Irons.	1785-1792A	
Powder compacts, Microstructure		
The Structure of Rapidly Solidified Al—Fe—Cr Alloys.	1891-1898A	
Powder metallurgy parts, Mechanical properties		
The Effect of Defects on the Fatigue Crack Initiation Process in Two P/M Superalloys. I.—Fatigue Origins.	33-43A	
The Effect of Defects on the Fatigue Crack Initiation Process in Two P/M Superalloys. II.—Surface—Subsurface Transition.	45-52A	
Powder metallurgy parts, Metallography		
Phase Analysis of Sintered and Heat Treated Alloy 718.	5-12A	
Powders		
See Metal powders		
Power supplies		
See Turbogenerators		
Precious metal alloys		
See Iridium base alloys		
Palladium base alloys		
Silver base alloys		
Precious metals		
See Palladium		
Silver		
Precipitates		
Formation Modes of the Alpha-Phase of Ti—6Al—4V as a Function of Oxygen Concentration and Aging Temperature.	889-899A	
The Morphology, Crystallography and Chemistry of Phases in As-Cast Nickel—Aluminum Bronze.	1337-1345A	
The Isothermal Austenite—Ferrite Transformation in Some Deformed Vanadium Steels.	1347-1353A	
The Usefulness of Integral Mean Curvature Measurements in the Study of the Kinetics of Coarsening.	1389-1395A	
The Structure of Rapidly Solidified Al—Fe—Cr Alloys.	1891-1898A	
Precipitates, Crystal lattices		
Silicide Precipitation in Alloy Ti—6Al—5Zr—0.5Mo—0.25Si.	771-775A	
Precipitates, Metallography		
Phase Analysis of Sintered and Heat Treated Alloy 718.	5-12A	
Precipitates, Phases (state of matter)		
Electron Microscopic Analysis of Heterogeneous Precipitates in Hastelloy C-276.	979-984A	
Precipitation		
See also Intergranular precipitation		
Calorimetric Studies of Precipitation and Dissolution Kinetics in Aluminum Alloys 2219 and 7075.	761-769A	
Precipitation, Radiation effects		
Irradiation-Induced Mo ₂ C Precipitation in Ni—Mo.	213-219A	
Precipitation hardening		
See also Aging (artificial)		
Secondary hardening		
Strain aging		
Effect of Composition and High-Energy Rate Forging on the Onset of Precipitation in an Iron-Base Superalloy.	345-353A	
Carbide Transformations During Aging of Wear-Resistant Cobalt Alloys.	545-550A	
Aging Effects in Copper-Based Shape Memory Alloys.	551-555A	
Combined Recrystallization and Precipitation in a Cu—9Ni—6Sn Alloy.	565-573A	
Mechanical Behavior of Alloy 800 at 838°K.	637-648A	
Thermomechanical Strengthening of High-Strength, Chromium—Molybdenum Steel.	671-673A	
Silicide Precipitation in Alloy Ti—6Al—5Zr—0.5Mo—0.25Si.	771-775A	
Influence of Grain Size and Age-Hardening on Dislocation Pile-Ups and Tensile Fracture for a Ti—Al Alloy.	1283-1292A	
Aging Susceptibility of Retained and Epitaxial Ferrite in Dual-Phase Steels.	2061-2064A	
Precipitation hardening, Alloying effects		
Microstructure—Property Relationships of Two Al—3Li—2Cu—0.2Zr—X Cd Alloys.	401-410A	
Precipitation hardening, Composition effects		
Tempering of 2.25%Cr—1%Mo Low-Carbon Steels.	557-563A	
Effects of Cobalt on Structure, Microchemistry and Properties of a Wrought Nickel-Base Superalloy.	1021-1032A	
Precipitation hardening, Vibration effects		
Surface Hardening and Microstructural Changes in 304 Stainless Steel Resulting From Elevated-Temperature Ultrasonic Vibration.	1167-1176A	

Reduction (electrolytic)

Precipitation hardening alloys, Mechanical properties		
Cyclic Hardening of Ni—14.4 At.-% Al Alloy Containing Coherent Precipitates.	1187-1198A	
Flow Localization and Shear Band Formation in a Precipitation Strengthened Austenitic Stainless Steel.	1263-1274A	
Influence of Test Temperature and Microstructure on the Tensile Properties of Titanium Alloys.	1435-1443A	
Induced Creep and Creep/Fatigue of a Nickel-Based Superalloy at Ambient Temperatures.	1951-1955A	
Precipitation heat treatment		
See Aging (artificial)		
Precipitation hardening		
Secondary hardening		
Preferential attack (corrosion)		
See also Intergranular corrosion		
Low-Temperature Hot Corrosion of Cobalt-Based Alloys. II.—Reaction Mechanism.	1853-1864A	
Pressure		
See Vapor pressure		
Pressure measurement		
Oxygen Pressure Measurements of Silica Saturated Fe—O—SiO ₂ Melts by the E.M.F. Method Using Zirconia Solid Electrolyte.	423-427B	
Probes		
See Oxygen probes		
Projection (forecasting)		
See Forecasting		
Propagation		
See Crack propagation		
Propeller shafts		
See Shafts (power)		
Properzi process		
See Continuous casting		
Protective atmospheres		
See Controlled atmospheres		
Quantitative analysis		
See also Electrolytic analysis		
A New Procedure for Determining Volume Fraction of Primary Carbides in High-Speed and Related Tool Steels.	185-191A	
Quench aging		
Studies on the Development of High-Strength Dual-Phase Steel Sheets With High r_m Values.	1257-1262A	
Quench hardenability, Alloying effects		
Relative Hardenabilities and Interaction Effects of Molybdenum and Vanadium in 4330 Alloy Steel.	319-320A	
Quenching (cooling)		
See also Quench aging		
Quenching and tempering		
Rapid solidification		
Splat cooling		
The Effect of Quenching on the Solidification Structure and Transformation Behavior of Stainless Steel Welds.	1141-1152A	
Quenching and tempering		
Fatigue Crack Initiation and Propagation in a Quenched and Tempered Niobium-Bearing HSLA Steel.	393-399A	
The Fracture Behavior of Quenched and Tempered Manganese Steels.	827-836A	
The Stress Corrosion Susceptibility of a Quenched and Tempered 12% CrMoV Martensitic Stainless Steel.	913-921A	
Quenching stresses		
See Residual stress		
R H process		
See Vacuum degassing		
Radiant heating		
See Laser beam heating		
Radioactive tracers		
Tracer Diffusivity of O ¹⁸ in CaO—SiO ₂ Melts at 1600°C.	237-240B	
The Relative Uptake of Several Vaporized Radiotracers at 1300°C as a Function of Basicity in Selected Oxide Melts.	645-648B	
Radiocrystallography		
See Crystallography		
Rail steels, Mechanical properties		
Cyclic Deformation of Pearlite Eutectoid Rail Steel.	2035-2047A	
Rapid solidification		
Microstructures of Rapidly Solidified Aluminum Alloy Sub-micron Powders.	13-23A	
Heat Flow During Rapid Solidification of Undercooled Metal Droplets.	221-234A	
Microstructures, Mechanical Properties and Electrical Resistivity of Rapidly Quenched Fe—Cr—Al Alloys.	337-343A	
Oxidation Behavior of a Fine-Grained Rapidly Solidified 18-8 Stainless Steel.	473-485A	
Rapid Solidification Effects in Martensitic Cu—Zn—Al Alloys.	1367-1372A	
Characterization of a Rapidly Solidified Iron-Based Superalloy.	1535-1546A	
Superplasticity in Rapidly Solidified White Cast Irons.	1785-1792A	
The Structure of Rapidly Solidified Al—Fe—Cr Alloys.	1891-1898A	
Rare earth compounds		
See Samarium compounds		
Rare earth metals		
See also Cerium		
Rare earth metals, Alloying additive		
Effect of Rare Earth Additions on the Inclusions and Properties of a Ca—Al Deoxidized Steel.	185-192B	
Rayleigh waves		
See Surface waves		
Reaction kinetics		
Steady-State Rates of Dissolution of Stationary Iron, Cobalt and Nickel Cylinders in Liquid Copper.	175-184B	
Carburization and Gas Reactions of Hydrocarbon—Nitrogen Mixtures at 850 and 925°C.	267-273B	
Lime-Enhanced Hydrogen Reduction of Molybdenite.	275-282B	
Oxidation of Fe(II) in Sulfuric Acid Solutions With Dissolved Molecular Oxygen.	311-318B	
Kinetics of Chlorination of Cobalt and Co—10 At.-% Pt Alloy by Reaction With HCl Gas.	349-356B	
Prediction of the Effects of Surface-Active Elements on Gas—Liquid Metal Kinetics.	357-367B	
The Reaction of Coke Specimens in an Environment Where Both the Temperature and the Gas Composition Are Time Dependent.	513-515B	
Mechanism of the Solid-State Displacement Reaction Between Iron and Nickel Oxide at 1000°C.	585-594A	
Kinetics of Vaporization of Lead Sulfide.	633-641B	
Calorimetric Studies of Precipitation and Dissolution Kinetics in Aluminum Alloys 2219 and 7075.	761-769A	
Mechanism of Oxidation—Sulfation Reactions of CoO in the Presence of Na ₂ SO ₄ .	1647-1654A	
Reaction kinetics, Impurity effects		
Rate of Decarburization of Iron—Carbon Melts. I.—Experimental Determination of the Effect of Sulfur.	403-409B	
Rate of Decarburization of Iron—Carbon Melts. II.—A Mixed-Control Model.	411-421B	
Reactions (chemical)		
See also Chlorination		
Deoxidizing		
Desulfurizing		
Desiccation		
Fluidized bed electrolysis		
Hydrogen reduction		
Hydrogenation		
Oxidation		
Sulfation		
Limestone Calcination in a Rotary Kiln.	369-378B	
Dry Method Preparation and Melting Point of Cu ₂ SO ₄ .	515-517B	
Electromagnetic Containerless Reaction of Samarium With Cobalt for the Formation of Samarium—Cobalt Alloys.	1868-1871A	
Reactivity (chemical)		
See Activity (chemical)		
Reactor vessels (chemical)		
See Chemical reactors		
Reactors		
See Chemical reactors		
Reclamation		
See Recycling		
Recovery		
Operation of Near-Surface Dislocation Sources.	1199-1205A	
Recrystallization		
See also Grain refinement		
Temperature Dependence of Sustained-Load Subcritical Crack Growth in Ti—6Al—6V—2Sn.	497-500A	
Combined Recrystallization and Precipitation in a Cu—3Ni—6Sn Alloy.	565-573A	
Effect of the Degree of Prior Cold Work on the Grain Volume Distribution and the Rate of Grain Growth of Recrystallized Aluminum.	985-993A	
On Fracture Initiation Mechanisms and Dynamic Recrystallization During Hot Deformation of Pure Nickel.	1233-1238A	
Recrystallization and Formation of Austenite in Deformed Lath Martensitic Structure of Low-Carbon Steels.	1379-1388A	
Recrystallization and Grain Growth in NiAl.	1563-1566A	
The Influence of Gamma Prime on the Recrystallization of an Oxide Dispersion Strengthened Superalloy—MA 6000E.	1665-1674A	
The Influence of Grain Structure on the Ductility of the Al—Cu—Li—Mn—Cd Alloy 2020.	2259-2269A	
Recrystallization, Alloying effects		
Microstructure—Property Relationships of Two Al—3Li—2Cu—0.27—X Cd Alloys.	401-410A	
Recrystallization, Deformation effects		
The Influence of Hot Working on the Subsequent Recrystallization of a Dispersion Strengthened Superalloy—MA 6000.	1463-1470A	
Recrystallization, Heating effects		
Heating Rate Effects on Recrystallized Grain Size in Two Al—Zn—Mg—Cu Alloys.	193-198A	
Primary Recrystallization Textures in Dilute Fe—C Alloys.	199-202A	
Recycling		
The Extractive Metallurgy of Old Scrap Recycle.	135-139B	
Red hardness		
See Hardness		
Reducing atmospheres		
The Effect of Oxygen Potential on Phosphorus in the CaO—Al ₂ O ₃ System.	643-644B	
Reduction (chemical)		
See Direct reduction		
Flash smelting		
Hydrogen reduction		
Reduction (electrolytic)		
See Electrowinning		

Reduction (metal working)

Reduction (metal working)		
See Cold rolling		
Hot rolling		
Refining		
<i>See also</i> Electroslag refining		
Vacuum refining		
The Effect of Melt Refining Upon Inclusions in Aluminum.	31-34B	
Lime-Enhanced Hydrogen Reduction of Molybdenum.	275-282B	
Refractory alloys		
<i>See</i> Niobium base alloys		
Tantalum base alloys		
Refractory metal compounds		
<i>See</i> Molybdenum compounds		
Molybdenum disulfide		
Niobium compounds		
Refractory metals		
<i>See</i> Chromium		
Molybdenum		
Niobium		
Tantalum		
Tungsten		
Vanadium		
Reinforcement		
<i>See</i> Fiber composites		
Repair welding		
High-Cycle Fatigue of Weld Repaired Cast Ti—6Al—4V.	1589-1594A	
Residual stress		
The Plastic Zone and Residual Stress Near a Notch and a Fatigue Crack in HSLA Steel.	1987-1995A	
Residual stress, Mechanical properties		
The State of Residual Stress in the Near Surface Region of Homogeneous and Heterogeneous Materials After Grinding.	1239-1244A	
Resistance welds		
<i>See</i> Welded joints		
Resistivity		
Microstructures, Mechanical Properties and Electrical Resistivity of Rapidly Quenched Fe—Cr—Al Alloys.	337-343A	
Retained austenite		
Mechanical Stability of Retained Austenite in Quenched and Tempered AISI 4340 Steel.	676-680A	
Tempering Characteristics of a Vanadium-Containing Dual-Phase Steel.	1679-1686A	
Retained austenite, Cooling effects		
Influence of Cooling Rate on the Microstructure and Retained Austenite in an Intercritically Annealed Vanadium-Containing HSLA Steel.	1899-1906A	
Retained austenite, Heating effects		
Fracture Toughness of AISI M2 High-Speed Steel and Corresponding Matrix Tool Steel.	1595-1605A	
Optimization of Fe/Cr/C Base Structural Steels for Improved Strength and Toughness.	2227-2237A	
Revaporation		
<i>See</i> Vaporizing		
Rheocasting		
Effect of Strain Rate on Deformation Behavior of Semisolid Dendritic Alloys.	1809-1819A	
Rheological properties		
<i>See also</i> Thixotropy		
Viscosity		
Study of the Rheological Behavior of the Beta Prime Phase of an Equiaxed Ag—Mg Alloy.	251-255A	
Ribbons (metallic)		
<i>See</i> Tapes (metallic)		
Roasting		
Regenerative Heat Transfer in Rotary Kilns (for Limestone). Limestone Calcination in a Rotary Kiln.	153-163B 369-378B	
Rolling		
<i>See</i> Cold rolling		
Hot rolling		
Rolling texture		
On Penetration of Shear Texture Into Rolled Aluminum and Copper.	665-669A	
Rolling texture, Deformation effects		
Grain Boundary Strengthening in Strongly Textured Magnesium Produced by Hot Rolling.	2219-2226A	
Rolling texture, Heating effects		
Primary Recrystallization Textures in Dilute Fe—C Alloys.	199-202A	
Room temperature		
Aging Susceptibility of Retained and Epitaxial Ferrite in Dual-Phase Steels.	2061-2064A	
Rotary furnaces		
Regenerative Heat Transfer in Rotary Kilns (for Limestone).	153-163B	
Rotary kilns		
<i>See</i> Kilns		
Rotating generators		
<i>See</i> Turbogenerators		
Rotating machines		
<i>See</i> Turbogenerators		
Roughing (rolling)		
<i>See</i> Hot rolling		
Roughness		
A Geometric Model for Fatigue Crack Closure Induced by Fracture Surface Roughness.	1627-1631A	
Rupture strength		
<i>See</i> Creep rupture strength		
Saline water		
<i>See</i> Salt water		
Salt (sodium chloride)		
<i>See</i> Sodium chloride		
Salt water, Environment		
Theoretical Considerations on Corrosion Fatigue Crack Initiation.	649-655A	
Samarium compounds, Crystal growth		
Electromagnetic Containerless Reaction of Samarium With Cobalt for the Formation of Samarium—Cobalt Alloys.	1868-1871A	
Sap process		
<i>See</i> Dispersion hardening		
Scale (corrosion)		
Kinetics and Mechanism of the Reaction of Iron—Chromium and Iron—Chromium—Molybdenum Alloys With Chlorine Gas.	153-159A	
Mechanism of the Solid-State Displacement Reaction Between Iron and Nickel Oxide at 1000°C.	585-594A	
Scale (corrosion), Chemical analysis		
Microstructural Investigation of the Oxidation of an Fe—3% Cr Alloy.	2103-2112A	
Scale (corrosion), Phases (state of matter)		
Oxidation Behavior of a Fine-Grained Rapidly Solidified 18-8 Stainless Steel.	473-485A	
Corrosion of Fe—Ni—Cr, Fe—Cr—Al and Fe—Ni—Cr—Al Alloys in $H_2/O/H_2S$ Mixtures at 1200°C.	1299-1311A	
Scanning electron microscopy		
The Detection of Monolayer Grain Boundary Segregations in Steels Using STEM-EDS X-Ray Microanalysis.	1397-1403A	
Schottky defect		
<i>See</i> Lattice vacancies		
Scrap		
<i>See</i> Metal scrap		
Scrap metal		
<i>See</i> Metal scrap		
Season cracking		
<i>See</i> Stress corrosion cracking		
Secondary hardening		
Structure—Property Relationships in Dual-Phase Cu—Al Alloys. I.—Individual Phases.	837-846A	
Seeding		
<i>See</i> Nucleation		
Segregations		
Microstructures of Rapidly Solidified Aluminum Alloy Submicron Powders.	13-23A	
Effect of Sulfur and Antimony on the Intergranular Fracture of Iron at Cathodic Potentials.	241-249A	
The Effect of Melt Composition on Solidification Cracking of Steel, With Particular Reference to Continuous Casting.	259-266B	
The Effect of Mold Precession on Channel and Macrosegregation in Ammonium Chloride—Water Analog Castings.	495-501B	
Carbide Transformations During Aging of Wear-Resistant Cobalt Alloys.	545-550A	
The Influence of Grain Boundary Phosphorus Concentration on Liquid Metal and Hydrogen Embrittlement of Monel 400.	611-618A	
Coarsening and Microsegregation During Solidification of Ni—Al—Cr Dendritic Monocrystals.	1153-1159A	
The Detection of Monolayer Grain Boundary Segregations in Steels Using STEM-EDS X-Ray Microanalysis.	1397-1403A	
The Thermodynamics of Interactive Cosegregation of Phosphorus and Alloying Elements in Iron and Temper-Brittle Steels.	1693-1711A	
Temper Embrittlement Diagram of NiCr Steel Doped With Phosphorus.	2205-2207A	
Segregations, Chemical analysis		
Surface Segregation in Austenitic Stainless Steel.	745-752A	
Segregations, High temperature effects		
The Role of Sulfur in the Air Embrittlement of Nickel and Its Alloys.	1223-1232A	
Self diffusion		
<i>See</i> Diffusion		
Semicontinuous casting		
<i>See</i> Continuous casting		
Semikilling		
<i>See</i> Deoxidizing		
Sensing		
<i>See</i> Detection		
Sensitivity		
<i>See</i> Notch sensitivity		
Sensitizing		
Stress Corrosion Cracking of Sensitized Type 304 Stainless Steel in Thioulate Solutions.	2015-2026A	
On Grain Boundary Segregation in Austenitic Stainless Steels.	2281-2285A	
Shaft kilns		
<i>See</i> Kilns		

Sodium compounds

Shafts (power), Mechanical properties			
Mode III Fatigue Crack Propagation in Low-Alloy Steel.	101-110A		
Effects of Friction and High Torque on Fatigue Crack Propagation in Mode III.	2197-2204A		
Shape			
See Particle shape			
Shape memory			
Deformation by Moving Interfaces.	509-538A		
Shape memory, Heating effects			
Aging Effects in Copper-Based Shape Memory Alloys.	551-555A		
Observations of Aging Effects in a Cu—Sn Shape Memory Alloy.	1687-1692A		
Shear properties			
See Shear strength			
Shear stress			
Shear strength			
Althermal Solid Solution Hardening in Tantalum.	1015-1020A		
Characterization of In-Based Eutectic Alloys Used in Josephson Packaging.	1547-1562A		
Shear strength, Temperature effects			
The Influence of Substructure on the Elevated- and Room-Temperature Strength of a 26Cr—1Mo Ferritic Stainless Steel.	447-456A		
Shear stress			
The Occurrence of Shear Bands in Isothermal, Hot Forging. Effects of Strain State and Strain Rate on Deformation-Induced Transformation in 304 Stainless Steel. II.—Microstructural Study.	275-288A		
On Penetration of Shear Texture Into Rolled Aluminum and Copper.	627-635A		
Correlation of Substructure With Time-Dependent Fatigue Properties of AISI 304 Stainless Steel.	665-669A		
1577-1588A			
Sheet metal			
Studies on the Development of High-Strength Dual-Phase Steel Sheets With High r_m Values.	1257-1262A		
Sheet metal, Mechanical properties			
Plastic Behavior of 70/30 Brass Sheet.	1491-1500A		
Sheet metal, Welding			
The Fatigue Crack Growth Behavior of Electron-Beam Welded A286 Superalloy.	1483-1489A		
Shielded arc welding			
See Gas metal arc welding			
Gas tungsten arc welding			
Short arc welding			
See Gas metal arc welding			
Short range order			
Measurement of Structural Parameters Important in Creep of Ni—Mo and Ni—W Solid Solutions.	1827-1836A		
Short-Range Ordering Kinetics in 316 Austenitic Stainless Steel.	1915-1919A		
Sigma hard facing			
See Gas metal arc welding			
Sigma welding			
See Gas metal arc welding			
Silicates, Chemical analysis			
The Relative Uptake of Several Vaporized Radiotracers at 1300°C as a Function of Basicity in Selected Oxide Melts.	645-648B		
Silicates, Diffusion			
Tracer Diffusivity of O ¹⁸ in CaO—SiO ₂ Melts at 1600°C.	237-240B		
Silicides, Crystal growth			
Silicide Precipitation in Alloy Ti—6Al—5Zr—0.5Mo—0.25Si.	771-775A		
Silicon carbide, Composite materials			
Effect of Lithium on the Mechanical Properties and Microstructure of SiC Whisker-Reinforced Aluminum Alloys.	1511-1519A		
Fatigue Behavior of SiC Reinforced Ti(6Al—4V) at 650°C.	1933-1938A		
Silicon compounds			
See Silicon carbide			
Silicon nitride			
Silicon iron			
See Silicon steels			
Silicon nitride, Coating			
Low-Temperature Strain Behavior of Lead Thin Films on a Substrate.	383-391A		
Silicon steels, Crystal lattices			
Operation of Near-Surface Dislocation Sources.	1199-1205A		
Silicon steels, Mechanical properties			
Studies on the Development of High-Strength Dual-Phase Steel Sheets With High r_m Values.	1257-1262A		
Silicon steels, Phase transformations			
The Bainite Reaction in Fe—Si—C Alloys: the Primary Stage.	777-787A		
The Bainite Reaction in Fe—Si—C Alloys: the Secondary Stage.	789-800A		
Silver, Binary systems			
Thermochemistry of Alloys of Transition Metals: III.—Copper—Silver, —Titanium, —Zirconium and —Hafnium at 1373°C.	391-401B		
The Coordination Cluster Theory—Description of the Activity Coefficients of Dilute Solutions of Oxygen and Sulfur in Binary Alloys.	429-437B		
Silver base alloys, Electrochemistry			
Potentiodynamic Polarization Analysis of Silver—Palladium Alloys in Chloride Solutions.	313-317A		
Silver base alloys, Mechanical properties			
Study of the Rheological Behavior of the Beta Prime Phase of an Equiatomic Ag—Mg Alloy.	251-255A		
Silver base alloys, Phases (state of matter)			
The Constitution and Phase Stability of Overlapping Melt Trails in Ag—Cu Alloys Produced by Continuous Laser Melting Quenching.	1879-1889A		
Simulation			
See also Computer simulation			
The Velocity Field in the Molten Slag Region of ESR Systems: a Comparison of Measurements in a Model System With Theoretical Predictions.	35-43B		
The Effect of Mold Precession on Channel and Macrosegregation in Ammonium Chloride—Water Analog Castings.	495-501B		
Single crystals, Mechanical properties			
The Influence of Orientation on the Stress Rupture Properties of Nickel-Based Superalloy Single Crystals.	1747-1754A		
Single crystals, Oxidation			
Observations on the Early Stages of Oxidation of Titanium Carbide.	1837-1841A		
Sintered metal			
See Powder metallurgy parts			
Sintering			
Factors Influencing the Production Rate and Quality of Lead Sinter.	15-29B		
Changes in Diffusivity Due to Sintering in Metallized Iron Oxide Pellets.	518-520B		
Kinetics of Grain Coarsening During Sintering of Co—Cu and Fe—Cu Alloys With Low Liquid Contents.	1405-1411A		
Sintering (powder metallurgy)			
See Vacuum sintering			
Size distribution (particle)			
See Particle size distribution			
Skull casting			
See Casting			
Slags			
Volatilization of Bismuth in Copper Matte Converting—Computer Simulation.	339-348B		
Slags, Chemical analysis			
The Relative Uptake of Several Vaporized Radiotracers at 1300°C as a Function of Basicity in Selected Oxide Melts.	645-648B		
Slags, Diffusion			
Tracer Diffusivity of O ¹⁸ in CaO—SiO ₂ Melts at 1600°C.	237-240B		
Slags, Phases (state of matter)			
CaS Formation and Oxidation in the System CaO—SiO ₂ —Al ₂ O ₃ Measured by Electron Paramagnetic Resonance.	1997-2002A		
Slags, Solubility			
Oxygen Pressure Measurements of Silica Saturated Fe—O—SiO ₂ Melts by the E.M.F. Method Using Zirconia Solid Electrolyte.	423-427B		
Slip			
See also Slip planes			
C Component Dislocations in Deformed Ti ₃ Al.	324-328A		
Enhanced Densification of White Cast Iron Powders by Cyclic Phase Transformations Under Stress.	355-361A		
Evidence for Dislocation Transport of Hydrogen in Aluminum. Deformation Modes of the Alpha-Phase of Ti—6Al—4V as a Function of Oxygen Concentration and Aging Temperature.	811-820A		
Stress-Substructure Relationships in Cyclically and Monotonically Deformed Wavy Slip Mode Metals.	889-899A		
Induced Creep and Creep/Fatigue of a Nickel-Based Superalloy at Ambient Temperatures.	1033-1041A		
Slip planes			
The Influence of Orientation on the Stress Rupture Properties of Nickel-Based Superalloy Single Crystals.	1951-1955A		
Smelting			
See also Flash smelting			
Activities of CoS and FeS in Copper Mattes and the Behavior of Cobalt in Copper Smelting.	461-470B		
Heteronuclear Compounds of Arsenic and Antimony.	511-513B		
Sodium, Ternary systems			
Recomputation of Phase Equilibria in the Sodium—Carbon—Oxygen System: Effect of Oxygen.	1101-1102A		
Sodium aluminum fluoride			
See Cryolite			
Sodium chlorides, Environment			
Environmental Factors Affecting Localized Corrosion of 7075-T7351 Aluminum Alloy Plate.	161-166A		
The Effect of Heat Treatments on the Corrosion Fatigue Properties of 13% Chromium Stainless Steel in 3% NaCl Aqueous Solution.	1521-1529A		
Sodium compounds			
See also Sodium chloride			
Sodium hydroxide			
Sodium compounds, Environment			
Low-Temperature Hot Corrosion of Cobalt-Based Alloys. I.—Morphology of the Reaction Product.	1843-1852A		
Low-Temperature Hot Corrosion of Cobalt-Based Alloys. II.—Reaction Mechanism.	1853-1864A		

Sodium compounds

Stress Corrosion Cracking of Sensitized Type 304 Stainless Steel in Thiosulfate Solutions.	2015-2026A	Steel constituents
		See Austenite Bainite Cementite Ferrite Martensite Pearlite Retained austenite
Sodium hydroxide, Environment		
The Stress Corrosion Susceptibility of a Quenched and Tempered 12% CrMoV Martensitic Stainless Steel.	913-921A	Steel converters
Caustic Stress Corrosion Cracking of Mild Steel.	1091-1098A	See Bottom blown converters
Soft solders		Steel making
See Solders		Effective Viscosity Models for Gas Stirred Ladles.
Softening		125-127B
See Strain softening		Steels
Solders, Mechanical properties		See also Aluminum killed steels
Characterization of In-Based Eutectic Alloys Used in Josephson Packaging.	1547-1562A	Austenitic stainless steels Boron steels Carbon steels Chromium manganese steels Chromium molybdenum steels Chromium steels Chromium vanadium steels Dual phase steels Ferritic stainless steels High alloy steels High speed tool steels High strength low alloy steels Low alloy steels Martensitic stainless steels Nickel chromium molybdenum steels Nickel chromium steels Rail steels Silicon steels Stainless steels TRIP steels
Solidification		Steels, Casting
See also Directional solidification Rapid solidification		The Effect of Melt Composition on Solidification Cracking of Steel, With Particular Reference to Continuous Casting.
The Effect of Melt Composition on Solidification Cracking of Steel, With Particular Reference to Continuous Casting.	259-266B	259-266B
The Use of Heat Flow Modeling to Explore Solidification Phenomena.	471-478B	Steels, Chemical analysis
Solidification, Alloying effects		Oxygen Probes Based on Calcia-Doped Hafnia or Calcium Zirconate for Use in Metallic Melts.
Effect of Manganese and Nitrogen on the Solidification Mode in Austenitic Stainless Steel Welds.	2121-2130A	227-235B
Solubility		Steels, Coating
Phase Stability Investigations of the Palladium—Cadmium System. I.—Thermodynamic Studies.	1115-1121A	Pulsed Laser Treatment of Plasma-Sprayed Coatings.
Solubility, Alloying effects		479-483B
The Influence of Solutes on Kinetics and Thermodynamics of Liquid Indium—Oxygen Systems.	53-59B	Steels, Diffusion
Solution hardening		Diffusion Driven Grain Boundary Migration in Iron During Zincification.
See Solution strengthening		1567-1572A
Solution strengthening		Steels, Metallography
Athermal Solid Solution Hardening in Tantalum.	1015-1020A	The Detection of Monolayer Grain Boundary Segregations in Steels Using STEM-EDS X-Ray Microanalysis.
Peierls—Nabarro Plastic Deformation in the Presence of Solute Clusters.	1429-1434A	1397-1403A
Sorption		Steels, Recovering
See Absorption (material) Desorption		The Extractive Metallurgy of Old Scrap Recycle.
Specific resistance		135-139B
See Resistivity		Steels, Refining
Specimen preparation		Effects of the Electromagnetic Stirring on the Removal of Inclusions of Oxide From Liquid Steel.
The Cleavage Plane of Pearlite.	1865-1868A	45-52B
Spectroscopy		Vacuum Distillation of Liquid Metals. I.—Theory and Experimental Study.
See Auger electron spectroscopy		581-588B
Speed		Vacuum Distillation of Liquid Metals. II.—Photographic Study.
See Velocity		589-591B
Spelter		Stirring
See Zinc		See also Electromagnetic stirring Effective Viscosity Models for Gas Stirred Ladles.
Spinodal decomposition		Hydrodynamics of Gas Stirred Melts. I.—Gas/Liquid Coupling.
Modulated Structures and G—P Zones in Al—Mg Alloys.	1373-1378A	193-202B
Splat cooling		Hydrodynamics of Gas Stirred Melts. II.—Axisymmetric Flows.
The Constitution and Phase Stability of Overlapping Melt Trails in Ag—Cu Alloys Produced by Continuous Laser Melt Quenching.	1879-1889A	203-211B
Splitting, Microstructural effects		Strain aging
Splitting of Tungsten Wire in the Knife-Edge Compression Test.	1501-1510A	Dynamic Strain Aging of Various Steels. Strain Aging and Strain Rate Sensitivity of Oxygen-Enriched (Alpha + Beta) Zircaloy-2.
Sponginess		1793-1797A 1957-1964A
See Porosity		Strain hardening
Sprayed coatings, Irradiation		The Large Strain Deformation of Some Aluminum Alloys. Plastic Behavior of 70/30 Brass Sheet.
Pulsed Laser Treatment of Plasma-Sprayed Coatings.	479-483B	1445-1452A 1491-1500A
Spraying		Strain hardenability, Composition effects
See Plasma spraying		Effect of Carbon Content on the Plastic Flow of Plain Carbon Steels at Elevated Temperatures.
Stability		125-134A
See also Phase stability		Strain hardening
Plastic Instability in U-Notched Bend Specimens of Spheroidized AISI 1090 Steel.	2209-2218A	Fatigue Crack Initiation and Strain-Controlled Fatigue of Some High-Strength Low-Alloy Steels.
Stacking fault energy		59-72A
Stress-Substructure Relationships in Cyclically and Monotonically Deformed Wavy Slip Mode Metals.	1033-1041A	Mechanical Behavior of Alloy 800 at 838°K.
Stacking faults		637-648A
Phase Transformations in a Wrought Co—Cr—Mo—C Alloy.	1161-1166A	Cyclic Hardening of Ni—14.4 At.-% Al Alloy Containing Coherent Precipitates.
Stainless steels		1187-1198A
See also Austenitic stainless steels Ferritic stainless steels Martensitic stainless steels		The Separate Roles of Subgrains and Forest Dislocations in the Isotropic Hardening of Type 304 Stainless Steel.
Stainless steels, Corrosion		1977-1986A
Theoretical Considerations on Corrosion Fatigue Crack Initiation.	649-655A	Strain hardening, Microstructural effects
Stainless steels, Mechanical properties		Cyclic Deformation of Pearlitic Eutectoid Rail Steel.
Surface Wave Studies of Hydrogen Damage Incubation Time.	487-491A	2035-2047A
Stainless steels, Refining		Strain rate
The Effect of Oxygen Potential on Phosphorus in the CaO—Al ₂ O ₃ System.	643-644B	Correction to "The Significance of the Dimensionless Constant in the Rate Equation for Superplastic Flow".
Static casting		2289A
See Casting		Effects of Strain State and Strain Rate on Deformation-Induced Transformation in 304 Stainless Steel. I.—Magnetic Measurements and Mechanical Behavior.
Static fatigue		619-626A
See Creep rupture strength		Effects of Strain State and Strain Rate on Deformation-Induced Transformation in 304 Stainless Steel. II.—Microstructural Study.
Statistical distributions		627-635A
See Normal distribution		The Mechanical Properties of Superplastic Materials.
		689-701A
		Influences of Materials Parameters and Microstructure on Superplastic Forming.
		733-743A
		Deformation Behavior of Duplex Zircaloy-4—Oxygen Alloys.
		1077-1082A

Plastic Behavior of 70/30 Brass Sheet.	1491-1500A	Submerged arc welds <i>See</i> Welded joints	
Correlation of Substructure With Time-Dependent Fatigue Properties of AISI 304 Stainless Steel.	1577-1588A	Substructures (crystalline)	
Effect of Strain Rate on Deformation Behavior of Semisolid Dendritic Alloys.	1809-1819A	The Influence of Substructure on the Elevated- and Room-Temperature Strength of a 26Cr-1Mo Ferritic Stainless Steel.	447-456A
Strain Aging and Strain Rate Sensitivity of Oxygen-Enriched (Alpha + Beta) Zircaloy-2.	1957-1964A	Correlation of Substructure With Time-Dependent Fatigue Properties of AISI 304 Stainless Steel.	1577-1588A
The Separate Roles of Subgrains and Forest Dislocations in the Isotropic Hardening of Type 304 Stainless Steel.	1977-1986A		
The Significance of the Dimensionless Constant in the Rate Equation for Superplastic Flow.	2059-2061A	Substructures (crystalline), Stress effects Stress-Substructure Relationships in Cyclically and Monotonically Deformed Wavy Slip Mode Metals.	1033-1041A
Strain softening			
Fatigue Crack Initiation and Strain-Controlled Fatigue of Some High-Strength Low-Alloy Steels.	59-72A	Sulfates <i>See also</i> Sulfuric acid Oxidation of Alkaline Earth Sulfides to Sulfates: Thermodynamic Aspects.	387-390B
Effect of Carbon Content on the Plastic Flow of Plain Carbon Steels at Elevated Temperatures.	125-134A		
Strengthening (solution) <i>See</i> Solution strengthening		Sulfates, Environment Environmental Factors Affecting Localized Corrosion of 7075-T351 Aluminum Alloy Plate.	161-166A
Stress aging <i>See</i> Strain aging		Mechanism of Oxidation—Sulfation Reactions of CoO in the Presence of Na ₂ SO ₄ .	1647-1654A
Stress analysis <i>See also</i> X ray stress analysis		Low-Temperature Hot Corrosion of Cobalt-Based Alloys. I.—Morphology of the Reaction Product.	1843-1852A
Measurement of a Stress Gradient Through the Bulk of an Aluminum Alloy Using Neutrons.	1069-1076A	Low-Temperature Hot Corrosion of Cobalt-Based Alloys. II.—Reaction Mechanism.	1853-1864A
Stress corrosion cracking		Sulfates, Synthesis Dry Method Preparation and Melting Point of Cu ₂ SO ₄ .	515-517B
Effects of Texture and Microstructure on the Propagation of Iodine Stress Corrosion Cracks in Zircaloy.	73-83A	Sulfation Mechanism of Oxidation—Sulfation Reactions of CoO in the Presence of Na ₂ SO ₄ .	1647-1654A
Claustic Stress Corrosion Cracking of Mild Steel.	1091-1098A		
Stress Corrosion Cracking of Sensitized Type 304 Stainless Steel in Thiosulfate Solutions.	2015-2026A	Sulfides <i>See also</i> Hydrogen sulfide Molybdenum disulfide	
Stress Corrosion of Cu-Zn and Cu-Zn-Ni Alloys: the Role of Dealloying.	2027-2033A	Sulfides, Impurities Effect of Volume Fraction and Shape of Sulfide Inclusions on Through-Thickness Ductility and Impact Energy of High-Strength 4340 Plate Steels.	2239-2258A
Stress corrosion cracking, Alloying effects		Sulfides, Oxidation Oxidation of Alkaline Earth Sulfides to Sulfates: Thermodynamic Aspects.	387-390B
The Role of Molybdenum in the Enhanced Resistance to Hydrogen Stress Cracking of AISI 4100 Steels.	1099-1101A	Sulfides, Physical properties Standard Free Energy of Formation of NiAsS.	285-288B
Stress corrosion cracking, Heating effects		Sulfides, Reduction (chemical) Kinetics of Vaporization of Lead Sulfide.	633-641B
The Stress Corrosion Susceptibility of a Quenched and Tempered 12% CrMoV Martensitic Stainless Steel.	913-921A	Sulfur, Diffusion On Grain Boundary Segregation in Austenitic Stainless Steels.	2281-2285A
On Grain Boundary Segregation in Austenitic Stainless Steels.	2281-2285A	Sulfur, Impurities Rate of Decarburization of Iron-Carbon Melts.	
Stress corrosion resistance <i>See</i> Corrosion resistance		I.—Experimental Determination of the Effect of Sulfur.	403-409B
Stress intensity		Rate of Decarburization of Iron-Carbon Melts. II.—A Mixed-Control Model.	411-421B
Some Considerations on Fatigue Crack Closure at Near-Threshold Stress Intensities Due to Fracture Surface Morphology.	937-940A	The Role of Sulfur in the Air Embrittlement of Nickel and its Alloys.	1223-1232A
The Effect of Stress State on Internal Hydrogen-Induced Crack Growth in Ti-6Al-6V-2Sn.	1055-1061A	Sulfur, Solubility The Coordination Cluster Theory—Description of the Activity Coefficients of Dilute Solutions of Oxygen and Sulfur in Binary Alloys.	429-437B
Stress relieving		Sulfur, Ternary systems Extension of the Associated Solution Model to Ternary Metal-Sulfur Melts: Cu-Ni-S.	379-385B
See Grain refinement		Sulfur, Trace elements Effect of Sulfur and Antimony on the Intergranular Fracture of Iron at Cathodic Potentials.	241-249A
Stress rupture strength <i>See</i> Creep rupture strength		Sulfur compounds See Hydrogen sulfide	
Stress strain curves		Sulfuric acid, Environment Oxidation of Fe(II) in Sulfuric Acid Solutions With Dissolved Molecular Oxygen.	311-318B
Fatigue Crack Initiation and Strain-Controlled Fatigue of Some High-Strength Low-Alloy Steels.	59-72A	An Examination of Chromium Substitution in Stainless Steels.	2003-2013A
Finite Element Method (FEM) Calculations of Stress—Strain Behavior of Alpha-Beta Ti-Mn Alloys. I.—Stress—Strain Relations.	595-601A	Sulfuric acid leaching Passive and Transpassive Anodic Behavior of Chalcocite in Acid Solutions.	571-579B
Finite Element Method (FEM) Calculations of Stress—Strain Behavior of Alpha-Beta Ti-Mn Alloys. II.—Stress and Strain Distributions.	603-609A	Sulfurization Elevated-Temperature Fatigue Crack Growth in Incoloy Alloy 800 in Sulfidizing Environments.	
Effects of Strain State and Strain Rate on Deformation-Induced Transformation in 304 Stainless Steel.	619-626A	Corrosion of Fe-Ni-Cr, Fe-Cr-Al and Fe-Ni-Cr-Al Alloys in H ₂ /H ₂ O/H ₂ S Mixtures at 1200°C.	145-152A
I.—Magnetic Measurements and Mechanical Behavior.	689-701A	Sulphur <i>See</i> Sulfur	1299-1311A
The Mechanical Properties of Superplastic Materials.	1445-1452A	Superalloys, Corrosion Elevated-Temperature Fatigue Crack Growth in Incoloy Alloy 800 in Sulfidizing Environments.	
The Large Strain Deformation of Some Aluminum Alloys.	1619-1626A	The Effect of High-Temperature Low-Cycle Fatigue on the Corrosion Resistance of Austenitic Stainless Steels.	145-152A
Cavitation and Cavity Growth During Superplastic Flow in Microduplex Cu-Zn-Ni Alloys.	2035-2047A	Superalloys, Crystal growth The Influence of Hot Working on the Subsequent Recrystallization of a Dispersion Strengthened Superalloy—MA 6000.	923-927A
Cyclic Deformation of Pearlite Eutectoid Rail Steel.		The Influence of Gamma Prime on the Recrystallization of an Oxide Dispersion Strengthened Superalloy—MA 6000E.	1463-1470A
Stresses		Superalloys, Diffusion Hydrogen Transport in Nickel-Based Stainless Alloys.	1685-1674A
See Residual stress			1181-1186A
Shear stress			
Stress intensity			
Tensile stress			
Strontium, Alloying additive			
Structure and Properties of Hypoeutectic Al-Si-Mg Alloys Modified With Pure Strontium.	945-951A		
Structural hardening			
See Aging (artificial)			
Precipitation hardening			
Secondary hardening			
Strain aging			
Surface hardening			
Structural steels			
See Rail steels			
Structures (crystalline)			
See Banded structure			
Columnar structure			
Crystal structure			
Dendritic structure			
Fibrous structure			
Grain structure			
Intergranular structure			
Lamellar structure			
Microstructure			
Substructures (crystalline)			
Widmanstatten structure			

Superalloys

Superalloys, Mechanical properties	Surface properties
Hydrogen Embrittlement of Ultra-Pure Alloys of the Inconel 600 Type: Influence of the Additions of Elements (Carbon, Phosphorus, Tin, Antimony).	See Roughness Surface structure
Mechanical Behavior of Alloy 800 at 838°K.	
A Note on the Microstructural Dependence of Creep Strength in Inconel 700.	Surface roughness
Microstructural Aspects of Superplasticity.	See Roughness
Effects of Cobalt on Structure, Microchemistry and Properties of a Wrought Nickel-Based Superalloy.	Surface structure
Effect of Environment on Fatigue and Creep Crack Growth in Inconel X-750 at Elevated Temperature.	Surface Wave Studies of Hydrogen Damage Incubation Time. 487-491A
The Role of Sulfur in the Air Embrittlement of Nickel and Its Alloys.	
High-Cycle Fatigue Life of the Cast Nickel-Based-Superalloys IN 738 LC and IN 939.	Surface structure, Radiation effects
Creep and Rupture of an ODS Alloy With High Stress Rupture Ductility.	Pulsed Laser Treatment of Plasma-Sprayed Coatings. 479-483B
The Influence of Orientation on the Stress Rupture Properties of Nickel-Based Superalloy Single Crystals.	
Fatigue and Creep—Fatigue Deformation of Several Nickel-Based Superalloys at 650°C.	Surface waves
The Influence of Cobalt on the Tensile and Stress Rupture Properties of the Nickel-Based Superalloy MAR-M247.	Surface Wave Studies of Hydrogen Damage Incubation Time. 487-491A
Induced Creep and Creep/Fatigue of a Nickel-Based Superalloy at Ambient Temperatures.	Surface waves, Field effects
Creep Fracture Processes of Oxide Dispersion Strengthened Mechanically Alloyed Inconel Alloy MA 754.	Effect of Wave Motion on Chill Cast Surfaces. 503-509B
Superalloys, Microstructure	Surfactants
The Influence of Cobalt on the Microstructure of the Nickel-Based Superalloy MAR-M247.	Prediction of the Effects of Surface-Active Elements on Gas—Liquid Metal Kinetics. 357-367B
Superalloys, Powder technology	
The Effect of Defects on the Fatigue Crack Initiation Process in Two P/M Superalloys. I.—Fatigue Origins.	Suspensions
33-43A	See Dispersions
The Effect of Defects on the Fatigue Crack Initiation Process in Two P/M Superalloys. II.—Surface—Subsurface Transition.	Swaging
45-52A	Superplastic Behavior of the Sn—Pb Eutectic in the As-Worked State. 53-58A
Characterization of a Rapidly Solidified Iron-Based Superalloy.	
1535-1546A	Synthetic coke
	See Coke
Superalloys, Refining	Systems (metallurgical)
Understanding the Role of Cerium During VIM Refining of Nickel—Chromium and Nickel—Iron Alloys.	See Binary systems Ternary systems
Superalloys, Structural hardening	Tanks (electrolytic)
Effect of Composition and High-Energy Rate Forging on the Onset of Precipitation in an Iron-Based Superalloy.	See Electrolytic cells
Electron Microscopic Analysis of Heterogeneous Precipitates in Hastelloy C-276.	Tantalum, Diffusion
	Thermotransport of Hydrogen and Deuterium in Vanadium, Niobium and Tantalum. 821-825A
Superalloys, Thermal properties	Tantalum, Refining
Thermodynamics of the Superalloys.	Doxidation of High-Melting-Point Metals and Alloys in Vacuum. 241-249B
Superalloys, Welding	Tantalum base alloys, Diffusion
The Fatigue Crack Growth Behavior of Electron-Beam Welded A286 Superalloy.	Hydrogen Diffusion in Nb—Ta Alloys. 1675-1678A
Superlattices	Tantalum base alloys, Structural hardening
"C" Component Dislocations in Deformed Ti ₃ Al.	Athermal Solid Solution Hardening in Tantalum. 1015-1020A
Superplastic forming	Tapes (metallic), Corrosion
Cavitation and Cavity Growth During Superplastic Flow in Microduplex Cu—Zn—Ni Alloys.	Corrosion Behavior of Amorphous Fe—Cr—Al—P—C Ribbon Alloys. 901-905A
Microstructural Observations of Superplastic Cavitation in Fine-Grained 7475 Al.	Tellurium, Binary systems
1721-1727A	Defective Two Sublattice Model for a Binary Liquid. 1107-1114A
Superplastic forming, Microstructural effects	Temper brittleness
Influences of Materials Parameters and Microstructure on Superplastic Forming.	Fracture Toughness of AISI M2 High-Speed Steel and Corresponding Matrix Tool Steel. 1595-1605A
Superplasticity	The Thermodynamics of Interactive Cosegregation of Phosphorus and Alloying Elements in Iron and Temper-Brittle Steels.
Correction to "The Significance of the Dimensionless Constant in the Rate Equation for Superplastic Flow".	1693-1711A
Superplastic Behavior of the Sn—Pb Eutectic in the As-Worked State.	Indentation Loading Studies of Acoustic Emission From Temper and Hydrogen Embrittled A533B Steel. 1965-1975A
The Mechanical Properties of Superplastic Materials.	Temper brittleness, Composition effects
Microstructural Aspects of Superplasticity.	Effects of Compositional Variations and Aging Treatments on the Fracture Behavior of HY 130 Steel in Air and Hydrogen. 111-116A
The Rate-Controlling Deformation Mechanisms in Superplasticity—a Critical Assessment.	Temper brittleness, Impurity effects
Superplasticity in Rapidly Solidified White Cast Irons.	Temper Embrittlement Diagram of NiCr Steel Doped With Phosphorus. 2205-2207A
The Significance of the Dimensionless Constant in the Rate Equation for Superplastic Flow.	Temper hardening
2059-2061A	See Secondary hardening
Surface active agents	Temperature
See Surfactants	See also Critical temperature High temperature Melting points Room temperature
Surface analysis (chemical)	
Experimental and Theoretical Concentration Profiles at the Surface of Chromized Iron.	Temperature, Stress effects
	Thermal Effects During Uniaxial Straining of Steels. 1063-1067A
Surface chemistry	Temperature measuring instruments
Surface Segregation in Austenitic Stainless Steel.	See Thermocouples
Surface defects	Tempering
Effect of Wave Motion on Chill Cast Surfaces.	See also Quenching and tempering Secondary hardening
	Tempering of 2.25%Cr—1%Mo Low-Carbon Steels. 557-563A
Surface diffusion	Structure—Property Relationships in Dual-Phase Cu—Al Alloys. II.—Alloy Behavior. 847-853A
See Diffusion	The Effect of Heat Treatments on the Corrosion Fatigue Properties of 13% Chromium Stainless Steel in 3% NaCl Aqueous Solution.
Surface energy	Tempering Characteristics of a Vanadium-Containing Dual-Phase Steel. 1521-1529A
Calorimetric Measurements of the Plastic Work of Fatigue Crack Propagation in 4140 Steel.	1679-1686A
Surface hardening	Tenacity
See also Carburizing Gas carburizing	See Tensile strength
Surface hardening, Vibration effects	Tensile modulus
Surface Hardening and Microstructural Changes in 304 Stainless Steel Resulting From Elevated-Temperature Ultrasonic Vibration.	See Modulus of elasticity
	Tensile properties
	See also Tensile strength Yield strength
	A Method for Fabrication of Aluminum / Alumina Composites. 93-100A
	Microstructures, Mechanical Properties and Electrical Resistivity of Rapidly Quenched Fe—Cr—Al Alloys. 337-343A
	Mechanical Properties of Fe—Si—B Amorphous Wires Produced by In-Rotating-Water Spinning Method. 373-382A

Preparation and Properties of Aluminum Alloy Coconut Shell Char Particulate Composites.	485-494B	Thermal flux
Fatigue Initiation Study of TMT Eutectoid Steel.	855-864A	<i>See Heat transmission</i>
Structure and Properties of Hypoeutectic Al—Si—Mg Alloys Modified With Pure Strontium.	945-951A	Thermal power
Thermal Effects During Uniaxial Straining of Steels.	1063-1067A	<i>See Thermoelectricity</i>
Cyclic Hardening of Ni—14.4 At.-% Al Alloy Containing Coherent Precipitates.	1187-1198A	Thermal properties
Studies on the Development of High-Strength Dual-Phase Steel Sheets With High r_m Values.	1257-1262A	<i>See Heat of activation</i>
Flow Localization and Shear Band Formation in a Precipitation Strengthened Austenitic Stainless Steel.	1263-1274A	Heat of formation
The Effects of Copper and Chromium on the Aging Response of Dilute Al—Mg—Si Alloys.	1318-1321A	Heat of fusion
Near-Threshold Fatigue Crack Growth Behavior in Copper. Dynamic Strain Aging of Various Steels.	1607-1618A	Heat of mixing
	1793-1797A	Melting points
		Thermal expansion
		Thermoelectricity
		Vapor pressure
Tensile properties, Alloying effects		Thermal reduction
Microstructure—Property Relationships of Two Al—3Li—2Cu—0.22Cr—Xcd Alloys.	401-410A	<i>See Flash smelting</i>
The Influence of Cobalt on the Tensile and Stress Rupture Properties of the Nickel-Based Superalloy MAR-M247.	1767-1774A	Thermoanalysis
		<i>See Thermal analysis</i>
Tensile properties, Composition effects		Thermochemistry
The Influence of Microstructure and Strength on the Fracture Mode and Toughness of 7XXX Series Aluminum Alloys.	411-425A	Kinetics and Mechanism of the Reaction of Iron—Chromium and Iron—Chromium—Molybdenum Alloys With Chlorine Gas.
Effects of Cobalt on Structure, Microchemistry and Properties of a Wrought Nickel-Based Superalloy.	1021-1032A	153-159A
Compositional Effects on the High-Temperature Ductility of 1Cr—1.25Mo—0.25V Steel.	1471-1481A	Thermocouples, Service life
An Examination of Chromium Substitution in Stainless Steels.	2003-2013A	Deterioration of Electromotive Force of Chromel—Alumel Thermocouples in Reducing Atmospheres at High Temperatures.
		167-172A
Tensile properties, Heating effects		Thermocycling
Tempering Characteristics of a Vanadium-Containing Dual-Phase Steel.	1679-1686A	<i>See Thermal cycling</i>
Tensile properties, Impurity effects		Thermodynamics
Hydrogen Effects on the Tensile Properties of 21-6-9 Stainless Steel.	2049-2058A	The Influence of Solutes on Kinetics and Thermodynamics of Liquid Iodium—Oxygen Systems.
		A Gaussian-Based Formalism for the Representation of Free Energy as a Function of Composition of Binary Metallic Solutions.
Tensile properties, Microstructural effects		213-225B
Structure—Property Relationships in Dual-Phase Cu—Al Alloys. II.—Alloy Behavior.	847-853A	Thermodynamics of Copper Matte Converting. III.—Steady-State Volatilization of Gold, Silver, Lead, Zinc, Nickel, Selenium, Tellurium, Bismuth, Antimony and Arsenic From Slag, Matte and Metallic Copper.
Deformation Modes of the Alpha-Phase of Ti—6Al—4V as a Function of Oxygen Concentration and Aging Temperature.	889-899A	319-329B
Influence of Grain Size and Age-Hardening on Dislocation Pile-Ups and Tensile Fracture for a Ti—Al Alloy.	1283-1292A	Thermodynamics of Copper Matte Converting. IV.— <i>A Priori</i> Predictions of the Behavior of Gold, Silver, Lead, Zinc, Nickel, Selenium, Tellurium, Bismuth, Antimony and Arsenic in the Noranda Process Reactor.
Influence of Test Temperature and Microstructure on the Tensile Properties of Titanium Alloys.	1435-1443A	331-338B
The Influence of Grain Structure on the Ductility of the Al—Cu—Li—Mn—Cd Alloy 2020.	2259-2269A	Extension of the Associated Solution Model to Ternary Metal—Sulfur Melts: Cu—Ni—S.
		379-385B
Tensile properties, Stress effects		Oxidation of Alkaline Earth Sulfides to Sulfates: Thermodynamic Aspects.
Tensile and Fracture Properties of Type 316 Stainless Steel After Creep.	2155-2163A	387-390B
		Thermodynamics of the Superalloys.
Tensile properties, Welding effects		395-965A
Microstructure and Mechanical Properties of Laser Welded Titanium 6Al—4V.	865-871A	The Thermodynamics of Interactive Cosegregation of Phosphorus and Alloying Elements in Iron and Temper-Brittle Steels.
Weld Metal Grain Structure and Mechanical Properties of a Thallium-Doped Ir—0.3% W Alloy (DOP-26).	1043-1053A	1329-1336A
		A Simple Bisection Technique for the Calculation of a Two-Solid or Two-Liquid Miscibility Gap in Binary Metallic Systems.
		1693-1711A
		2097-2102A
Tensile shear strength		Thermoelastic properties
<i>See Shear strength</i>		<i>See Internal friction</i>
Tensile strength		Shape memory
Mechanical Behavior of Alloy 800 at 838°C.	637-648A	Thermoelectric effect
Fatigue Behavior of SiC Reinforced Ti(6Al—4V) at 650°C.	1933-1938A	<i>See Thermoelectricity</i>
Tensile strength, Microstructural effects		Thermoelectric EMF
Deformation Characteristics of Dual-Phase Steels.	85-92A	<i>See Thermoelectricity</i>
Tensile stress		Thermoelectricity, Corrosion effects
Low-Temperature Strain Behavior of Lead Thin Films on a Substrate.	383-391A	Deterioration of Electromotive Force of Chromel—Alumel Thermocouples in Reducing Atmospheres at High Temperatures.
Tensile tests		167-172A
<i>See Tension tests</i>		Thermomechanical treatment
Tensile yield strength		Heating Rate Effects on Recrystallized Grain Size in Two Al—Zn—Mg—Cu Alloys.
<i>See Yield strength</i>		193-198A
Tension tests		Thermomechanical Strengthening of High-Strength, Chromium—Molybdenum Steel.
Thermal Effects During Uniaxial Straining of Steels.	1063-1067A	671-673A
Calorimetric Measurements of the Plastic Work of Fatigue Crack Propagation in 4140 Steel.	2165-2172A	855-864A
Ternary systems		The Influence of Grain Structure on the Ductility of the Al—Cu—Li—Mn—Cd Alloy 2020.
Extension of the Associated Solution Model to Ternary Metal—Sulfur Melts: Cu—Ni—S.	379-385B	2259-2269A
Ternary systems, Phases (state of matter)		Thickness
Recomputation of Phase Equilibria in the Sodium—Carbon—Oxygen System: Effect of Oxygen.	1101-1102A	<i>See Wall thickness</i>
Texture		Thixotropy
<i>See also Rolling texture</i>		Effect of Strain Rate on Deformation Behavior of Semisolid Dendritic Alloys.
Effects of Texture and Microstructure on the Propagation of Iodine Stress Corrosion Cracks in Zircaloy.	73-83A	1809-1819A
Thermal analysis		Thorium, Diffusion
Thermal Analysis of Trapped Hydrogen in Pure Iron.	135-140A	Internal Friction Studies of Fast Diffusing Solutes in Thorium.
Thermal cycling		995-1001A
Work of Fracture in Aluminum Metal-Matrix Composites.	289-297A	Thorium, Dopants
Enhanced Densification of White Cast Iron Powders by Cyclic Phase Transformations Under Stress.	355-361A	Weld Metal Grain Structure and Mechanical Properties of a Thallium-Doped Ir—0.3% W Alloy (DOP-26).
Low-Temperature Strain Behavior of Lead Thin Films on a Substrate.	383-391A	1043-1053A
Thermal EMF		Tig arc welding
<i>See Thermoelectricity</i>		<i>See Gas tungsten arc welding</i>
Thermal expansion		Tilting furnaces
The Thermal Distortion of Continuous-Casting Billet Molds.	91-104B	<i>See Bottom blown converters</i>
Characterization of In-Based Eutectic Alloys Used in Josephson Packaging.	1547-1562A	Tin, Alloying additive
		Hydrogen Embrittlement of Ultra-Pure Alloys of the Inconel 600 Type: Influence of the Additions of Elements (Carbon, Phosphorus, Tin, Antimony).
		141-144A
		Tin, Alloying elements
		Observations of Aging Effects in a Cu—Sn Shape Memory Alloy.
		1687-1692A

Tin

Tin, Binary systems		
The Coordination Cluster Theory—Description of the Activity Coefficients of Dilute Solutions of Oxygen and Sulfur in Binary Alloys.	429-437B	
Tin, Diffusion		
Vacuum Distillation of Liquid Metals. II.—Photographic Study.	589-591B	
Tin, Dopants		
Compositional Effects on the High-Temperature Ductility of 1Cr—1.25Mo—0.25V Steel.	1471-1481A	
Tin, Physical properties		
Fluid Dynamics of Vertical Submerged Gas Jets in Liquid Metal Processing Systems.	165-173B	
Tin base alloys, Casting		
Effect of Wave Motion on Chill Cast Surfaces.	503-509B	
Tin base alloys, Crystal growth		
The Influence of Acceleration Forces on Dendritic Growth and Grain Structure.	85-90B	
Tin base alloys, Diffusion		
The Rate-Controlling Deformation Mechanisms in Superplasticity—a Critical Assessment.	717-732A	
Tin base alloys, Mechanical properties		
The Mechanical Properties of Superplastic Materials.	689-701A	
Tin base alloys, Metal working		
Effect of Strain Rate on Deformation Behavior of Semisolid Dendritic Alloys.	1809-1819A	
Tin base alloys, Solubility		
Dissolution of Solid Copper Cylinder in Molten Tin—Lead Alloys Under Dynamic Conditions.	439-445B	
Tin base alloys, Thermal properties		
A Gaussian-Based Formalism for the Representation of Free Energy as a Function of Composition of Binary Metallic Solutions.	213-225B	
Tin compounds, Powder technology		
The Production of Niobium/Tin Powders by Vapor-Deposition Processes.	625-631B	
Titanium, Binary systems		
Thermochemistry of Alloys of Transition Metals: III.—Copper—Silver, —Titanium, —Zirconium and —Hafnium at 1373°K.	391-401B	
Thermodynamics of the Ti—H System.	1329-1336A	
Titanium, Mechanical properties		
A Geometric Model for Fatigue Crack Closure Induced by Fracture Surface Roughness.	1627-1631A	
Titanium, Refining		
Deoxidation of High-Melting-Point Metals and Alloys in Vacuum.	241-249B	
Titanium base alloys, Castings		
High-Cycle Fatigue of Weld Repaired Cast Ti—6Al—4V.	1589-1594A	
Titanium base alloys, Composite materials		
Fatigue Behavior of SiC Reinforced Ti(6Al—4V) at 650°C.	1933-1936A	
Titanium base alloys, Forging		
The Occurrence of Shear Bands in Isothermal, Hot Forging.	275-288A	
Titanium base alloys, Mechanical properties		
Low-Cycle Fatigue Behavior of Ti—6Al—2Sn—4Zr—6Mo. I.—The Role of Microstructure in Low-Cycle Crack Nucleation and Early Crack Growth.	257-268A	
Low-Cycle Fatigue Behavior of Ti—6Al—2Sn—4Zr—6Mo. II.—Cyclic Deformation Behavior and Low Cycle Fatigue. Effects of Dwell on High-Temperature Low-Cycle Fatigue of a Titanium Alloy.	269-274A	
Temperature Dependence of Sustained-Load Subcritical Crack Growth in Ti—6Al—6V—2Sn.	322-324A	
Finite Element Method (FEM) Calculations of Stress—Strain Behavior of Alpha-Beta Ti—Mn Alloys. I.—Stress—Strain Relations.	497-500A	
Finite Element Method (FEM) Calculations of Stress—Strain Behavior of Alpha-Beta Ti—Mn Alloys. II.—Stress and Strain Distributions.	595-601A	
The Effect of Stress State on Internal Hydrogen-Induced Crack Growth in Ti—6Al—6V—2Sn.	603-609A	
The State of Residual Stress in the Near Surface Region of Homogeneous and Heterogeneous Materials After Grinding.	1055-1061A	
Low-Cycle Fatigue Behavior of Ti—Mn Alloys: Fatigue Life, Influence of Grain Size and Age-Hardening on Dislocation Pile-Ups and Tensile Fracture for a Ti—Al Alloy.	1239-1244A	
Influence of Test Temperature and Microstructure on the Tensile Properties of Titanium Alloys.	1275-1281A	
Creep of Hydrogen-Charged Ti—5Al—2.5Sn at Room Temperature.	1283-1292A	
The Influence of Microstructure on the Susceptibility of Titanium Alloys to Internal Hydrogen Embrittlement.	1435-1443A	
Fracture Toughness: a Rationalization of the Role of Microstructure in an Alpha—Beta Titanium Alloy.	1531-1532A	
Titanium base alloys, Metal working		
Influences of Materials Parameters and Microstructure on Superplastic Forming.	1729-1738A	
Titanium base alloys, Phases (state of matter)		
Identification of the Interface Phase in Titanium Alloys.	2191-2195A	
Titanium base alloys, Structural hardening		
Silicide Precipitation in Alloy Ti—6Al—5Zr—0.5Mo—0.25Si.	733-743A	
Deformation Modes of the Alpha-Phase of Ti—6Al—4V as a Function of Oxygen Concentration and Aging Temperature.	681-684A	
	771-775A	
	689-699A	
Titanium base alloys, Welding		
Microstructure and Mechanical Properties of Laser Welded Titanium 6Al—4V.		865-871A
Titanium carbide, Oxidation		
Observations on the Early Stages of Oxidation of Titanium Carbide.		1837-1841A
Titanium compounds		
See also Titanium carbide		
Titanium compounds, Crystal lattices		
"C" Component Dislocations in Deformed Ti ₃ Al.		324-328A
Tool steels		
See High speed tool steels		
Tools		
See High speed tool steels		
Torque		
Effects of Friction and High Torque on Fatigue Crack Propagation in Mode III.		2197-2204A
Torsion tests		
Mode III Fatigue Crack Propagation in Low-Alloy Steel.		101-110A
Torsional strength		
See Shear strength		
Toughness		
See Fracture toughness		
Tracers		
See Radioactive tracers		
Tracing (radioactive)		
See Radioactive tracers		
Transferring		
See Heat transfer		
Mass transfer		
Transformations (materials)		
See Martensitic transformations		
Phase transformations		
Transition metal alloys		
See Cobalt base alloys		
Ferrous alloys		
Iridium base alloys		
Nickel base alloys		
Niobium base alloys		
Palladium base alloys		
Tantalum base alloys		
Titanium base alloys		
Zirconium base alloys		
Transition metal compounds		
See Cobalt compounds		
Iron compounds		
Iron oxides		
Manganese compounds		
Molybdenum compounds		
Molybdenum disulfide		
Nickel compounds		
Niobium compounds		
Titanium carbide		
Titanium compounds		
Transition metals		
See also Chromium		
Cobalt		
Hafnium		
Iron		
Manganese		
Molybdenum		
Nickel		
Niobium		
Palladium		
Tantalum		
Titanium		
Tungsten		
Vanadium		
Zirconium		
Transition metals, Alloying elements		
Athermal Solid Solution Hardening in Tantalum.		1015-1020A
Transmission		
See Heat transmission		
Transmission electron microscopy		
The Cleavage Plane of Pearlite.		1865-1868A
Traps		
Application of the McNabb—Foster Trapping Equations to the Diffusion of Oxygen in Dilute Niobium Alloys.		539-543A
A SIMS Study of the Diffusion and Trapping of Deuterium in 302 Stainless Steel.		581-584A
TRIP steels, Phase transformations		
Stress-Assisted Isothermal Martensitic Transformation: Application to TRIP Steels.		1907-1914A
Tungsten, Alloying elements		
Measurement of Structural Parameters Important in Creep of Ni—Mo and Ni—W Solid Solutions.		1827-1836A
Tungsten, Extraction		
Solution Chemistry of Tungsten Leaching Systems.		555-564B
Tungsten, Mechanical properties		
Splitting of Tungsten Wire in the Knife-Edge Compression Test.		1501-1510A
Tungsten, Refining		
Deoxidation of High-Melting-Point Metals and Alloys in Vacuum.		241-249B

Work hardenability

Tungsten arc welding		
<i>See</i> Gas tungsten arc welding		
Turbine blades		
The Influence of Orientation on the Stress Rupture Properties of Nickel-Based Superalloy Single Crystals.	1747-1754A	
Turbine blades, Service life		
The Effect of Heat Treatments on the Corrosion Fatigue Properties of 13% Chromium Stainless Steel in 3% NaCl Aqueous Solution.	1521-1529A	
Turbine generators		
<i>See</i> Turbogenerators		
Turbines		
<i>See</i> Gas turbines		
Turbogenerators		
Mode III Fatigue Crack Propagation in Low-Alloy Steel.	101-110A	
Twinning		
Deformation by Moving Interfaces.	509-538A	
The Bainite Reaction in Fe—Si—C Alloys: the Primary Stage.	777-787A	
The Growth of Hematite Blades During the High-Temperature Oxidation of Iron.	929-935A	
Surface Hardening and Microstructural Changes in 304 Stainless Steel Resulting From Elevated-Temperature Ultrasonic Vibration.	1167-1176A	
Twinning, Cooling effects		
Influence of Cooling Rate on the Microstructure and Retained Austenite in an Intercritically Annealed Vanadium-Containing HSLA Steel.	1899-1906A	
Ultimate shear strength		
<i>See</i> Shear strength		
Ultimate tensile strength		
<i>See</i> Tensile strength		
Ultrasonic attenuation		
Surface Wave Studies of Hydrogen Damage Incubation Time.	487-491A	
Ultrasonic vibration		
Surface Hardening and Microstructural Changes in 304 Stainless Steel Resulting From Elevated-Temperature Ultrasonic Vibration.	1167-1176A	
Vacancies (crystal defects)		
<i>See</i> Lattice vacancies		
Vacancies (lattice)		
<i>See</i> Lattice vacancies		
Vacuum degassing		
Deoxidation of High-Melting-Point Metals and Alloys in Vacuum.	241-249B	
Vacuum distillation		
Vacuum Distillation of Liquid Metals. I.—Theory and Experimental Study.	581-588B	
Vacuum induction melting		
Understanding the Role of Cerium During VIM Refining of Nickel—Chromium and Nickel—Iron Alloys.	603-611B	
Vacuum melting		
<i>See</i> Vacuum induction melting		
Vacuum refining		
Vacuum Distillation of Liquid Metals. II.—Photographic Study.	589-591B	
Understanding the Role of Cerium During VIM Refining of Nickel—Chromium and Nickel—Iron Alloys.	603-611B	
Vacuum sintering		
Phase Analysis of Sintered and Heat Treated Alloy 718.	5-12A	
Vanadium, Alloying additive		
Relative Hardenabilities and Interaction Effects of Molybdenum and Vanadium in 4330 Alloy Steel.	319-320A	
Vanadium, Alloying elements		
Tempering Characteristics of a Vanadium-Containing Dual-Phase Steel.	1679-1686A	
Vanadium, Diffusion		
Thermotransport of Hydrogen and Deuterium in Vanadium, Niobium and Tantalum.	821-825A	
Vanadium, Refining		
Deoxidation of High-Melting-Point Metals and Alloys in Vacuum.	241-249B	
Vanadium chromium steels		
<i>See</i> Chromium vanadium steels		
Vanadium steels		
<i>See</i> Chromium vanadium steels		
Vapor deposition		
Diffusion Driven Grain Boundary Migration in Iron During Zincification.	1567-1572A	
Vapor pressure		
Phase Stability Investigations of the Palladium—Cadmium System. I.—Thermodynamic Studies.	1115-1121A	
Vaporizing		
<i>See also</i> Nucleate boiling		
Vacuum distillation		
Thermodynamics of Copper Matte Converting. III.—Steady-State Volatilization of Gold, Silver, Lead, Zinc, Nickel, Selenium, Tellurium, Bismuth, Antimony and Arsenic From Slag, Matte and Metallic Copper.	319-329B	
Thermodynamics of Copper Matte Converting. IV.— <i>A Priori</i> Predictions of the Behavior of Gold, Silver, Lead, Zinc,		
Nickel, Selenium, Tellurium, Bismuth, Antimony and Arsenic in the Noranda Process Reactor.		331-338B
Volatilization of Bismuth in Copper Matte Converting—Computer Simulation.		339-348B
Heteronuclear Compounds of Arsenic and Antimony.		511-513B
Kinetics of Vaporization of Lead Sulfide.		633-641B
Veining (cracks)		
<i>See</i> Cracks		
Velocity		
The Velocity Field in the Molten Slag Region of ESR Systems: a Comparison of Measurements in a Model System With Theoretical Predictions.		35-43B
Vibration		
<i>See</i> Ultrasonic vibration		
Viscosity		
Effective Viscosity Models for Gas Stirred Ladles.		125-127B
Voids		
Deformation Characteristics of Dual-Phase Steels.		85-92A
The Growth of Creep Cavities in a Low-Alloy Steel.		1739-1745A
A Study of the Deformation and Fracture of a Dual-Phase Steel.		1821-1826A
Fracture Toughness: a Rationalization of the Role of Microstructure in an Alpha—Beta Titanium Alloy.		2191-2195A
Volatilizing		
<i>See</i> Vaporizing		
Voltage		
<i>See</i> Electric potential		
Voltage drop		
<i>See</i> Electric potential		
Wall thickness		
The Influence of Mold Behavior on the Production of Continuously Cast Steel Billets.		105-116B
Waste disposal		
The Extractive Metallurgy of Old Scrap Recycle.		135-139B
Waste incineration		
<i>See</i> Waste disposal		
Water		
<i>See</i> Salt water		
Wave numbers		
<i>See</i> Wavelengths		
Wavelengths		
Effects of Dwell on High-Temperature Low-Cycle Fatigue of a Titanium Alloy.		322-324A
Waves		
<i>See</i> Surface waves		
Weld metal		
Tempering of 2.25%Cr—1%Mo Low-Carbon Steels.		557-563A
Weld metal, Microstructure		
The Effect of Quenching on the Solidification Structure and Transformation Behavior of Stainless Steel Welds.		1141-1152A
Welded joints		
<i>See also</i> Butt welds		
Welded joints, Crystal growth		
Carbide Formation in a Low-Ferrite Austenitic Stainless Steel Weld Metal at 649°C		173-174A
Welded joints, Diffusion		
Discussion of "An Approximate Analytical Demonstration of the Famous Darken Experiment".		1658-1659A
Welded joints, Mechanical properties		
The Fatigue Crack Growth Behavior of Electron-Beam Welded A286 Superalloy.		1483-1489A
Welded joints, Microstructure		
Effect of Manganese and Nitrogen on the Solidification Mode in Austenitic Stainless Steel Welds.		2121-2130A
Welding		
<i>See</i> Electron beam welding		
Gas metal arc welding		
Gas tungsten arc welding		
Laser beam welding		
Repair welding		
Welds		
<i>See</i> Welded joints		
White iron, Powder technology		
Enhanced Densification of White Cast Iron Powders by Cyclic Phase Transformations Under Stress.		355-361A
Superplasticity in Rapidly Solidified White Cast Irons.		1785-1792A
Widmanstätten structure		
Low-Cycle Fatigue Behavior of Ti—6Al—2Sn—4Zr—6Mo. II.—Cyclic Deformation Behavior and Low Cycle Fatigue.		269-274A
Effect of Composition and High-Energy Rate Forging on the Onset of Precipitation in an Iron-Base Superalloy.		345-353A
Wire, Mechanical properties		
Mechanical Properties of Fe—Si—B Amorphous Wires Produced by In-Rotating-Water Spinning Method.		373-382A
Splitting of Tungsten Wire in the Knife-Edge Compression Test.		1501-1510A
Wolfram		
<i>See</i> Tungsten		
Work hardenability		
<i>See</i> Strain hardenability		

Work hardening

Work hardening See Strain hardening	
Work softening See Strain softening	
Work strengthening See Strain hardening	
Workability See also Formability The Occurrence of Shear Bands in Isothermal, Hot Forging.	275-288A
Wustite, Reduction (chemical) Microstructural Features Produced by the Reduction of Wustite in H ₂ /H ₂ O Gas Mixtures.	117-124B
X ray analysis See also X ray diffraction X ray stress analysis A New Procedure for Determining Volume Fraction of Primary Carbides in High-Speed and Related Tool Steels.	185-191A
X ray diffraction See also X ray stress analysis Identification of the Interface Phase in Titanium Alloys.	681-684A
X ray diffractometer See X ray diffraction	
X ray stress analysis The State of Residual Stress in the Near Surface Region of Homogeneous and Heterogeneous Materials After Grinding.	1239-1244A
Yield strength Hydrogen Embrittlement in a 2000 Series Aluminum Alloy. Low-Cycle Fatigue Behavior of Ti—6Al—2Sn—4Zr—6Mo. I.—The Role of Microstructure in Low-Cycle Crack Nucleation and Early Crack Growth. Deformation by Moving Interfaces. Crack Arrest Toughness of Two High-Strength Steels (AISI 4140 and AISI 4340). The Effect of Phosphorus Content on the Hydrogen Stress Cracking of High-Strength 4130 Steel. Deformation Behavior of Duplex Zircaloy-4—Oxygen Alloys. Plastic Behavior of 70/30 Brass Sheet.	235-239A 257-268A 509-538A 657-664A 907-912A 1077-1082A 1491-1500A
Yield strength, Alloying effects The Effect of an Inert Oxide Particle Dispersion on the Morphology of Martensite in Fe—27Ni—0.025C Alloys.	203-211A
Yield strength, Cooling effects Influence of Cooling Rate on the Microstructure and Retained Austenite in an Intercritically Annealed Vanadium-Containing HSLA Steel.	1899-1906A
Yield strength, Heating effects Strain Aging and Strain Rate Sensitivity of Oxygen-Enriched (Alpha + Beta) Zircaloy-2.	1957-1964A
Yield strength, Microstructural effects The Influence of a Duplex-Microstructure in Steels on Fatigue Crack Growth in the Near-Threshold Region. The Influence of Substructure on the Elevated- and Room-Temperature Strength of a 26Cr—1Mo Ferritic Stainless Steel. Influence of Test Temperature and Microstructure on the Tensile Properties of Titanium Alloys. Grain Boundary Strengthening in Strongly Textured Magnesium Produced by Hot Rolling. Optimization of Fe/Cr/C Base Structural Steels for Improved Strength and Toughness.	439-445A 447-456A 1435-1443A 2219-2226A 2227-2237A
Yield strength, Temperature effects Stress-Assisted Isothermal Martensitic Transformation: Application to TRIP Steels. The Separate Roles of Subgrains and Forest Dislocations in the Isotropic Hardening of Type 304 Stainless Steel.	1907-1914A 1977-1986A
Yield stress See Yield strength	
Young's modulus See Modulus of elasticity	
Zinc, Alloying elements A Localized Soft Mode Model for the Nucleation of Thermoelastic Martensitic Transformation: Application to the Beta → 9R Transformation.	1127-1134A
Zinc, Diffusion Intrinsic Diffusion Coefficients and the Vacancy Flow Factor in Dilute Cu—Zn Alloys. Diffusion Driven Grain Boundary Migration in Iron During Zincification.	1135-1139A 1567-1572A
Zinc base alloys, Mechanical properties Correction to "The Significance of the Dimensionless Constant in the Rate Equation for Superplastic Flow". The Mechanical Properties of Superplastic Materials. Microstructural Aspects of Superplasticity. The Rate-Controlling Deformation Mechanisms in Superplasticity—a Critical Assessment. The Significance of the Dimensionless Constant in the Rate Equation for Superplastic Flow.	2289A 689-701A 703-715A 717-732A 2059-2061A
Zinc base alloys, Thermal properties A Gaussian-Based Formalism for the Representation of Free Energy as a Function of Composition of Binary Metallic Solutions.	213-225B
Zirconium, Binary systems Thermochemistry of Alloys of Transition Metals: III.—Copper—Silver, —Titanium, —Zirconium and —Hafnium at 1373°K.	391-401B
Zirconium base alloys, Corrosion Effects of Texture and Microstructure on the Propagation of Iodine Stress Corrosion Cracks in Zircaloy.	73-83A
Zirconium base alloys, Mechanical properties Deformation Behavior of Duplex Zircaloy-4—Oxygen Alloys.	1077-1082A
Zirconium base alloys, Structural hardening Strain Aging and Strain Rate Sensitivity of Oxygen-Enriched (Alpha + Beta) Zircaloy-2.	1957-1964A

